Summer 2010

Phosphate post-treatment of cerium-based conversion coatings on Al 2024-T3

Daimon K. Heller

Department: Materials Science and Engineering

PHOSPHATE POST-TREATMENT OF CERIUM-BASED CONVERSION COATINGS ON Al 2024-T3

by

DAIMON K HELLER

A DISSERTATION

Presented to the Faculty of the Graduate School of the

MISSOURI UNIVERSITY OF SCIENCE AND TECHNOLOGY

In Partial Fulfillment of the Requirements for the Degree

DOCTOR OF PHILOSOPHY

in

MATERIALS SCIENCE AND ENGINEERING

2010

Approved by

William G. Fahrenholtz, Adviser

Matthew J. O'Keefe

F. Scott Miller

James O. Stoffer

Geoff E. Fair

PUBLICATION DISSERTATION OPTION

This dissertation has been prepared in the style utilized by Corrosion Science and the Journal of the Electrochemical Society. It consists of two papers that have been published, one that has been submitted for publication, and two papers to be submitted for publication. The first paper (pages 20-46) has been published in Corrosion Science. The second paper (pages 47-71) has been published in the Journal of the Electrochemical Society. The third paper is intended for submission to Surface and Coatings Technology (pages 72-98). The fourth paper (pages 99-118) has been submitted for publication in ECS Transactions and is intended for future publication in the Journal of the Electrochemical Society. The fifth paper, (pages 119-131), is intended for submission to Materials Characterization.

ABSTRACT

Phosphate post-treatment of cerium-based conversion coatings (CeCCs) on high strength aluminum alloys can significantly improve corrosion resistance. As-deposited CeCCs exhibit corrosion pits and salt tails across the specimen surface after 3 days of exposure, but post-treated CeCCs have withstood 14 days of salt spray exposure without visibly corroding. The morphology, phase, and electrochemical properties of spray deposited CeCCs were affected by post-treatment parameters such as immersion time, solution temperature, and phosphate source. The best performing coatings were post-treated in aqueous orthophosphate solutions for at least 5 min at temperatures of at least 85 °C. These conditions converted cerium hydroxy/peroxy species in the as-deposited CeCC to hydrated $CePO_4$ and minimized cracks in the coating. Despite demonstrating the kinetic dependence of processes active during post-treatment, these results suggested that the corrosion resistance of CeCCs was dependent on the coating phase and morphology. Using an aqueous precipitation technique, hydrated $CePO_4$ coatings were directly deposited onto Al 2024-T3 substrates and compared to as-deposited and post-treated CeCCs. After salt spray exposure, analysis revealed the formation of pits in the alloy where the substrate was exposed by cracks in the directly deposited $CePO_4$ coating. Post-treated CeCC specimens did not exhibit corrosion at crack/substrate interfaces, indicating that CeCCs can provide electrochemical protection. Post-treated CeCCs also formed an interfacial reaction layer at CeCC/substrate interfaces, a response not observed for directly deposited $CePO_4$ coatings or as-deposited CeCCs. These results demonstrate that post-treated CeCCs are not static barrier coatings, but respond actively to corrosion.

ACKNOWLEDGMENTS

I would like to extend my sincere gratitude to Dr. Bill Fahrenholtz for his guidance, support, and friendship while acting as my advisor. I also thank those who served on my committee, Dr. Matt O'Keefe, Dr. James Stoffer, Dr. Scott Miller, and Dr. Geoff Fair, for providing valuable insight, guidance, and hours of stimulating conversation.

I also extend my undying gratitude to my parents, Lance and Donna Heller. Without their influence and example I would have had neither the character, discipline, nor responsibility to pursue my academic and scientific aspirations. Their encouragement and unwavering support will never be forgotten.

The assistance and camaraderie of those in the corrosion group is also appreciated, including Will Pinc, Beth Kulp, Surender Maddela, Simon Joshi, and Becky Treu.

The work contained herein was funded by the Strategic Environmental Research and Development Program (SERDP) under contracts W912HQ-06-C-0030 and W912HQ-08-C-0008.

TABLE OF CONTENTS

Page

LIST OF FIGURES

Figure Page

Paper I

Paper II

LIST OF TABLES

SECTION

1. INTRODUCTION

Cerium-based conversion coatings have been recognized as an environmentally friendly alternative to chromate conversion coatings (CCCs) for the corrosion protection of high strength aluminum alloys, such as Al 2024-T3 and Al 7075-T6. Despite providing excellent corrosion protection, chromate conversion coatings contain hexavalent chromium, a known toxin and carcinogen. Federal mandates have required implementation of strict environmental controls to reduce workplace exposure to Cr^{6+}, motivating the development of environmentally benign alternatives.

The deposition of CeCCs occurs via a precipitation reaction driven by an increase in the near surface pH that is formed by electrochemical reactions between the coating solution and the alloy substrate. Immediately following deposition, an as-deposited CeCC consists of cerium hydroxide and peroxide species that transition to the more stable $CeO_2 \cdot 2H_2O$ over time. After three days of ASTM B117 salt spray exposure, these coatings exhibit corrosion pits and salt tails across the CeCC surface. However, as-deposited CeCCs that were treated in a heated orthophosphate solution immediately following deposition have withstood up to 14 days of salt spray exposure without exhibiting visible corrosion. While post-treating CeCCs has been shown to significantly increase the corrosion resistance of the coating, neither the changes to the coating that occur during post-treatment nor the mechanism of protection have been comprehensively examined. This dissertation examines the effect of post-treatment parameters on the

phase and morphology of CeCCs and analyzes how CeCCs respond to the salt spray corrosion testing in order to describe how they inhibit the corrosion of Al 2024-T3.

The effect of post-treatment time and temperature on the phase, morphology, and electrochemical properties of CeCCs was examined in a paper published in *Corrosion Science* and is included as Paper I. As-deposited CeCCs post-treated for times of at least 2 min (at 85 °C) or temperatures of at least 70 °C (for 5 min) converted as-deposited cerium hydroxy/peroxy species to hydrated $CePO_4$. These coatings exhibited more anodic pitting potentials and larger charge transfer resistances compared to CeCCs post-treated for shorter times or at lower temperatures. Increasing post-treatment time and temperature also decreased cracks in the CeCC. The phase and morphology of CeCCs is strongly influenced by the time and temperature of phosphate post-treatment, indicating the kinetic dependence of processes active during post-treatment.

A study on the effect of the phosphate source used to post-treat CeCCs was published in the *Journal of the Electrochemical Society* and is included as Paper II. This study characterized the phase and morphology of CeCCs post-treated in solutions produced from orthophosphate, pyrophosphate, and polyphosphate sources. CeCCs that were post-treated in 2.5 wt. % orthophosphate (i.e., $NH_4H_2PO_4$, Na_3PO_4) solutions at 85 °C for 5 min minimized the formation of cracks in the CeCC, converted as-deposited species to $CePO_4{\cdot}H_2O$, and exhibited the least corrosion after 14 days of salt spray exposure. Pyrophosphate (i.e., $K_4P_2O_7$, $Na_2H_2P_2O_7$) and polyphosphate (i.e., $Na_5P_3O_{10}$) post-treatments also reduce cracking in the coating but did not produce the $CePO_4{\cdot}H_2O$ phase, exhibiting intermediate corrosion performance after salt spray testing. Post-treatment in 2.5 wt. % $Na_5P_3O_{10}$ introduced other defects into the coating and performed

the worst in salt spray tests. Results from electrochemical impedance spectroscopy and polarization scans correlated to salt spray results, with orthophosphate post-treatments exhibiting more anodic pitting potentials and larger passivation regions than pyrophosphate or polyphosphate post-treatments. The results indicated that the corrosion resistance of CeCCs is dependent on the phase and morphology of the coating.

Paper III describes the chemical and structural changes that occur in as-deposited and post-treated CeCCs during salt spray exposure and will be submitted to *Surface and Coatings Technology*. Cross-sectional transmission electron microscopy (TEM) was performed on as-deposited and post-treated CeCCs before and after exposure to neutral salt spray. The interface between as-deposited CeCCs and the alloy did not change in thickness (10 – 20 nm) or composition (predominately Al and O) after six days of salt spray exposure. In contrast, post-treated CeCC specimens developed an interfacial reaction layer that grew from an as-deposited thickness of 10 – 20 nm to a thickness of 60 – 100 nm during seven days of salt spray exposure. Since Cl was not detected in either as-deposited or post-treated CeCCs after salt spray exposure, these coatings are believed to be effective barriers to chloride ions. Therefore, the coatings would seem to be more susceptible to corrosion at defects (i.e., cracks and/or subsurface crevices) than by degradation of the CeCC due to chloride attack. The interfacial reaction layer observed only for post-treated CeCC may form by the attack of aluminum oxide or hydroxide species by chloride ions at the interface, facilitating reaction with neighboring Ce species that may be metastable. These results demonstrate that the corrosion inhibition provided by post-treated CeCCs is not solely a result of a static barrier coating, but instead occurs by an active response to corrosion.

Paper IV examines the efficacy of using directly deposited $CePO_4$ coatings for corrosion protection and compares their response to the salt spray environment to that of post-treated CeCCs. This work has been submitted to *ECS Transactions*. Experimental data indicated that CeCCs containing hydrated $CePO_4$ exhibited the best corrosion performance, despite containing subsurface crevices that were formed by the presence of soluble chloride ions and hydrogen peroxide in the deposition solution. Using aqueous precursor solutions of cerium citrate and phosphoric acid, $CePO_4{\cdot}H_2O$ coatings were directly deposited onto Al 2024-T3 substrates without forming subsurface crevices. The directly deposited coatings were not sensitive to surface activation processes and did not significantly alter the electrochemical properties of the substrate, indicating that deposition proceeded independently of the local galvanic activity used to deposit CeCCs. After 18 hours of salt spray exposure, specimens with directly deposited $CePO_4$ coatings exhibited many corrosion pits and tails. Post salt spray cross-sectional analyses of directly deposited $CePO_4$ coatings showed the formation of pits at crack/substrate interfaces, suggesting that coatings functioned as static barriers. In contrast, corrosion pits were not observed at crack/substrate interfaces on post-treated CeCC specimens after salt spray exposure. By inhibiting corrosion of the substrate exposed by defects, CeCCs not only respond actively to the salt spray environment by forming interfacial layers, but appear to provide some electrochemical protection.

The coating solution used to spontaneously deposited CeCCs contains a combination of soluble chlorides and H_2O_2, which aggressively etches the alloy substrate and forms subsurface crevices. Paper V studied the chemical and structural effect of post-treatment on these regions and will be submitted to *Materials Characterization*.

Cross-sectional TEM analysis of subsurface crevices in as-deposited and post-treated CeCCs revealed that an aluminum hydroxide phase had formed on crevices surfaces during coating deposition. For as-deposited specimens, this phase contained up to 8 at. % chlorine and was structurally amorphous. After post-treatment, EDS analysis showed that phosphate post-treatment had reduced the concentration of chlorine in these regions to $\leq$ 1.5 at. % and acted to crystallize the $Al(OH)_3$ phase. Post-treatment will act to improve the corrosion resistance of subsurface crevices separately of its affect on the CeCC by causing more anodic pitting potentials due to reduced chlorine concentration and by forming an improved barrier film by promoting formation of a crystalline aluminum hydroxide (i.e., gibbsite) or hydrated oxide phase.

The series of papers presented within this dissertation describes the effect of post-treatment parameters on the physical, chemical, and electrochemical properties of CeCCs and relates those changes to corrosion performance. Processes active during post-treatment are kinetically dependent. The phase and morphology of CeCCs is strongly dependent on post-treatment time, temperature, and phosphate source. In each case, CeCCs in which $CePO_4$ was formed exhibited the best electrochemical properties (i.e., more anodic pitting potentials, larger passivation, and higher impedance), which correlated to results from accelerated salt spray corrosion testing. The analysis of directly deposited coatings demonstrated that the presence of hydrated $CePO_4$ did not guarantee corrosion protection, and provided the first published evidence that post-treated CeCCs deliver some electrochemical protection by inhibiting corrosion in areas where the substrate is exposed by defects (i.e., cracks). Cross-sectional comparison of as-deposited and post-treated CeCCs revealed that post-treatment facilitates the formation of an

interfacial reaction layer between the CeCC and alloy substrate after salt spray exposure, a response that was not observed for as-deposited CeCCs or directly deposited $CePO_4$ coatings. The formation of an interfacial layer appears to be a vital component of the corrosion protection mechanism and demonstrates that post-treated CeCCs are not static barrier coatings, but respond actively to inhibit corrosion.

The appendices unpublished data and published manuscripts that were not included within the main sections of the dissertation. Appendix A consists of a manuscript published in the *Department of Defense Corrosion Conference 2009 Proceedings* on the development of multifunctional ultraviolet light curable coatings for use with CeCCs and Appendix B contains work published in *ECS Transactions* that describes the electrochemical response of CeCCs to the salt spray environment. Appendix C contains experimental data that was not included for publication elsewhere.

2. LITERATURE REVIEW

2.1. CORROSION OF HIGH STRENGTH ALUMINUM ALLOYS

Aluminum is commonly selected for use in aerospace applications because of its high strength to weight ratio. However, nominally pure aluminum lacks the requisite strength for many applications and must be alloyed to improve its mechanical properties. Copper and zinc are the primary alloying elements in high strength aluminum alloys 2024-T3 and 7075-T6 respectively (Table 2.1), and allow the metals to be precipitation strengthened after solution treatment. The T3 temper designates an alloy that has been solution treated, cold worked, and naturally aged whereas the T6 temper specifies alloys that have been solution treated and artificially aged.[1]

Table 2.1. Alloy composition (wt. %) of Al 2024-T3 and Al 7075-T6. [1]

Element	Si	Fe	Cu	Mn	Mg	Cr	Zn	Ti	Al
AA2024	0.5	0.5	3.8-4.9	0.3-0.9	1.2-1.8	0.1	0.25	0.15	Bal
AA7075	0.4	0.5	1.2-2.0	0.3	2.1-2.9	0.18-0.28	5.1-6.1	0.2	Bal

The formation of small second phase particles during heat treatment increases the strength and hardness of these alloys but has a deleterious effect on the corrosion resistance. When exposed to halide environments in the presence of an electrolyte, many small galvanic cells are created across the metal surface between intermetallic particles and the alloy matrix. These electrochemical cells result in the oxidation of aluminum

metal according to Equations 1 and 2 below. Here the aluminum matrix serves as the anode and water is reduced at intermetallic phases acting as cathodes.

$$Al \rightarrow Al^{3+} + 3e^{-} \quad (1)$$

$$2H_2O + 2e^{-} \rightarrow H_2 + 2OH^{-} \quad (2)$$

High strength aluminum alloys are used widely in applications where high strengths are required without a disproportionate amount of added weight (i.e., high strength to weight ratio). As such, the automotive and aerospace industries use these alloys extensively for structural applications such as truck wheels, gears, fasteners, ordnance, airframes, missile housings, engines, etc.[2] Because of their widespread use on military aircraft and weapons that are exposed to severe environments, extensive research has been conducted on methods to effectively prevent corrosion. In some situations, acceptable corrosion resistance is achieved by utilizing alloys clad in nominally pure aluminum, which lacks second phase particles and consequently exhibits markedly improved corrosion resistance. However, for the most demanding applications a coating system is used, consisting of a conversion coating, primer, and topcoat.[3]

2.2. CHROMATES FOR CORROSION PROTECTION

The conversion coating is a pretreatment that chemically transforms the metallic substrate and forms a thin, typically 100 to 500 nm thick, layer that provides corrosion protection and improves the adhesion of subsequent organic coatings (i.e., primer and topcoat). Based on military performance requirements for conversion coatings such as those described in MIL-DTL-81706, the goal is for conversion coatings to prevent the formation of corrosion pits and salt tails for 2 weeks (336 hours) of salt spray exposure.

In the current system, a primer containing corrosion inhibitor (traditionally chromate compounds) is then deposited on top of the conversion coating. Once a primer is applied, MIL-PRF-85582 dictates that the substrate must not exhibit pitting or corrosion in the scribe after 2000 hrs of salt spray exposure. The primer is followed by a topcoat that provides weatherability and the desired exterior appearance.

Chromate conversion coatings (CCCs) have long been used for the corrosion protection of high strength aluminum alloys. The inclusion of chromate species for chemical oxidation of aluminum was first reported in 1915 by Bauer and Vogel.[4] The solution contained a mixture of metal carbonates and potassium dichromate. The resulting film was claimed to provide improved corrosion protection compared to untreated substrates in neutral salt solution. Biestek and Weber list a number of patents awarded throughout the 1920s and 1930s for using chromates to form chemical oxide coatings on other metals such as cadmium, zinc, magnesium, and copper.[5] More modern chromating processes appeared in the 1940s and were available on a commercial scale in 1950 largely because of their use on military equipment during the Second World War.[6] The chromate conversion coatings in use today most closely resemble the process described in a patent by Ostrander in 1957, who dictates the use of chromic acid, a ferricyanide accelerator, and additives such as soluble dichromate salts, silicates, and/or fluorides.[7]

Chromated coatings actively protect the substrate from corrosion by slowing the kinetics of the oxygen reduction reaction occurring at local cathodes and the anodic reactions occurring across the alloy matrix.[8,9,10] These coatings are believed to protect by the transport of Cr^{6+} ions to sites of active corrosion on the substrate where they are

reduced, forming an insoluble Cr^{3+} oxide film.[11,12,13,14] While providing excellent corrosion protection, chromated coatings contain hexavalent chromium, a known toxin and carcinogen.[15] This becomes a significant health issue when chromium-containing particulates are dispersed into the air during removal and reapplication of these coatings for scheduled aircraft maintenance.[16] Additionally, recent regulations have increased the restrictions on the use and handling of chromates, which increases the life-cycle costs associated with use and maintenance of chromated coatings.[17]

The deposition of CCCs is believed to proceed by a redox mechanism in which the chromate ions present in solution are reduced in conjunction with aluminum oxidation.[5,18] The presence of fluoride in the solution facilitates aluminum dissolution and assists in breaching the native oxide layer, allowing Cr^{6+} access to the Al surface. The resulting near surface pH increase favors the precipitation of a Cr oxide/hydroxide with a gel-like morphology onto the substrate. Several investigators have suggested that CCCs first deposit on cathodic second-phase particles and later deposit on the alloy matrix due to local inhomogeneities that exhibit a weaker galvanic couple than those between the matrix and intermetallic particles.[19,20,21]

Conversion coatings and primers containing chromates have seen prolific use in the past decades because of their effectiveness, despite the associated health and environmental risks. Because hexavalent chromium is a well-documented carcinogen, recent regulations will dramatically increase the expense of using chromated systems by limiting the permissible exposure limit to 5 $\mu g/m^3$ in facilities that process these coatings. To maintain compliance with these regulations, implementation of costly, more stringent

environmental controls will be required, providing an incentive for the development of environmentally friendly coating systems.[3]

2.3. CORROSION INHIBITION BASED ON RARE EARTH COATINGS

Hinton et al. were the first to publish on the use of cerium species to inhibit corrosion of aluminum alloys.[22,23] Since then, continuing studies of coatings based on rare earth elements, particularly cerium, have shown that rare earth based coatings can provide corrosion protection to high strength aluminum alloys in saline environments.[24,25] Solutions containing dissolved rare earth salts are believed to inhibit corrosion by providing ions that selectively precipitate onto local cathodes (i.e., Cu-rich intermetallics) and slow the oxygen reduction reaction.[9,26,27,28,29] Investigations examining the efficacy of using cerium containing films for the corrosion protection of other substrates including magnesium, tinplate, zinc, and select metal matrix composites have also been published.[30,31,32,33]

Cerium-based conversion coatings (CeCCs) have been developed as a possible alternative to CCCs for the corrosion protection of high strength aluminum alloys.[34,35] The deposition mechanism arises from an increase in the near surface pH when the coating solution contacts the substrate; this results in precipitation of cerium peroxide/hydroxide compounds that decompose over time into hydrated cerium oxide ($CeO_2 \cdot 2H_2O$).[36,37,38] Electrolytic, immersion, and spray techniques can be used to deposit CeCCs with different surface morphologies and corrosion resistances.[39,40,41] Because CeCCs are environmentally friendly, their implementation would eliminate the increased cost and environmental risks incurred by using chromated coatings.

The deposition of CeCCs is highly sensitive to deposition parameters such as the surface activation, substrate microstructure, and the composition of the coating solution.[42,43,44] The role of the surface activation process is to remove the native oxide layer, exposing intermetallic compounds and allowing the constituents in the coating solution to react directly with the alloy surface. Because of the amphoteric nature of aluminum, a wide variety of processes can be used to activate 2024 or 7075 substrates, such as immersion in solutions comprised of NaOH, H_2SO_4, Na_2CO_3, HBF_4, HF, H_3PO_4, or HNO_3. The strength and duration of the surface activation will affect the resulting chemistry of the sample surface and, in turn, can modify the deposition and properties of CeCCs.[42,45,46] In some cases a combination of activation solutions is used to remove the surface oxide and then desmut the resulting surface. The deposition and morphology of the cerium-based coating can also be dramatically influenced by the composition of the coating solution and the concentration of species therein.[47,48] Adding gelatin to the coating solution has been shown to stabilize bubble formation during deposition and provide a mechanism that controls the rate of coating formation.[49] Hydrogen peroxide has been shown to significantly increase the rate of coating deposition for solutions based on $CeCl_3$ or $Ce(NO_3)_3$ salts, allowing CeCCs to be deposited from room temperature solutions in minutes rather than hours or days.[50]

2.4. RARE EARTH TOXICOLOGY

The use of rare earth elements is continually increasing as new materials are developed and applications utilizing their properties are produced. These elements are commonly used in superconductors, lasers, catalysts, magnets, ceramics, and abrasives.

As the use of rare earth elements increases, so does the need to understand their toxicological effect on living organisms.

The absorption of rare earth elements, including cerium, into the body through the skin is negligible, except when abrasions are present. In this case, increased absorption may occur, but the dominant response is irritation and scarring caused by reaction with tissue constituents (e.g., phosphates).[51] Intradermal injection of rare earth chlorides or nitrates can produce granulomas or lesions at the injection site and moderate adsorption. Intravenous injection causes rapid absorption of rare earth elements, which are removed from the bloodstream with 24 hours. The absorption and clearance of rare earth elements depends on their stability in the bloodstream. More stable chelated forms, such as citrate complexes, were quickly removed through the body's waste stream, whereas ionic forms were absorbed into the body. Rare earth elements are primarily transported to the liver, spleen, and bone where the half-life of removal is between 150 – 250 days for most rare earth elements.[51,52,53] Removal time varies with organ, as half-life for removal from the liver is approximately 15 days. However, 66 % of the rare earth concentration in bone remained eight months after initial exposure, with heavier rare earth elements having a larger propensity to be incorporated into bone compared to light rare earths. Once transported to the organs, rare earth elements can cause development of a fatty liver and premature death of liver or spleen tissue.[51,52] Because of the similar ionic radii, many rare earth elements exhibit a propensity to remove Ca^{2+} and deposit in bone, resulting in increased calcium concentration in other organs.[53] Eye exposure and inhalation generally leads to irritation of the affected tissue, but long term exposure to rare earth dust can cause pneumoconiosis (restricted lung capacity) caused by fibrosis.[52,54] Rare earth

elements are poorly absorbed through the intestinal tract and no toxic side effects were observed after long term ingestion. Exposure to rare earth elements is not highly toxic, with LD_{50} values from 10 – 100 mg/kg when intravenously injected and generally from 250 – 1000 mg/kg for intraperitoneal (i.e., into a body cavity) injections.[52] The development of carcinomas was not reported after exposure to rare earth elements.

2.5. POST-TREATMENT (SEALING)

Electrolytic processes (e.g., anodizing, electroplating) and/or chemical pre-treatments/conversion coatings are used to inhibit the corrosion of metals such as aluminum, iron (steels), titanium, zinc, and magnesium.[55,56] While the formation of anodized and phosphate conversion layers provide some corrosion protection, these coatings typically contain a significant amount of porosity that allows corrosive species such as chloride ions to react with the underlying substrate. These coatings exhibit optimal corrosion resistance after being subjected to a post-treatment (a.k.a. sealing) process that acts to fill porosity and/or alter the structure of the as-deposited coatings. For example, sealing of an anodized alumina layer by immersion in a boiling aqueous solution of nickel acetate results in the precipitation of nickel hydroxide in pores and converts the as-deposited amorphous film to boehmite.[56] Anodized layers function as barriers to corrosion and therefore do not actively protect the substrate. The incorporation of rare earth elements into anodized coatings during the sealing process has been shown to further improve corrosion resistance, presumably a result of rare earth compounds functioning as corrosion inhibitors.[57,58,59,60]

The corrosion resistance of phosphate layers formed during phosphating of galvanized steel or magnesium can also be improved by post-treatment in molybdate or silicate solutions.[61,62,63] These treatments were observed to fill pores in between zinc phosphate crystals, creating continuous coatings containing molybdate and silicate species respectively. In each case, the corrosion resistance improved and electrochemical analysis revealed a decrease in anodic and cathodic corrosion current densities.

Sealing processes have also been used to increase the corrosion resistance of coatings deposited with sol-gel techniques or vapor deposition processes. Silane and silicate based sols have been used to seal Zn-TiO_2 coatings on rare earth magnets, reportedly by filling pores and other defects present in the coating.[64] Similarly, polymethyl methacrylate based sealing processes filled pinholes in CrTiAlN coatings deposited by magnetron sputtering and significantly improved corrosion resistance.[65]

Several researchers have shown that the corrosion resistance of CeCCs increases after post-treatment in a phosphate solution.[30,47,48,66,67] This process has typically been performed by immersing the sample for 5 to 20 min in an aqueous solution of 2.5 to 3.0 wt% Na_3PO_4 heated to at least 80 °C. The results have shown that phosphate post-treatment can convert the as-deposited nanocrystalline cerium species, (i.e., hydrated CeO_2 and/or cerium hydroxides/peroxides), to hydrated $CePO_4$. Coatings that had been post-treated were observed to have less cracking and improved electrochemical properties as shown via polarization and electrochemical impedance spectroscopy (EIS) testing. Additives such as gelatin can aid in controlling the deposition rate and morphology of the resulting coating, but have also been shown to affect the ability of the as-deposited coating to transform to hydrated $CePO_4$.[49]

2.6. REFERENCES

1. R.B.C. Cayless, "Alloy and Temper Designation Systems for Aluminum and Aluminum Alloys," *ASM Handbook*, Vol. 2, in ASM Handbooks Online http://products.asminternational.org/matinfo, ASM International, 2002.

2. J.R. Davis, *Corrosion of Aluminum and Aluminum Alloys*, ASM International, Materials Park, OH, 1999.

3. R.L. Twite, G.P. Bierwagen, *Prog. Org. Coat.*, **33**, 91-100 (1998).

4. S. Wernick, R. Pinner, and P.G. Sheasby, *The Surface Treatment and Finishing of Aluminum and Its Alloys*, 5th ed., Finishing Publications, Teddington (1987).

5. T. Biestak and J. Weber, Eletrolytic and Chemical Conversion Coatings, 1st ed., Portcullis Press, Redhill (1976).

6. R. Stricklen, *Materials and Methods*, **35**(2), 91-95 (1952).

7. C.W. Ostrander, N.R. Congiundi, U.S. Patent 2,796,370, issued June 18, 1957.

8. W. J. Clark, J. D. Ramsey, R. L. McCreery, G. S. Frankel, J. Electrochem. Soc., **149**(5), B179-B185 (2002).

9. M. Kendig and C. Yan, J. Electrochem. Soc., **151**(12), B679-B682 (2004).

10. J. Zhao, G. Frenkel, R.L. McCreery, *J. Electrochem. Soc.*, **145**(7), 2258-2264 (1998).

11. L. Xia, E. Akiyama, G. Frankel, and R. McCreery, *J. Electrochem. Soc.*, **147**, 2556 (2000).

12. M. Kendig, S. Jeanjaquet, R. Addison, J. Waldrop, *Surf. Coat. Technol.*, **140**, 58-66 (2001).

13. J. Zhao, L. Xia, A. Sehgal, D. Lu, R. L. McCreery, G. S. Frankel, *Surf. Coat. Technol.*, **140**, 51-57 (2001).

14. O. Lunder, J.C. Walmsley, P. Mack, K. Nisancioglu, *Corr. Science*, **47**, 1604-1624 (2005).

15. Agency for Toxic Substances and Disease Registry (ATSDR), Toxicological profile for Chromium, (2008).

16. D.C. Perry, *Specialized Cleaning, Finishing and Coating Processes*, Conference Proceedings 5-6 Feb. 1981, American Society for Metals, 3-16 (1981).

17. OSHA 29 CFR Part 1910.1026.

18. A.E. Hughes, R.J. Taylor, B.R.W. Hinton, *Surf. Interface Anal.*, **25**, 223-234 (1997).

19. S.A. Kulunkich, A.S. Akhtar, D. Susac, P.C. Wong, K.C. Wong, K.A.R. Mitchell, *Appl. Surf. Sci.*, **253**, 3144-3153 (2007).

20. P. Campestrini, E.P.M. van Westing, J.H.W. de Wit, *Electrochimica Acta*, **46**, 2553-2571 (2001).

21. P.L. Hagans, C.M. Haas, *Surf. Interface Anal.*, **21**, 65 (1994).

22. B.R. Hinton, D. R. Arnott, and N. E. Ryan, *Met. Forum*, **7**, 211 (1984).

23. B.R. Hinton, D. R. Arnott, and N. E. Ryan, *Materials Forum*, **9**, 162 (1986).

24. M. Bethencourt, F. J. Botana, J. J. Calvino, M. Marcos, M. A. Rodriquez-Chacoń, *Corr. Science*, **40** (11), 1803-1819 (1998).

25. B.R.W. Hinton, *J. Alloy Compd.*, **180**, 15-25 (1992).

26. Y. Xingwen, C. Chunan, Y. Zhiming, Z. Derui, Y. Zhongda, *Mat. Sci. and Engr.*, **A284**, 56-63 (2000).

27. M.A. Jakab, F. Presuel-Moreno, J.R. Scully, *J. Electrochem. Soc.*, **153** (7), B244-B252 (2006).

28. A. Kolics, A. S. Besing, P. Baradlai, and A. Wieckowski, *J. Electrochem. Soc.*, **150** (11), B512-B516 (2003).

29. M. Kendig, S. Jeanjaquet, *J. Electrochem. Soc.*, **149** (2), B47-B51 (2002).

30. C. Wang, S. Zhu, F. Jiang, F. Wang, *Corr. Science*, doi:10.1016/j.corsci.2009.08.003 (2009).

31. N. Mora, E. Cano, J. L. Polo, J. M. Puente, J. M. Bastidas, *Corr. Science*, **46**, 563-578 (2004).

32. K. Aramaki, *Corr. Science*, **46**, 1565-1579 (2004).

33. A. Pardo, M. C. Merino, R. Arrabal, F. Viejo, and M. Carboneras, *J. Electrochem. Soc.*, **153** (2), B52-B60 (2006).

34. S.M. Cohen, *Corrosion Engineering*, **51**(1), 71-78 (1995).

35. R.L. Twite and G. P. Bierwagen, *Progress in Organic Coatings*, **33**, 91-100 (1998).

36. A.E. Hughes, R.J. Taylor, B.R.W. Hinton, L. Wilson, *Surf. Interface Anal.*, **23**, 540-550 (1995).

37. S.A. Hayes, P. Yu, T.J. O'Keefe, M.J. O'Keefe, J.O. Stoffer, *J. Electrochem Soc.*, **149**(12), C623-C630 (2002).

38. A.J. Aldykiewicz, A.J. Davenport, H.S. Isaacs, *J. Electrochem Soc.*, **143**(1), 147-154 (1996).

39. B.Y. Johnson, J. Edington, A. Williams, M.J. O'Keefe, *Mat. Characterization*, **54**, 41-48 (2005).

40. W. G. Fahrenholtz, M. J. O'Keefe, H. Zhou, J. T. Grant, *Surf. Coat. Technol.*, **155**, 208 (2002).

41. J. Stoffer, T. O'Keefe, S. P. Sitaram, P. Yu, X. Lin, E. L. Morris, U.S. Patent 5,932,083, issued Aug. 3, 1999.

42. P. S. Jones, P. Yu, W. R. Pinc, M. J. O'Keefe, W. G. Fahrenholtz, and T. J. O'Keefe, *Int. J. Appl. Ceram. Technol.*, **5**(1), 63 (2008).

43. W. Pinc, S. Geng, M. O'Keefe, W. Fahrenholtz, T. O'Keefe, *Appl. Surf. Sci.*, **255**(7), 4061-4065 (2009).

44. A. Decroly, J. Petitjean, *Surf. Coat. Technol.*, **194**, 1-9 (2005).

45. P. Campestrini, H. Terryn, A. Havestad, J.H.W. de Wit, *Surf. Coat. Technol.*, **176**, 365-381 (2004).

46. L.E.M. Palomino, I.V. Aoki, H.G. Melo, *Electrochemica Acta*, **51**, 5943-5953 (2006).

47. B.Y. Johnson, J. Edington, M.J. O'Keefe, *Mat. Sci. and Engr.*, **A361**, 225-231 (2003).

48. B. F. Rivera, B.Y. Johnson, M.J. O'Keefe, W.G. Fahrenholtz, *Surf. Coat. Technol.*, **176**, 349-356 (2004).

49. W. Pinc, P. Yu, M. O'Keefe, W. Fahrenholtz, *Surf. Coat. Technol.*, **203**(23), 3533-3540 (2009).

50. F.H. Scholes, C. Soste, A.E. Hughes, S.G. Hardin, P.R. Curtis, *Appl. Surf. Sci.*, **253**, 1770-1780 (2006).

51. T.J. Haley, *J. Pharm. Sci.*, **54**(5), 663-670 (1965).

52. S. Hirano, K.T. Suzuki, *Environ. Health Perspectives*, **104**(1), 85-95 (1996).

53. Y. Nakamura, Y. Tsumura, Y. Tonogai, T. Shibata, Y. Ito, *Fund. Appl. Toxicol.*, **37**, 106-111 (1997).

54. W. Lin, Y. Huang, X. Zhou, Y. Ma, *Int. J. Toxicol.*, **25**, 451-457 (2006).

55. T.S.N.S. Narayanan, *Rev. Adv. Mater. Sci.*, **9**, 130-177 (2005).

56. M.F. Stevenson, "Anodizing," *ASM Handbook*, Vol. 5, in ASM Handbooks Online http://products.asminternational.org/matinfo, ASM International, 2002.

57. F. Mansfeld, C. Chen, C.B. Breslin, D.Dull, *J. Electrochem. Soc.*, **145**(8), 2792-2798 (1998).

58. X. Yu, C. Yan, C. Cao, *Mater. Chem. Phys.*, **76**, 228-235 (2002).

59. X. Yu, C. Cao, *Thin Solid Films*, **423**, 252-256 (2003).

60. A.S. Hamdy, *Surf. Coat. Technol.*, **200**, 3786-3792 (2006).

61. B. Lin, J. Lu, G. Kong, *Corr. Science*, **50**, 962-967 (2008).

62. B. Lin, J. Lu, G. Kong, *Surf. Coat. Technol.*, **202**, 1831-1838 (2008).

63. X. Shi, G. Jarjoura, and G.J. Kipouros, *Magnesium Technology*, 273-280 (2006).

64. X. Yang, Q. Li, S. Zhang, F. Liu, S. Wang, H. Zhang, *J. Alloy Compd.*, **495**, 189-195 (2010).

65. Q. Yang, F. Cai, L.R. Zhao, X. Huang, *Surf. Coat. Technol.*, **203**, 606-609 (2008).

66. H. Zhang, Y. Zuo, *Appl. Surf. Sci.*, **254**, 4930 (2008).

67. S. You, P. Jones, A. Padwal, P. Yu, M. O'Keefe, W. Fahrenholtz, T. O'Keefe, *Mat. Letters*, **61**, 3778-3782 (2007).

PAPER

I. THE EFFECT OF POST-TREATMENT TIME AND TEMPERATURE ON CERIUM-BASED CONVERSION COATINGS ON Al 2024-T3

Daimon K Heller, William G. Fahrenholtz, Matthew J. O'Keefe

Materials Research Center, Department of Materials Science and Engineering,

Missouri University of Science and Technology, Rolla, MO 65409, USA

ABSTRACT

Corrosion performance, morphology, and electrochemical characteristics of cerium-based conversion coatings on Al 2024-T3 were examined as a function of phosphate post-treatment time and temperature. Corrosion resistance improved after post-treatment in 2.5 wt% $NH_4H_2PO_4$ for times up to 10 minutes or temperatures up to 85 °C. Electrochemical impedance spectroscopy and polarization testing correlated to neutral salt spray corrosion performance. Hydrated cerium oxide and peroxide species present in the as-deposited coatings were transformed to $CePO_4{\cdot}H_2O$ for post-treatments at longer times and/or higher temperatures. Based on these results, processes active during post-treatment are kinetically dependent and strongly influenced by the post-treatment time and temperature.

1. INTRODUCTION

Aluminum is widely used in the aerospace industry because of its high strength to weight ratio. However, nominally pure aluminum lacks the requisite strength for many applications and must be alloyed to improve its mechanical properties. For example, high strength aluminum alloys such as AA2024-T3 and AA7075-T6 are commonly used in the aerospace industry. The intermetallic particles that give these alloys their strength are also culpable for their susceptibility to galvanic corrosion [1]. Chromate based conversion coatings and primers have traditionally been used for corrosion protection of commercial and military aircraft [2,3]. These coatings actively protect the substrate by slowing the kinetics of the oxygen reduction reaction that occurs at local cathodes (i.e., intermetallics) and anodic reactions across the alloy matrix [4]. This mechanism is believed to proceed by the transport of Cr^{6+} ions to active sites where they are reduced to form an insoluble hydrated Cr^{3+} oxide layer [5,6]. Despite excellent protective capacity, Cr^{6+} is toxic and carcinogenic. As a result, modified regulations such as OSHA's 29 CFR 1910 have been put into place to decrease the permissible workplace exposure limit by more than a factor of ten to 5 $\mu g/m^3$ [7].

Human health and environmental diligence provide the impetus to develop and employ environmentally benign coating systems to replace chromate-containing systems. Research has shown that rare earth compounds have the ability to protect aluminum alloys in saline environments; these compounds, particularly cerium compounds, are environmentally benign and have excellent potential for use in protective coatings [8,9,10,11]. Cerium-based conversion coatings have been shown to protect Al 2024-T3 and Al 7075-T6 alloys, as well as other materials such as magnesium alloys, stainless

steels, and metal matrix composites [12,13,14]. In the case of aluminum alloys, published results show these coatings can be deposited with spontaneous or electrolytic (i.e., current driven) processes [5,15]. Spontaneous processes take advantage of the electrochemical potential created between the alloy matrix and intermetallic particles to drive reactions which produce a pH gradient that allows Ce species to precipitate onto the substrate [16,17].

In several reports, the corrosion protection of CeCCs was improved by the use of a phosphate post-treatment, which leads to a reduction in surface cracking and the formation of a hydrated $CePO_4$ phase [18,19,20]. The phosphate post-treatment, referred to as sealing, is typically performed at or above 80 °C, but literature that addresses phosphate post-treatments has limited examination on the effects of varying process parameters such as immersion time and temperature on coating performance.

The purpose of this study was to examine the effects of post-treatment variables on the corrosion protection of CeCCs and to elucidate the processes that occurred during sealing. In this work, CeCCs were deposited on Al 2024-T3 panels from aqueous solutions using a spontaneous spray process [21,22]. The coatings were subsequently treated in phosphate solutions for various times and temperatures. Coating performance was evaluated with salt spray testing and electrochemical analysis. Physical and chemical analyses were also used to identify the effects of time and temperature on the coating characteristics, which were then correlated to corrosion performance and electrochemical measurements.

2. EXPERIMENTAL

Copper is the primary alloying element in the precipitation strengthened aluminum 2024-T3 alloy, present from 3.8 to 4.9 wt % as shown in Table 1 [23,24]. The T3 temper designates an alloy that was solution treated, cold worked, and allowed to age naturally.

Prior to coating deposition, coupons of Al 2024-T3 (AMI Metals) measuring 3.8 x 7.6 cm were acetone wiped, rinsed with tap water, and immersed in a 5.0 wt% solution of alkaline cleaner (Turco 4215 NCLT) for five minutes at 55 °C. Upon removal, samples were rinsed with deionized water and immersed in 1.0 wt% sulfuric acid at 50 °C for ten minutes followed by rinsing with deionized water. At this point the panels were ready for the spray deposition process.

To prepare the coating solution, a stock solution was first produced by dissolving 40 g of hydrated $CeCl_3$ (Alfa Aesar, 99.9%) into 780 g of deionized water. The solution pH was then adjusted to 2.07 with hydrochloric acid. Next, 0.8 g of gelatin (Rousselot, DSF) was dissolved into 25 g of deionized water and added to 205 g of stock solution. Lastly, 20 ml of H_2O_2 (Fisher Scientific, 30%) was added to the solution, which was mixed for several minutes with a magnetic stirrer prior to spray deposition.

The coating solution was sprayed onto the panel surface using a Husky Model 515-547 detail spray gun operated at 205-245 kPa. Each panel was coated using five spray-drain cycles where each cycle consisted of spraying the panels for ≈3 seconds and then allowing them to drain for ≈35 seconds. After five cycles, the panels were rinsed with deionized water and then submerged in the post-treatment solution, which consisted of 2.5 wt% $NH_4H_2PO_4$ (Aldrich, 98%) in deionized water. The post-treatment times and

temperatures varied, but all were followed by a final rinse in deionized water. For the experiments discussed herein, conditions analyzed included unsealed (as-deposited), post-treatment times of 10, 30, 120, and 600 seconds, and temperatures of 55, 70, and 85 °C.

A Q-FOG cyclic corrosion tester (A-Panel Lab Products) was used to evaluate the neutral salt spray corrosion performance of all panels. Tests were conducted to the specifications detailed in ASTM B117.

Electrochemical tests were conducted using a flat cell (model K0235, Princeton Applied Research) in conjunction with a saturated calomel electrode and platinum mesh counter electrode. The area tested was 1.0 cm^2; the electrolyte was a mixture of 0.6 wt% NaCl and 0.6 wt% $(NH_4)_2SO_4$ in deionized water. Corrware (Scribner Associates) software was used to control the analytical equipment; CorrView and ZView were used for data analysis. Electrochemical impedance spectroscopy (EIS) was performed using a Schlumberger model SI1255 frequency response analyzer. Data were collected over a frequency range of 0.006 to $1x10^5$ Hz with an AC amplitude of 10 mV. The potentiostat was model 273A from Princeton Applied Research; scans were conducted from -0.4 to +0.7 V with respect to open circuit potential using a scan rate of 1.5 mV/s. A time of 1500 seconds was allowed for the cell to stabilize at ambient temperature before data collection began.

Microscopy was carried out with a Hitachi S570 scanning electron microscope (SEM) equipped with a LaB_6 electron source. Images were recorded using the secondary electron detector at an accelerating voltage of 12 kV. Grazing incidence x-ray diffraction (XRD) was performed using a Phillips X-Pert Diffractometer from 5° to 90° two theta

using Cu-Kα radiation. X-ray photoelectron spectra were collected with a Kratos Axis 165 x-ray photoelectron spectrometer (XPS) using a non-monochromated magnesium x-ray source.

3. RESULTS AND DISCUSSION

Neutral salt spray testing and electrochemical analyses indicated that the temperature and duration of phosphate post-treatment affected the corrosion resistance of CeCCs. Analysis revealed that the processes active during post-treatment affected the surface morphology of the coatings, altered the cerium oxidation state (from Ce^{4+} to Ce^{3+}), and changed the hydrated CeO_2 species present in the as-deposited coating to hydrated $CePO_4$. Furthermore, CeCCs post-treated in room temperature phosphate solutions for up to four weeks exhibited many of the same characteristics (i.e., morphology, phase) and comparable corrosion resistance to CeCCs post-treated at temperatures up to 85 °C for times less than 10 min. The results suggested that the post-treatment process is kinetically controlled and greatly influenced by time and temperature.

3.1. Corrosion Results

Samples treated for longer times or higher temperatures exhibited less salting and better electrochemical properties than those subjected to shorter or lower temperature sealing processes. Figure 1 shows optical images of CeCCs for different post-treatment temperatures after 14 days of neutral salt spray exposure. For the as-deposited condition, Figure 1a, many pits were present and numerous, large salt tails

were seen after ASTM B117 testing. Post-treatment at 55 °C, Figure 1b, decreased the density of corrosion pits and the size of salt tails that were observed. Continuing to increase the post-treatment temperature to 70 and 85 °C, Figures 1c and 1d, further reduced the number of pits and the size of salt tails observed after corrosion testing. Post-treatment at higher temperatures also changed the color of the coatings. Before corrosion testing, an as-deposited sample had a strong orange color whereas the color gradually transitioned to a light gold as the post-treatment temperature increased to 85 °C. The color change is believed to result from the elimination of cerium hydroxide and/or peroxide species formed during the deposition process.

Similar to the effects of temperature, corrosion performance was also affected by post-treatment duration. A treatment for 10 sec at 85 °C showed fewer pits and less tailing than an as-deposited sample. As post-treatment time increased, the number of pits and tails also decreased, Figures 2a-d; additionally, the same color change described previously as a function of temperature was also observed as a function post-treatment time. Salt spray corrosion testing revealed that the best corrosion performance was observed for CeCCs post-treated for the longest time (10 min) and at the highest temperature (85 °C). These panels, Figures 1d and 2d, showed only a few pits and tails, which were typically not visible to the unaided eye, but could only be resolved with magnification.

3.2. Surface Morphology

SEM analysis indicated that the size and extent of cracking decreased as post-treatment temperature increased. The as-deposited coating, Figure 3a, was the most

highly cracked of the samples evaluated during the study, and showed the worst salt spray corrosion performance. Examination of the morphology of CeCCs post-treated for 5 min at 55, 70, and 85 °C, Figures 3b-d, revealed that higher temperature post-treatment reduced the density and size of cracks. The 85 °C treatment exhibited fewer cracks, and the cracks were smaller in size compared to an as-deposited coating. In addition, coatings post-treated at 85 °C exhibited superior corrosion performance compared to CeCCs post-treated at lower temperatures.

Electron micrographs of CeCCs post-treated at 85 °C for different times are included as Figure 4. After post-treatment for 10 sec at 85 °C, the coatings showed a marginal decrease in cracking compared to as-deposited coatings, yet they had improved corrosion protection. Post-treatment for longer times (30 sec, 2 min, and 10 min) at 85 °C produced a clear reduction in cracking over as-deposited coatings, but little difference in cracking was observed between coatings post-treated for 30 seconds and those immersed for two or 10 minutes (Figure 4). The initial reduction in cracking likely plays a role in the improved corrosion performance as coatings with fewer cracks would be more effective barriers to corrosive species and reduce the probability of a crack exposing an active site on the substrate. The above results suggest that additional processes, aside from an improved coating morphology (decreased cracking), are responsible for the increased corrosion protection observed from samples post-treated for times longer than 30 sec.

3.3. Electrochemical Analysis

Electrochemical impedance spectra and potentiodynamic scans (Figure 5) indicated that increasing the post-treatment temperature resulted in a coating that was more electrochemically resistant to corrosion. Higher temperature treatments had higher charge transfer resistances than CeCCs post-treated at lower temperatures, Table 2. For example, the charge transfer resistance increased from ≈8 kΩ cm^2 for an as-deposited panel to ≈50 kΩ cm^2 after post-treatment for five minutes at 55 °C and to ≈90 kΩ cm^2 for a five minute post-treatment at 85 °C, which exhibited the least amount of corrosion after 14 days of salt spray testing. The resistance values were calculated by fitting the recorded data to an equivalent circuit model using a software application. Data collected from potentiodynamic scans revealed that higher temperature treatments resulted in more noble pitting potentials (E_{pit}), lower corrosion currents (i_{corr}), and larger passivation regions as depicted in Figure 5 and tabulated in Table 2.

Similar data were measured for CeCCs post-treated for increasing times at 85 °C. As the duration of post-treatment increased, more noble pitting potentials and passivation regions were observed as well as higher charge transfer resistances (Figure 6, Table 3). The larger passivation regions and more anodic E_{pit} values from samples post-treated for longer times and higher temperatures translate to better corrosion resistance by protecting against pit formation at lower potentials where coatings post-treated for shorter times or lower temperatures begin to form pits and corrode. These results correlate well to salt spray testing and show that improved corrosion protection was observed from samples post-treated at higher temperatures and longer times because they exhibited the highest

resistances, largest passivation regions, and most noble pitting potentials of samples included in the study.

3.4. Phase Analysis

CeCCs post-treated as a function of time and temperature were analyzed with grazing incidence x-ray diffraction. XRD analysis indicated that hydrated $CePO_4$ (most closely matching rhabdophane, PDF #35-0614) formed after post-treatment above 70 °C for five minutes or for treatments at 85 °C lasting two minutes or longer (Figure 7). Unsealed panels and panels treated at lower temperatures or shorter times did not show distinct peaks for hydrated $CePO_4$. Instead, these panels exhibited a broad, low angle peak believed to be due to the presence of nanocrystalline hydrated CeO_2 (i.e., $CeO_2 \cdot 2H_2O$) formed during deposition [19]. During post-treatment, cerium hydroxide and oxide species were transformed to $CePO_4 \cdot H_2O$ for some combinations of post-treatment time and temperature. The formation of hydrated $CePO_4$ in the CeCC is believed to improve the corrosion performance and was most evident by examining the coatings post-treated as a function of time at 85 °C. Since samples treated for at least 30 seconds all exhibited fewer cracks than the as-deposited coating, an explanation aside from coating morphology is needed to explain the improved corrosion performance observed as the post-treatment time was extended to two and ten minutes. The XRD pattern for the 30 second post-treatment exhibited the first indication of hydrated $CePO_4$ peaks although the pattern was predominated by the broad CeO_2 peak. However, distinct $CePO_4$ peaks were evident after two and ten minute post-treatments. These results correspond to the large increase in electrochemical resistance as the post-treatment time

increased from 30 seconds to two minutes and was also consistent with the smaller changes in charge transfer resistance and corrosion performance observed between the two and ten minute post-treatments. Despite the much longer duration in the phosphate solution, the ten minute post-treatment exhibited a marginal improvement in corrosion performance over the two minute immersion. Since the duration of the two minute immersion was sufficient to reduce cracking and form at least some hydrated $CePO_4$, it is likely that the additional immersion time from the ten minute post-treatment acted only to transform additional cerium oxide or hydroxide species to hydrated $CePO_4$. Since the resolution of the XRD peaks exhibited subtle, if any, changes between the two and ten minute treatments, it is believed that this additional transformation is relatively small compared to the transformation that occurred between the 30 second and two minute treatments. Combined with the SEM observations, the results suggest that both the morphology and phase of the CeCC are factors in determining its corrosion protection.

3.5. Cerium Oxidation State (Ce^{3+}/Ce^{4+})

XPS analysis of the Ce 3d and O 1s regions of the spectra showed that post-treatment affected the Ce valence state (Figure 8). The Ce 3d spectra is complex and the peak identification in the literature is inconsistent [25,26,27]. However, examination of the Ce 3d spectrum revealed similar amounts of Ce^{3+} and Ce^{4+} in the as-deposited panel. With increased post-treatment duration, the area under the Ce^{4+} peaks decreased, including the satellite unique to Ce^{4+} near 916 eV. The intensity of the Ce-OH peak in the O 1s spectra decreased as post-treatment time increased, supporting the contention that cerium hydroxide species were either removed or converted to hydrated

cerium phosphate during post-treatment. The spectrum from the panel treated for 10 minutes exhibits a peak centered at 531.0 eV, matching exactly to the binding energy of oxygen in $CePO_4$ [28]. The peak at 528.9 eV, identified as CeO_2, is only observed for as-deposited coatings and post-treatment times less than 30 seconds, indicating that CeO_2 also converts to $CePO_4$ during post-treatment.

Analysis of samples post-treated at different temperatures did not exhibit the gradual transition from Ce^{4+} to Ce^{3+} as temperature was increased. After post-treatment at 55 °C, quantitative analysis from calculated peak area from the O 1s spectra indicated that cerium was predominately present as Ce^{3+} (75 %), but $CePO_4$ was not detected at this temperature by XRD. As the post-treatment temperature was increased to 70 and 85 °C, the amount of Ce^{3+} calculated by area from the O 1s spectra did not change significantly, remaining between 75 and 80 %. At these temperatures, XRD indicated that hydrated $CePO_4$ formed, suggesting that the $CePO_4$ phase, not the Ce^{3+} valence, imparted the superior corrosion performance to samples post-treated at the highest temperatures and longest times.

Even though higher temperatures and longer times increased conversion to phosphate, the Ce 3d spectra indicated that some amount of Ce^{4+} remained even after the highest temperature post-treatment, whereas the O 1s spectra suggested that Ce^{4+} species were nearly all transformed to $CePO_4$ (Ce^{3+}). This discrepancy is likely explained by the instability of cerium species upon exposure to the x-ray radiation and results in the O 1s spectra being a better measure of the process. However, as a surface sensitive technique, XPS was unable to evaluate the bonding environment throughout the thickness of the coating, so Ce^{4+} species may have been present closer to the substrate/coating interface.

The Ce 3d and O 1s spectra both indicated that the as-deposited coating contained a mixture of Ce^{3+} and Ce^{4+}; after post-treatment, hydrated $CePO_4$ (Ce^{3+}) became the dominate constituent in the coating and was believed to increase the corrosion protection of CeCCs.

3.6. Room Temperature Post-treatment

Noting the large dependence on time and temperature explicated in previous sections, additional samples were evaluated after immersing CeCC panels in a room temperature solution of 2.5 wt% $NH_4H_2PO_4$ (pH adjusted to 4.5 by adding H_3PO_4) for one week. Salt spray corrosion testing of the panels post-treated at room temperature for one week showed fewer pits and tails compared to an as-deposited panel, thereby exhibiting improved corrosion resistance over the as-deposited condition but not equaling the performance of samples post-treated at 85 °C for 5 or 10 minutes. The surface morphology of the CeCC post-treated for one week showed less cracking compared to the as-deposited condition and the presence of hydrated $CePO_4$ was confirmed with XRD (Figure 9), indicating that conversion of cerium oxide and hydroxide species present in the as-deposited coating to hydrated $CePO_4$ was favorable at room temperature given sufficient time for the reaction to proceed. Furthermore, high temperature post-treatment was not a requisite factor to improve the surface morphology of a CeCC (reduce cracking) or to form $CePO_4$ hydrate within the coating, although increasing the post-treatment temperature dramatically increased the reaction kinetics, which produced similar morphologies and phases in much shorter times. These results provide strong evidence that the post-treatment processes are kinetically controlled and heavily

dependent on time and temperature. Subsequent CeCCs post-treated in a room temperature phosphate solution for up to four weeks showed corrosion performance comparable to samples post-treated at 85 °C for times greater than two minutes.

4. CONCLUSIONS

The duration and temperature of phosphate post-treatment affected the corrosion performance of CeCCs. Corrosion performance improved with longer immersion times, up to 10 min, and higher solution temperatures, up to 85 °C. As-deposited coatings exhibited pitting potentials near -435 mV(SCE) and charge transfer resistances of 8 kΩ cm^2, the lowest of all conditions examined in the study. As-deposited coatings also had the smallest passive region, ≈100 mV, compared to more than 300 mV for samples post-treated at higher temperatures and longer times. Post-treatment at 85 °C or for up to 10 minutes increased the pitting potential to about -250 mV(SCE), resulting in larger passivation regions (≥ 300 mV) and more noble potentials throughout the anodic sweep. The charge transfer resistance of CeCCs post-treated for up to ten minutes or at temperatures of at least 70 °C was greater than 60 kΩ cm^2, more than five times higher than an as-deposited coating. Potentiodynamic scans and EIS results correspond well to observed ASTM B117 corrosion performance since the largest charge transfer resistances and pitting potentials were measured for samples exhibiting the lowest density of pits and least tailing, these panels were post-treated at the highest temperatures and longest times. The formation of hydrated $CePO_4$ was observed for times of at least two minutes at 85 °C and for five minute treatments above 70 °C. Surface cracking seemed to be more strongly dependent on temperature than time, with higher temperature post-treatments

preventing much of the cracking observed in the as-deposited coating. However, post-treatment in a room temperature solution for at least one week also produced a similar morphology.

The processes active during post-treatment are kinetically controlled. This is evidenced by the improvement in corrosion performance for samples treated in a room temperature solution of $NH_4H_2PO_4$ for at least one week. XRD confirmed the presence of hydrated $CePO_4$ under these conditions and electron microscopy revealed reduced cracking compared to as-deposited coatings, indicating that high temperature is not required for transformation. Improved corrosion resistance from post-treatment is attributed to a combination of reduced cracking and the conversion of cerium oxide and hydroxides to hydrated $CePO_4$. Coatings in which hydrated $CePO_4$ was detected had the highest impedances and reduced cracking, which likely contributed to the corrosion resistance of the CeCC.

ACKNOWLEDGMENTS

The authors appreciated the support and guidance of Bruce Sartwell of the Strategic Environmental Research and Development Program (SERDP) and Donna Ballard of AFRL/MLLB. This project was funded by SERDP under Contract W912HQ-06-C-0030. Discussion and collaboration with John DeAntoni of Boeing is also acknowledged. The assistance of Eric Bohannan and Jeff Wight of the Materials Research Center at Missouri S&T is also appreciated.

REFERENCES

[1] J.G. Kaufman, Corrosion of Aluminum and Aluminum Alloys, *ASM Handbook*, Vol 13B, in ASM Handbooks Online http://products.asminternational.org/matinfo, ASM International, 2005.

[2] L. Roberts, A. Galanis, Nonchromated technology: Ready for prime time, Metal Finishing, 101 (2003) 36-39.

[3] C. Challener, Government coatings research: Fundamental to performance, J. Coatings Tech., 2 (2005) 32-36.

[4] R.G. Buchheit and A.E. Hughes, Chromate and Chromate-Free Conversion Coatings, ASM Handbook Vol 13A, in ASM Handbooks Online http://products.asminternational.org/matinfo, ASM International, 2003.

[5] B.R. W. Hinton, D.R. Arnott, N. E. Ryan, Cerium conversion coatings for the corrosion protection of aluminium, Met. Forum, 9 (1986) 162-173.

[6] M. Kendig, S. Jeanjaquet, Cr(VI) and Ce(III) inhibition of oxygen reduction on copper, J. Electrochem. Soc., 149 (2002) B47-B51.

[7] OSHA 29 CFR Part 1910.1026.

[8] B.R. Hinton, D.R. Arnott, N.E. Ryan, Inhibition of aluminum alloy corrosion by cerous cations, Met. Forum, 7 (1984) 211-217.

[9] M. A. Jakab, F. Presuel-Moreno, and J. R. Scully, Effect of molybdate, cerium, and cobalt ions on the oxygen reduction reaction on AA2024-T3 and selected intermetallics experimental and modeling studies, J. Electrochem. Soc., 153 (2006) B244-B252.

[10] M. Bethencourt, F.J. Botana, J.J. Calvino, M. Marcos, M.A. Rodríquez-Chacón, Lanthanide compounds as environmentally-friendly corrosion inhibitors of aluminium alloys: A review, Corr. Sci., 40 (1998) 1803-1819.

[11] A.K. Mishra, R. Balasubramaniam, Corrosion inhibition of aluminum alloy AA 2014 by rare earth chlorides, Corr. Sci., 49 (2007) 1027-1044.

[12] H. Ardelean, I. Frateur, P. Marcus, Corrosion protection of magnesium alloys by cerium, zirconium and niobium-based conversion coatings, Corr. Sci., 50 (2008) 1907-1918.

[13] C. Wang, F. Jiang, F. Wang, The characterization and corrosion resistance of cerium chemical conversion coatings for 304 stainless steel, Corr. Sci., 46 (2004) 75-89.

[14] A. Pardo, M.C. Merino, R. Arrabal, F. Viejo, M. Carboneras, J.A. Muñoz, Influence of Ce Surface treatments on corrosion behavior of A3xx.x/SiCp composites in 3.5 wt% NaCl, Corr. Sci., 48 (2006) 3035-3048.

[15] J.O. Stoffer, T. O'Keefe, S.P. Sitaram, P. Yu, X. Lin, E.L. Morris, U.S. Patent 5,932,083, issued Aug. 3, 1999.

[16] N. Birbilis and R.G. Buchheit, Electrochemical characteristics of intermetallic phases in aluminum alloys: An experimental survey and discussion, J. Electrochem. Soc., 152 (2005) B140-B151.

[17] F.H. Scholes, C. Soste, A.E. Hughes, S.G. Hardin, and P.R. Curtis, The role of hydrogen peroxide in the deposition of cerium-based conversion coatings, Appl. Surf. Sci., 253 (2006) 1770-1780.

[18] H. Zhang, Y. Zuo, The improvement of corrosion resistance of Ce conversion films on aluminum alloy by phosphate post-treatment, Appl. Surf. Sci., 254 (2008) 4930-4935.

[19] S. You, P. Jones, A. Padwal, P. Yu, M. O'Keefe, W. Fahrenholtz, T. O'Keefe, Response of nanocrystalline cerium-based conversion coatings on Al 2024-T3 to chloride environments, Mater. Lett., 61 (2007) 3778-3782.

[20] D.K Heller, W.G. Fahrenholtz, M.J. O'Keefe, The effect of phosphate source on the post-treatment of cerium based conversion coatings on Al 2024-T3 and its correlation to corrosion performance, ECS Trans., 16 (2009) 47.

[21] P.S. Jones, P. Yu, W.R. Pinc, M.J. O'Keefe, W.G. Fahrenholtz, and T.J. O'Keefe, Spray deposition of cerium oxide-based conversion coatings on Al 2024-T3, Int. J. Appl. Ceram. Tec., 5 (2008) 63-73.

[22] W.R. Pinc, S. Geng, M. O'Keefe, W. Fahrenholtz, and T. O'Keefe, Effects of acid and alkaline based surface preparations on spray deposited cerium based conversion coatings on Al 2024-T3, Appl. Sur. Sci., 255 (2009) 4061-4065.

[23] R.B.C. Cayless, Alloy and Temper Designation Systems for Aluminum and Aluminum Alloys, ASM Handbook Vol 2, in ASM Handbooks Online http://products.asminternational.org/matinfo, ASM International, 2002.

[24] Kaiser Aluminum, Certified Test Report Serial No. 4098982, Spokane, WA, 2007.

[25] X. Yu, G. Li, XPS study of cerium conversion coating on the anodized 2024 aluminum alloy, J. Alloy Compd., 364 (2004) 193-198.

[26] L. Qiu, F. Liu, L. Zhao, Y. Ma, J. Yao, Comparative XPS study of surface reduction for nanocrystalline and microcrystalline ceria powder, Appl. Surf. Sci., 252 (2006) 4931-4935.

[27] G. Wu, C. Wang, Q. Zhang, P. Kang, Characterization of Ce conversion coating on Gr-f/6061Al composite surface for corrosion protection, J. Alloy Compd., 461 (2008) 389-394.

[28] NIST XPS Database Version 3.5, http://srdata.nist.gov/xps/, (2007).

Table 1. Compositional limits of Al 2024 and reported actual chemistry as indicated by the manufacturer.

Element	Si	Fe	Cu	Mn	Mg	Cr	Zn	Ti	V	Zr	Other	Al
Alloy Limits (min/max)	0	0	3.8	0.3	1.2	0	0	0	0	0	0	Bal
	0.5	0.5	4.9	0.9	1.8	0.1	0.25	0.15	0.05	0.05	0.15	Bal
Actual	0.09	0.22	4.45	0.61	1.37	0.01	0.16	0.02	0.01	0	0.04	Bal

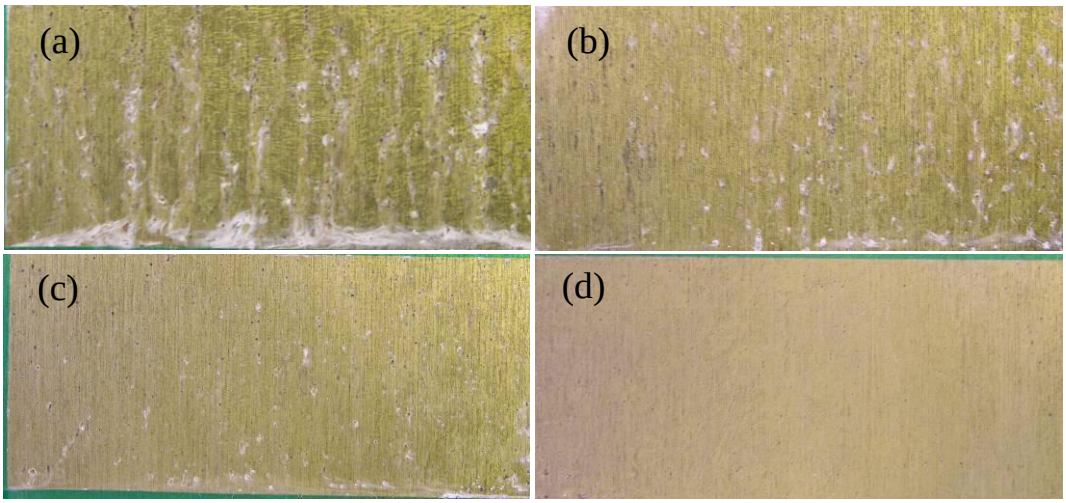

Figure 1. Optical images of CeCCs on Al 2024-T3 coupons measuring 3.8 cm x 7.6 cm after 14 days of salt spray exposure. The CeCCs were post-treated at different temperatures for 5 min, (a) as-deposited, (b) 55 °C, (c) 70 °C, and (d) 85 °C.

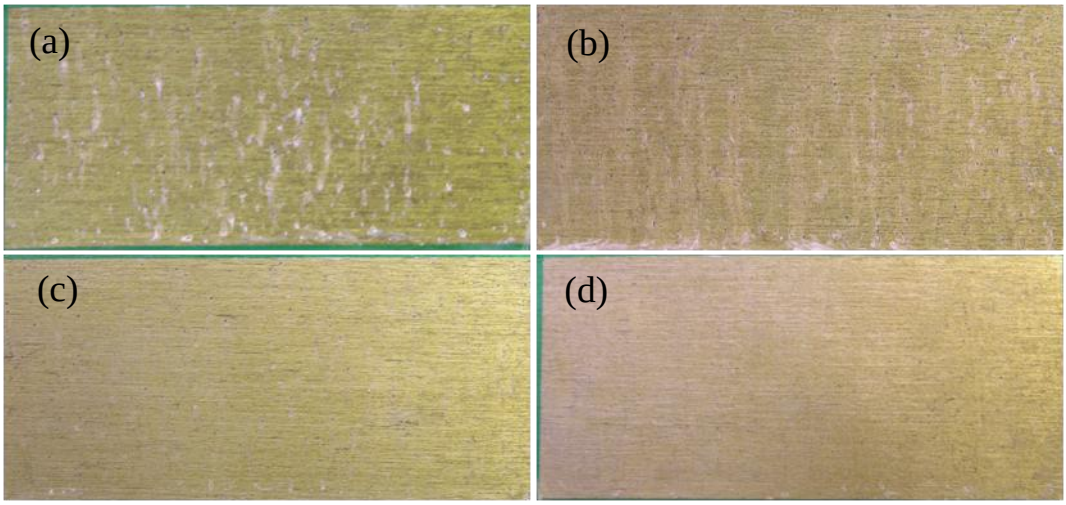

Figure 2. Optical images of CeCCs on Al 2024-T3 coupons measuring 3.8 cm x 7.6 cm after 14 days of salt spray exposure. The CeCCs were post-treated at 85 °C for (a) 10 sec, (b) 30 sec, (c) 2 min, and (d) 10 min.

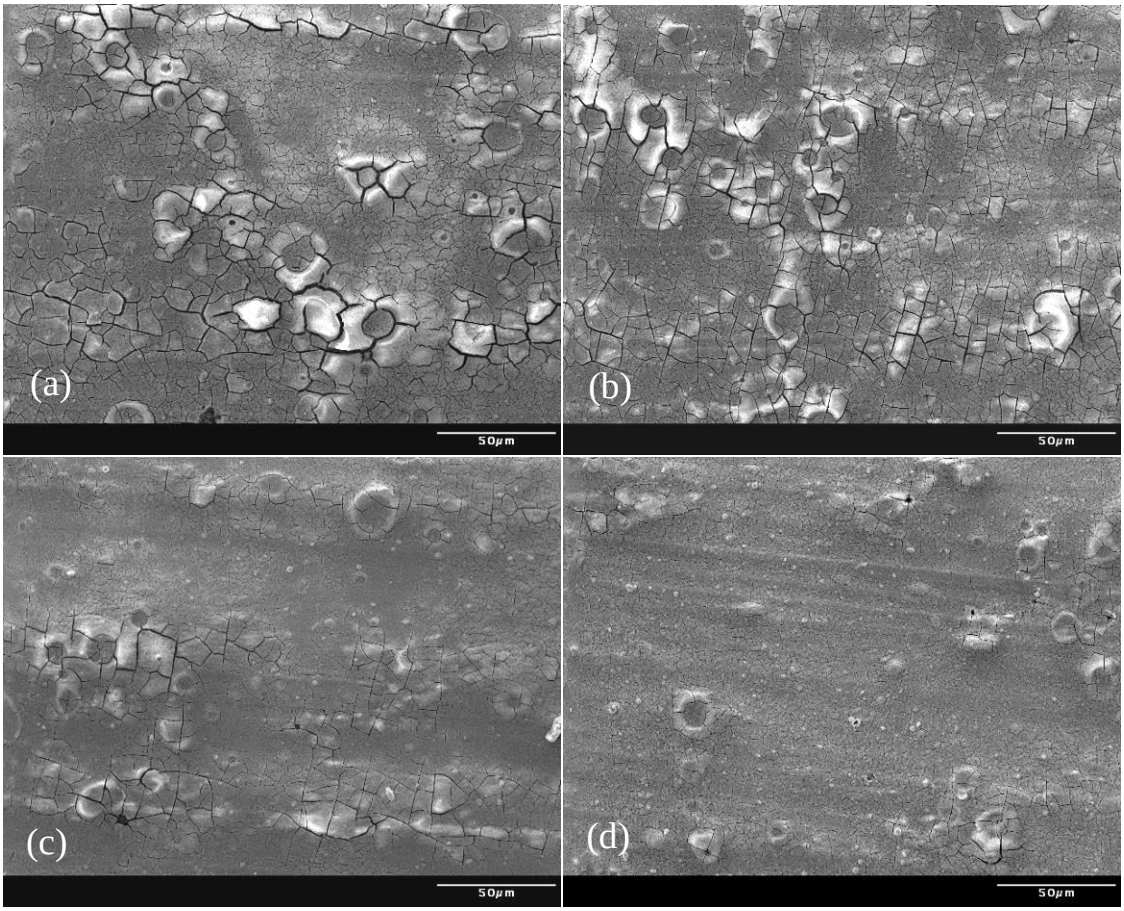

Figure 3. SEM micrographs of CeCCs post-treated for 5 min at different temperatures, (a) as-deposited, (b) 55 °C, (c) 70 °C, and (d) 85 °C. A reduction in surface cracking was evident as post-treatment temperature increased.

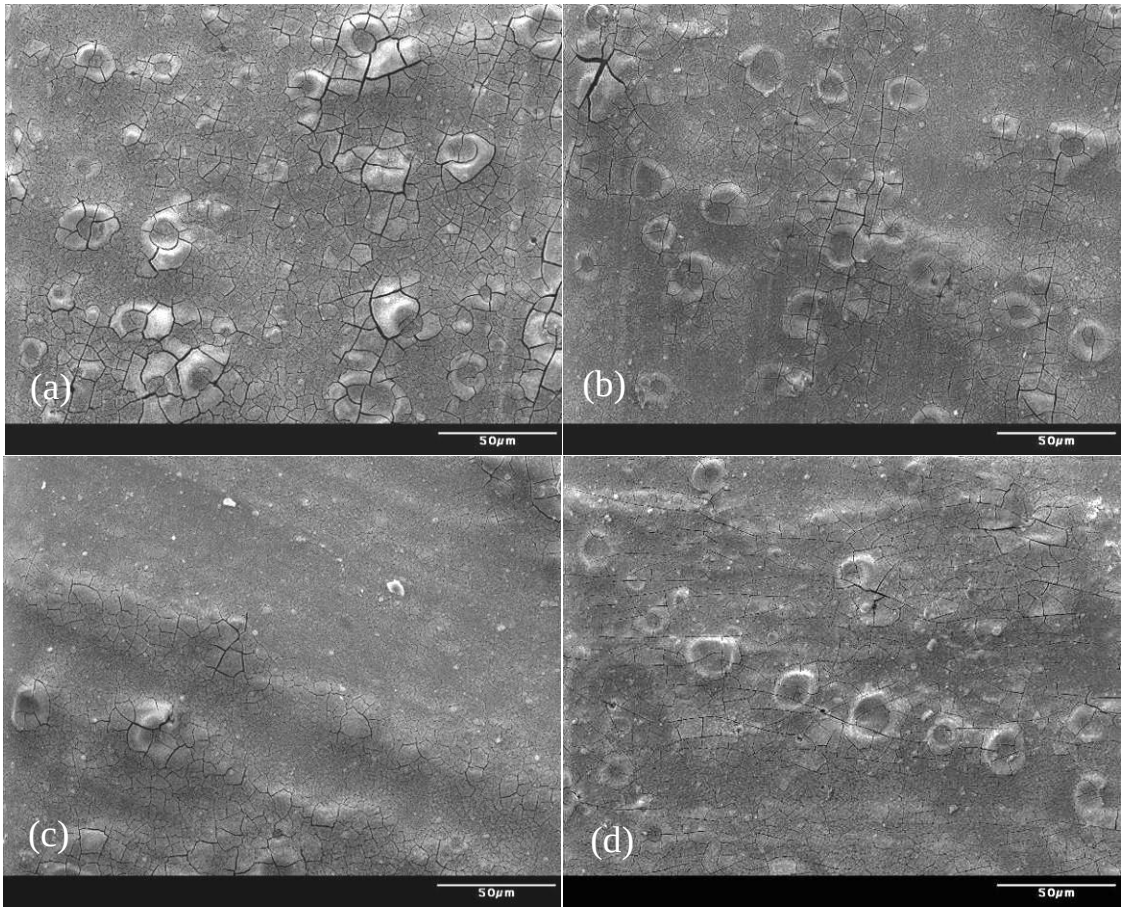

Figure 4. SEM images for CeCCs post-treated at 85°C for (a) 10 sec, (b) 30 sec, (c) 2 min, and (d) 10 min, showing decreased cracking with post-treatment times ≥ 30 sec.

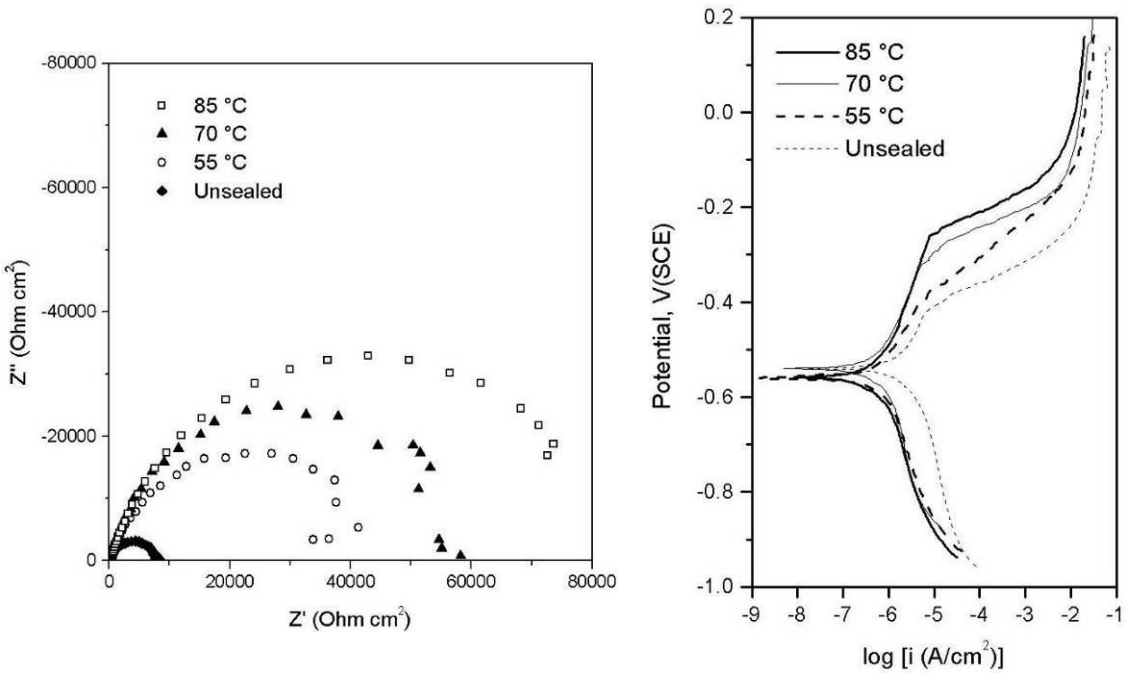

Figure 5. EIS spectra (left) showing higher coating impedance for samples treated at higher temperatures and potentiodynamic scans (right) illustrating the increased pitting potentials observed with higher post-treatment temperatures.

Table 2. Values obtained by fitting electrochemical data from CeCCs post-treated for different times at 85°C.

Condition	**Equiv. circuit model**	R_{ct} **(kΩ cm²)**	**FCP, mV(SCE)**	E_{pit}**, mV(SCE)**	**Passive Region (mV)**	i_{corr} **(μA/cm²)**
55 °C (5 min)	$R_s(Q_{coat}R_{ct})$	49	-559	-384	175	0.83
70 °C (5 min)	$R_s(Q_{ox}(R_p(Q_{dl}R_{ct})))$	63	-536	-320	216	0.66
85 °C (5 min)	$R_s(Q_{ox}(R_p(Q_{dl}R_{ct})))$	91	-558	-258	300	0.65

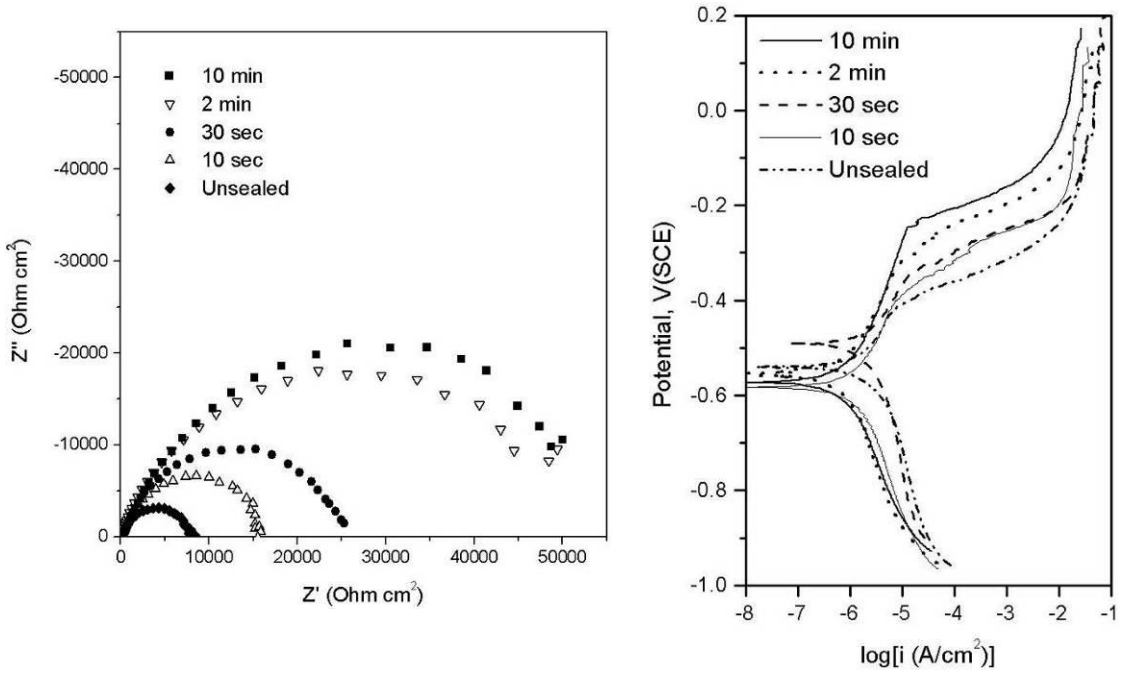

Figure 6. EIS spectra (left) illustrating the corresponding increase in coating impedance with respect to treatment time, and potentiodynamic scans (right) showing the increased passivation region observed as post-treatment time at 85°C was increased.

Table 3. Values obtained by fitting electrochemical data for CeCCs post-treated for 5 min at different temperatures.

Condition	**Equiv. circuit model**	R_{ct} **(kΩ cm²)**	**FCP, mV(SCE)**	E_{pit}, **mV(SCE)**	**Passive Region (mV)**	i_{corr} **(μA/cm²)**
Unsealed	$R_s(Q_{coat}R_{ct})$	8	-537	-435	102	1.50
10 sec (85 °C)	$R_s(Q_{coat}R_{ct})$	17	-578	-401	177	1.41
30 sec (85 °C)	$R_s(Q_{ox}(R_p(Q_{dl}R_{ct})))$	25	-492	-340	152	1.98
2 min (85 °C)	$R_s(Q_{ox}(R_p(Q_{dl}R_{ct})))$	52	-556	-329	227	0.84
10 min (85 °C)	$R_s(Q_{ox}(R_p(Q_{dl}R_{ct})))$	62	-582	-245	337	1.00

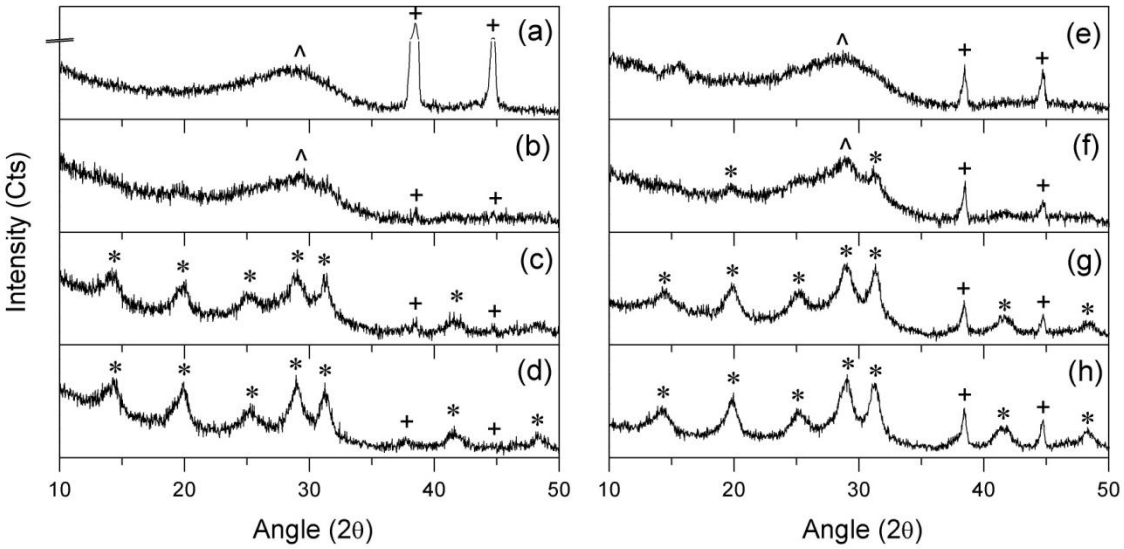

Figure 7. On the left, XRD spectra for (a) an as-deposited coating, and CeCCs post-treated for 5 min at (b) 55 °C, (c) 70 °C, and (d) 85 °C, showing the formation of hydrated $CePO_4$ for post-treatment temperatures ≥ 70°C. On the right, XRD spectra for (e) 10 sec, (f) 30 sec, (g) 2 min, and (h) 10 min post-treatment times at 85 °C, (*$CePO_4 \cdot H_2O$ PDF #35-0614, $^{\wedge}CeO_2$ PDF #43-1002, $^{+}$Aluminum PDF #04-0787).

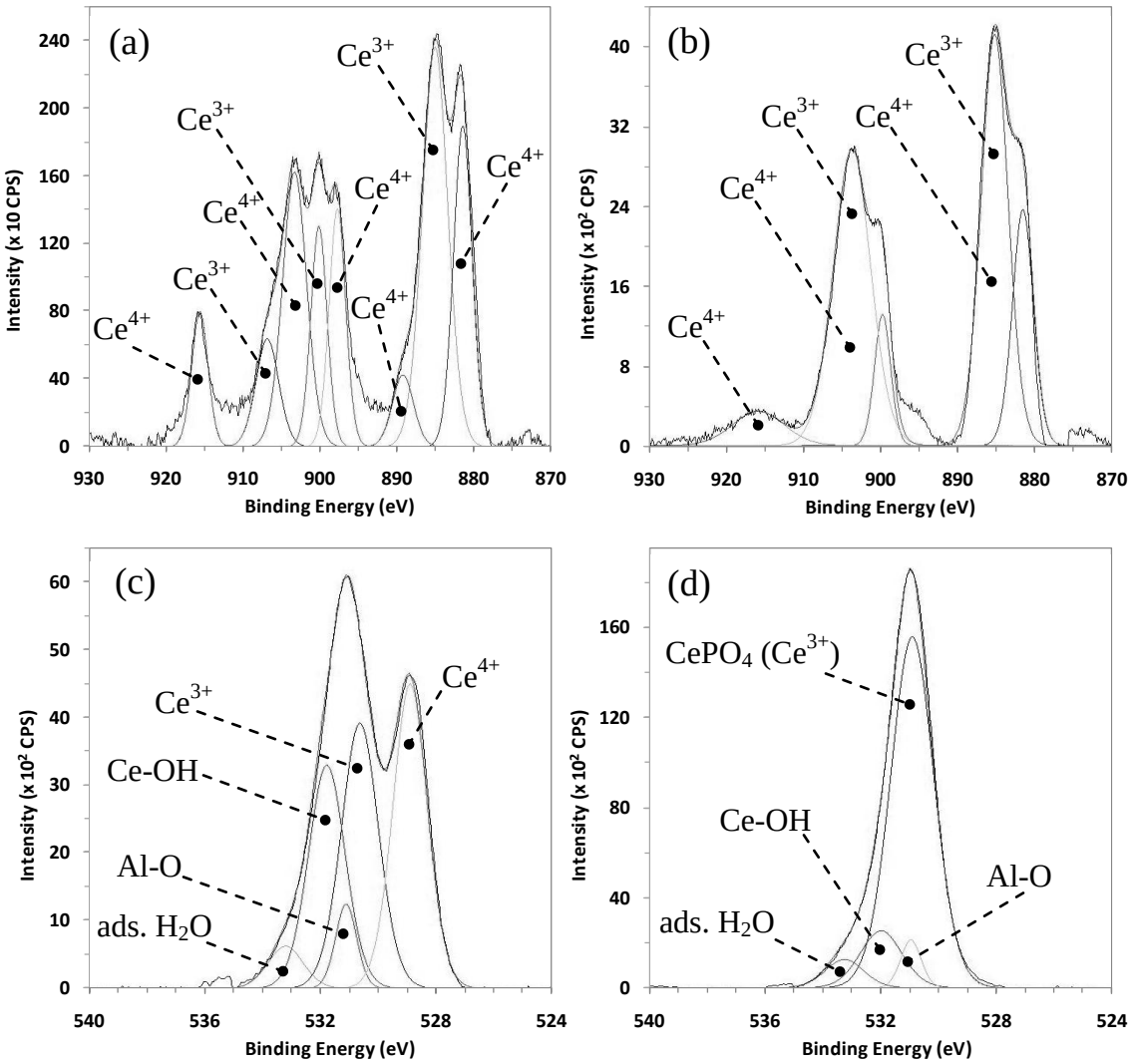

Figure 8. XPS spectra with respect to post-treatment time at 85°C, (a) Ce 3d of as-deposited CeCC, (b) Ce 3d after 10 minute post-treatment, (c) O 1s for an as-deposited CeCC and (d) O 1s after 10 minute post-treatment.

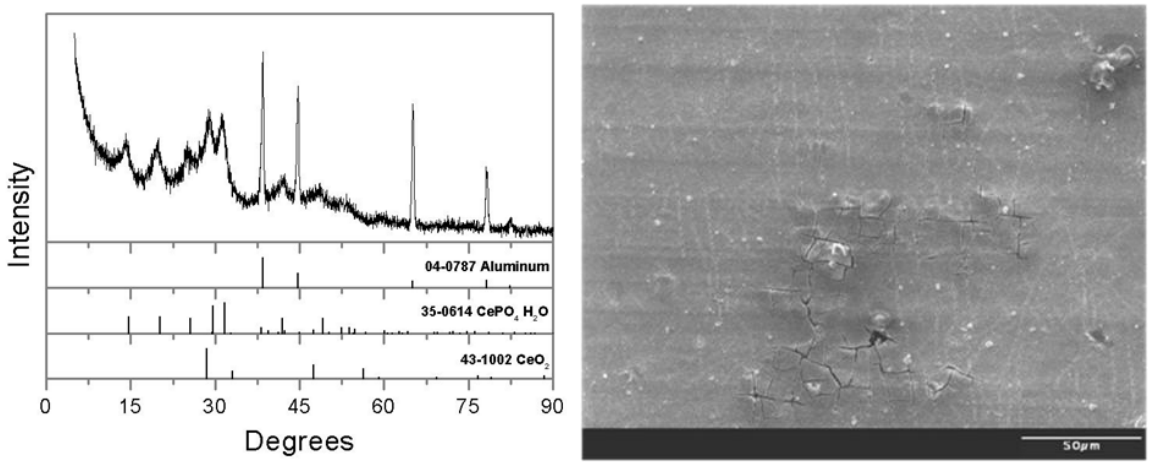

Figure 9. XRD pattern of a CeCC immersed in 2.5 wt% $NH_4H_2PO_4$ at room temperature for one week (left), and an SEM image of the coating surface (right) exhibiting less cracking than the as-deposited condition.

II. EFFECT OF PHOSPHATE SOURCE ON POST-TREATMENT OF CERIUM-BASED CONVERSION COATINGS ON Al 2024-T3

Daimon K Heller, William G. Fahrenholtz, Matthew J. O'Keefe

Materials Research Center, Department of Materials Science and Engineering,

Missouri University of Science and Technology, Rolla, MO 65409, USA

ABSTRACT

The surface morphology, electrochemical characteristics, and salt spray corrosion performance were studied for cerium-based conversion coatings on Al 2024-T3 that were post-treated in heated aqueous solutions of orthophosphate, pyrophosphate, and polyphosphate compounds. Phosphate post-treatment reduced cracking in the coatings, which resulted in better corrosion protection compared to coatings that were highly cracked or contained other defects. In addition, post-treatment in orthophosphate solutions converted the as-deposited hydrated cerium oxide to hydrated $CePO_4$, which further improved corrosion protection. Electrochemical analyses showed that cerium-based conversion coatings that contained hydrated cerium phosphate after post-treatment had the highest resistance (~100 $k\Omega$-cm^2), most noble pitting potentials (~ -270 mV), and best corrosion protection of the post-treatments that were tested. While pyrophosphate and polyphosphate post-treatments reduced cracks in the coatings, they did not promote formation of hydrated cerium phosphate. The results suggest that the corrosion

protection of cerium-based conversion coatings on Al 2024-T3 is dependent on both the surface morphology and phase of the coating.

INTRODUCTION

High strength aluminum alloys such as Al 2024-T3 and Al 7075-T6 are widely used for military and commercial aerospace applications. However, these alloys are susceptible to localized corrosion from the galvanic potential created between the alloy matrix and the intermetallic particles responsible for the increased strength of the alloys.[1,2,3,4] Chromate conversion coatings (CCCs) are commonly used to protect these alloys from corrosion and to improve the adhesion of subsequent organic coatings. Chromated coatings provide protection by controlling the kinetics of the oxygen reduction reaction occurring at local cathodes within the alloy matrix.[5,6] These coatings are believed to protect by the transport of Cr^{6+} ions to sites of active corrosion on the substrate where the Cr^{6+} ions are reduced, forming an insoluble Cr^{3+} oxide film.[7,8,9] While providing excellent corrosion protection, chromated coatings contain hexavalent chromium, which is known to be toxic and carcinogenic.[10] Additionally, recent regulations have increased the restrictions on the use and handling of chromates, which increases the life-cycle costs associated with the application, maintenance, and removal of chromated coatings.[11]

Cerium-based conversion coatings (CeCCs) are a possible alternative to CCCs.[12,13] Coatings containing rare earth elements, particularly cerium, have shown the ability to provide corrosion protection to high strength aluminum alloys in saline environments.[14,15] Investigations examining the efficacy of using cerium containing

films for the corrosion protection of other substrates including tinplate, zinc, and select metal matrix composites have been published.[16,17,18] Similar to chromated coatings, CeCCs are thought to inhibit the oxygen reduction reaction by providing ions that selectively precipitate onto cathodic sites (i.e., Cu-rich intermetallics).[9,19] The deposition mechanism arises from an increase in the near surface pH when the coating solution contacts the substrate, this results in precipitation of cerium peroxide/hydroxide compounds that decompose over time into hydrated cerium oxide ($CeO_2 \cdot 2H_2O$). Electrolytic, immersion, and spray techniques can be used to deposit CeCCs with different surface morphologies and corrosion resistances. All CeCCs are environmentally benign, eliminating the increased cost and environmental risks incurred by using chromated coatings.[20,21,22,23]

The corrosion protection provided by CeCCs is sensitive to deposition process parameters. Surface preparation prior to coating and the chemistry of the coating solution both impact the deposition rate, morphology, and corrosion resistance of CeCCs.[24,25,26] Previous studies have shown that one method to improve the corrosion protection of CeCCs is by post-treatment in a heated phosphate solution, which is referred to as sealing.[27,28] Zhang et al. examined the effect of post-treating electrodeposited CeCCs in a Na_3PO_4 solution, noting the formation of hydrated cerium phosphate ($CePO_4 \cdot H_2O$) and decreased cracking.[29] However, the effect of post-treatment conditions on corrosion performance and coating morphology has not been addressed in the literature.

The purpose of this study was to characterize the effect of phosphate source on the post-treatment of CeCCs, including corrosion performance, surface morphology, and electrochemical response. To collect these data, CeCCs were deposited on Al 2024-T3

coupons using a spontaneous spray deposition process and post-treated in heated solutions containing various phosphate sources, including Na_3PO_4, $NH_4H_2PO_4$, $Na_2H_2P_2O_7$, $K_4P_2O_7$, or $Na_5P_3O_{10}$. The surface morphology of the post-treated coatings was analyzed using scanning electron microscopy (SEM) and the crystalline phases of the coatings were characterized with x-ray diffraction (XRD) analysis. The coatings were also characterized using electrochemical impedance spectroscopy (EIS) and potentiodynamic scans.

EXPERIMENTAL

Prior to coating deposition, the substrates were first subjected to cleaning and surface activation processes. Coupons measuring 3.8 cm x 7.6 cm were cut from a sheet of Al 2024-T3 (AMI Metals) that was 0.81 mm thick. First, coupons were wiped with an acetone-soaked laboratory wiper, rinsed with tap water, and immersed for 5 min in an aqueous solution containing 5.0 wt% solution of an alkaline cleaner (Turco 4215 NCLT) that was heated to 55 °C. The panels were then rinsed with deionized water and placed in a 1.0 wt% sulfuric acid bath at 50 °C for 10 min. After the coupons were rinsed with deionized water, CeCCs were spray deposited from an aqueous solution (composition given below) using five spray cycles. Each cycle consisted of misting the solution onto the panel for ~3 sec and then allowing the solution to drain off of the panel for ~35 sec. After five spray cycles, the panels were rinsed with deionized water. A Husky Model 515-547 detail spray gun was used for spray deposition using an air pressure of ~35 psi.

The spray solution was prepared by first making a stock solution consisting of 780 g deionized water and 40 g $CeCl_3 \cdot xH_2O$ (Alfa Aesar, 99.9%). The stock solution

was adjusted to a pH of 2.07 by adding dilute hydrochloric acid. To prepare the spray solution, 0.8 g of gelatin (Rousselot, DSF) was dissolved in 25 g of deionized water. Then, the gelatin solution and 20 ml of H_2O_2 (Fisher Scientific, 30%) were added to 205 g of stock solution and mixed with a magnetic stirrer.

After CeCC deposition, the panels were post-treated for 5 min by immersion in an aqueous solution containing 2.5 wt% Na_3PO_4, $NH_4H_2PO_4$, $Na_2H_2P_2O_7$, $K_4P_2O_7$, or $Na_5P_3O_{10}$ heated to 85 °C. In each case the post-treatment solution pH was adjusted to 4.4 by adding appropriate quantities of phosphoric acid or sodium hydroxide (Table 1). After post-treatment, the panels were again rinsed with deionized water and allowed to dry in the ambient laboratory environment for at least 24 hours prior to salt spray testing or chemical and physical analyses.

Corrosion performance was evaluated by salt spray testing using a Q-FOG cyclic corrosion tester (Q-Panel Lab Products) with 5 wt% NaCl solution according to the specifications in ASTM B117. Based on military performance requirements for conversion coatings such as those described in MIL-DTL-81706, the goal for the CeCCs is to prevent the formation of corrosion pits and salt tails for 2 weeks (336 hours) of salt spray exposure.

The surface morphology of the coatings was examined using electron microscopy, which was conducted with a Hitachi S-570 SEM with a LaB_6 electron source at an accelerating voltage of 12 kV. Grazing incidence XRD was used to determine the crystalline phases present in the coatings. Patterns were collected from 5 to 90 degrees two theta using a Phillips X-Pert Diffractometer with a Cu-Kα x-ray source. Electrochemical impedance spectroscopy (EIS) was used to measure the capacitance and

impedance characteristics of the coatings. Analysis was performed using a Schlumberger model SI1255 frequency response analyzer from $6x10^{-3}$ to $1x10^{5}$ Hz using an AC amplitude of 10 mV. Potentiodynamic scans were collected at 1.5 mV/s from -0.4 to +0.7 V with respect to open circuit potential using a model 273A potentiostat from Princeton Applied Research. For each condition, the cell was allowed to stabilize for 1500 seconds before data were recorded and three to five tests were performed to establish reproducible behavior. A Princeton Applied Research model K0235 Flat Cell was used with an electrolyte composition of 0.6 wt% NaCl + 0.6 wt% $(NH_4)_2SO_4$ in deionized water. Electrochemical analysis was performed with a less aggressive electrolyte with respect to the salt spray tests because it was found that this composition resulted in data with the highest level of detail, exhibiting subtleties that were overpowered when more concentrated NaCl solutions were used. Tests performed with more aggressive electrolytes (up to 3.5 wt% NaCl) made differentiation of sample treatments and prediction of salt spray corrosion performance impossible. In contrast, the selected electrolyte repeatedly showed consistent differences in the measured R_{ct}, $i_{corr,}$ and E_{pit} values between the different coating treatments. These values were found to correspond well to salt spray corrosion performance. The sample area tested was 1.0 cm^2 and a saturated calomel electrode was used in all tests. Corrware (Scribner Associates) data acquisition software was used to control the electrochemical tests and data fitting was performed using complementary programs CView and ZView.

RESULTS AND DISCUSSION

Salt spray corrosion testing of the panels showed that corrosion performance of CeCCs on Al 2024-T3 varied as a function of the phosphate solution used during post-treatment, as shown optically in Figure 1. These images illustrate the range of corrosion performance observed with respect to the phosphate salt used to produce the post-treatment solution. Observations of corroded panels indicated that the as-deposited CeCC (Figure 1f) exhibited many pits and large salt tails after 14 days of salt spray exposure. The panels post-treated in the polyphosphate solution (2.5 wt% $Na_5P_3O_{10}$, Figure 1e) performed the worst among the phosphate sources tested and decreased the corrosion protection compared to the as-deposited coating. The panels treated in this solution showed salting on almost the entire panel surface after only four days of salt spray testing. In contrast, panels sealed with orthophosphate-based solutions (*i.e.*, $NH_4H_2PO_4$ and Na_3PO_4, Figure 1a & 1b) had just a few pits and some minor salt tailing after 14 days of salt spray exposure. Post-treatment in pyrophosphate solutions (*i.e.*, $K_4P_2O_7$ and $Na_2H_2P_2O_7$, Figure 1c & 1d) provided corrosion performance that was between that of the polyphosphate and orthophosphate treatments. The sample sealed with 2.5 wt% $Na_2H_2P_2O_7$ had numerous pits and significant salting after 14 days of salt spray exposure. The $K_4P_2O_7$ treatment resulted in better corrosion performance than the 2.5 wt% $Na_2H_2P_2O_7$ treatment, but after 14 days of exposure the panel had more pits and salt tails than either of the orthophosphate treatments. These initial observations suggested that the type of phosphate salt used to produce the post-treatment solution (*i.e.* orthophosphate, pyrophosphate, or polyphosphate) affected corrosion performance.

The effect of an orthophosphate treatment on bare Al 2024-T3 substrates and substrates that underwent the cleaning and activation process but did not receive a CeCC treatment were evaluated with salt spray testing and Auger electron spectroscopy (AES) depth profiling. It was found that the extent of corrosion on the substrate surface was comparable to that of an as received Al 2024-T3 panel after equal duration salt spray exposure, indicating that corrosion performance of an uncoated Al 2024-T3 substrate was not improved by the phosphate treatment. Data collected from AES analyses did not reveal the presence of a phosphorous rich film on the surface of the panel (less than one atomic percent detected). These experiments suggest that the improved corrosion resistance observed after phosphate post-treatment was a result of modification to the cerium-based coating and not from a reaction occurring between the phosphate solution and alloy substrate via defects in the coating.

SEM micrographs of the surfaces of representative coatings were taken for each phosphate post-treatment as well as from an as-deposited (unsealed) coating (Figure 2). The unsealed CeCCs were dominated by large, highly cracked regions. A CeCC that had fewer cracks that were much finer would be expected to be a more effective barrier to corrosion by limiting the access of attacking species to the underlying metal substrate. All phosphate post-treatments resulted in a reduction in surface cracking compared to the unsealed condition. However, the coatings post-treated in $Na_5P_3O_{10}$ and $Na_2H_2P_2O_7$ solutions had defects that resembled craters (circled in Figure 2d & 2e) that were not observed for any other panels that had been post-treated. These defects were prevalent in coatings that underwent the polyphosphate post-treatment and may help explain the poor corrosion performance observed for CeCCs post-treated with those solutions. While

inhibiting cracking seemed to improve the corrosion performance of CeCCs, as long as the coating was not compromised with other defects, elimination of cracking alone does not guarantee good corrosion protection. This is illustrated by the panels that were sealed in the pyrophosphate solutions. These panels had reduced levels of cracking and improved corrosion performance compared to unsealed coatings, but did not provide the same level of corrosion protection observed from panels post-treated with orthophosphate solutions.

Grazing incidence XRD was used to characterize the crystalline phases present in the CeCCs. Figure 3 shows XRD patterns for CeCCs post-treated in solutions produced from each of the phosphate sources. The broad peak centered at ~30° two theta was observed for panels post-treated in pyrophosphate and polyphosphate solutions as well as the as-deposited coating. This peak was consistent with the presence of nanocrystalline hydrated CeO_2 (PDF #43-1002) formed during the deposition process (Figure 3c – 3f).[26] Hence, post-treatment in pyrophosphate or polyphosphate solutions had no apparent effect on the crystalline phase present in the coatings. Analysis revealed that $CePO_4 \cdot H_2O$ (Rhabdophane, PDF #35-0614) was formed only after treatment in orthophosphate-based solutions (Figure 3a & 3b). In addition, salt spray testing showed that CeCCs subjected to post-treatment in either of the orthophosphate solutions provided the best corrosion protection. Combined with the SEM results discussed above, the XRD data suggested that the formation of the hydrated $CePO_4$ phase alone was not responsible for the reduction in cracking, but appeared to contribute to the enhanced corrosion performance exhibited by these coatings. Hence, a combination of coating surface morphology (fine

cracks) and crystalline phase ($CePO_4 \cdot H_2O$) was associated with improved corrosion performance during salt spray testing.

Electrochemical impedance spectroscopy revealed that coatings post-treated in orthophosphate-based solutions had higher charge transfer resistances (> 90 $k\Omega\text{-}cm^2$) than as-deposited coatings or coatings post-treated in other solutions (Figure 4 and Table 2). Further comparison with Figure 1 indicated a strong correlation between salt spray corrosion performance and charge transfer resistance (R_{ct}), i.e. better salt spray corrosion performance was observed for panels with a higher charge transfer resistance. These coatings were able to inhibit corrosion for up to two weeks in salt spray testing. The as-deposited (unsealed) and polyphosphate treated conditions had the lowest R_{ct}, < 8 $k\Omega\text{-}cm^2$. Likewise, these coatings had the poorest performance in salt spray testing, with both showing significant pitting and salt tailing within four days. The measured R_{ct} of coatings post-treated in pyrophosphate solutions was 35 to 40 $k\Omega\text{-}cm^2$, which was between the values recorded from CeCCs post-treated in orthophosphate or polyphosphate solutions. The performance in salt spray was also between those observed for the other coatings. Hence, the charge transfer resistance determined by EIS was able to predict the performance in salt spray testing in that coatings with higher R_{ct} had better salt spray performance.

More detailed analyses of the impedance spectra for unsealed panels revealed only one semicircle whereas panels post-treated in orthophosphate solutions clearly exhibit two semicircles (inset in Figure 4). This trend is further highlighted by examining the Bode plots (Figure 5). The Bode magnitude and phase plots emphasize the similarities between the responses observed from panels treated with the same type of

phosphate and more clearly demonstrates the transition from a system modeled with one time constant (unsealed, Figure 5a) to a system that must be fit with a two time constant model (orthophosphates, Figure 5c). The Bode phase plot for the unsealed and polyphosphate samples exhibit one maximum along the curve, while orthophosphate post-treatments exhibit two maxima, indicative of two time constants. A higher quality coating, or one with minimal defects, should exhibit a phase shift across the frequency spectrum and extend to low frequencies. At 10^{-2} Hz, the phase shift of the polyphosphate and unsealed conditions drops to zero, exhibiting poorer low frequency characteristics compared to orthophosphate post-treatments, which exhibit a phase shift of approximately -25 degrees at 10^{-2} Hz. Consistent with previous analysis, the behavior of panels post-treated in pyrophosphate solutions lies in between that of panels post-treated in orthophosphate solutions and the unsealed CeCC.

To better understand the effect of post-treatment, the electrochemical data were fit to equivalent circuit models and then compared to other physical and chemical characteristics of the coatings. Because of the change in behavior evident in the EIS analysis between the highly cracked unsealed coating and the finely cracked coatings produced by post-treatment in orthophosphate solutions, two models with corresponding physical representations are proposed. The as-deposited coating was highly cracked, exhibited poor salt spray corrosion performance, and the EIS data could be fit to one semicircle with a single associated time constant. Based on the combined analysis, the cracks in the coating dominated the behavior of the system. The cracks increased the probability that active sites vulnerable to corrosion were exposed through the coating, giving the electrolyte solution access to and from the coating substrate and providing a

direct path for both charge and mass transfer to occur. This situation was modeled by the equivalent circuit and physical representation shown in Figure 6a. For this case, the resistance and capacitance (modeled as a constant phase element) were attributed to that of the double layer capacitance at the electrolyte-substrate interface and its associated charge transfer resistance.

In contrast, CeCCs post-treated in orthophosphate solutions had relatively few, fine cracks, exhibited excellent salt spray corrosion performance, and EIS analysis confirmed the presence of two semicircles with associated time constants. In this case, the system was modeled as shown in Figure 6b and the coating was considered to dominate the corrosion resistance. In this model, the coating resistance and capacitance were included in addition to the resistance and capacitance of the double layer formed at the solution-substrate interface. Because cracks in the coating were sparse and very small, the electrolyte had a much smaller area for charge and mass transfer processes to occur directly with the substrate, which would reduce the probability that active sites were exposed to the external environment by cracks.

The behavior of the coatings post-treated in polyphosphate solutions most closely matched that of the unsealed, highly cracked condition. The quantity and size of the defects present in the unsealed coatings provided many sites for corrosion to occur, resulting in a completely salted surface after four days of salt spray testing. Coatings post-treated in pyrophosphate solutions again exhibited behavior in between that of the unsealed CeCCs and coating post-treated in orthophosphate solutions. These treatments were modeled using the fine crack model to calculate a value of the coating resistance, but comparable values were also obtained by using the large crack model. Values

calculated by fitting experimental data to the models described above are reported in Table 2. Coatings post-treated in orthophosphate solutions had the highest coating resistances (R_{coat}) near 200 Ω-cm^2, more than 100 Ω-cm^2 larger than panels post-treated with pyrophosphate and polyphosphate solutions. Orthophosphate post-treatment imparted a charge transfer resistance (R_{ct}) > 90 kΩ-cm^2 whereas all other post-treatments exhibit an $R_{ct} \leq 40$ kΩ-cm^2. The values also correlated well with salt spray corrosion testing as panels with higher R_{coat} and R_{ct} showed better corrosion resistance in salt spray testing.

Coatings that did not protect well, exemplified by the as-deposited (unsealed) samples, exhibited a high density of regions with large cracks or other defects. Unsealed CeCCs had the lowest combined and charge transfer resistances and performed poorly in salt spray corrosion testing. In this case, only double layer effects between the solution and metal substrate needed to be considered to accurately fit the data. The coating properties need not be considered as the response is believed to be dominated by the direct corrosive attack of the substrate that was exposed to the electrolyte in the cracked areas. In contrast, coatings that showed good corrosion protection had a lower density of large cracked regions and are instead dominated by regions of fine cracks (Figure 2) that reduced the area of the substrate exposed to the electrolyte. Accurately fitting the measured data from these samples required considering the electrochemical contribution of the coating and the double layer formed between the electrolyte and alloy substrate. The Nyquist and Bode plots indicated a change in behavior from one time constant (for as-deposited coatings) to two time constants as the post-treatment conditions became more effective at increasing the corrosion performance.

Potentiodynamic scans also provided insight into the protective capacity of CeCCs and the dependence on post-treatment. Data collected from panels sealed with each of the phosphate sources as well as an unsealed panel are shown as Figure 7. The anodic passivation regions were dependent on post-treatment. The pitting potential (E_{pit}) is a measure of stress (*i.e.*, applied voltage) that can be applied before a coating begins to breakdown. As seen in Figure 7, CeCCs that were post-treated and did not exhibit crater-like defects (i.e., post-treated in $NH_4H_2PO_4$, Na_3PO_4, or $K_4P_2O_7$ solutions, Fig. 1a – 1c) had similar pitting potentials, about -270 mV. The coatings post-treated in orthophosphate solutions maintained more noble potentials throughout the anodic sweep. Coatings that were highly cracked, such as unsealed CeCCs, or coatings that had crater-like defects, such as coatings post-treated in $Na_2H_2P_2O_7$ or $Na_5P_3O_{10}$ solutions, had lower pitting potentials (< -320 mV), indicating that these coatings were not as resistant to corrosive attack. These coatings exhibited a smaller passivation region when compared to the CeCCs post-treated in orthophosphate or $K_4P_2O_7$ solutions. As reported in Table 3, the calculated pitting potential and corrosion current (i_{corr} obtained by Tafel fit) correlated well to salt spray corrosion tests and reported EIS data. Samples with a lower i_{corr} and higher pitting potential exhibited the best corrosion protection in salt spray testing. Coatings post-treated in orthophosphate solutions again showed the best characteristics, having the largest passivation regions, highest pitting potentials (> -260 mV), and lowest corrosion currents (< 0.60 μA/cm^2). While the coatings post-treated in $K_4P_2O_7$ solutions showed potentiodynamic characteristics comparable to the orthophosphate samples (i_{corr} = 0.74 μA/cm^2, E_{pit} = -275 mV), those coatings did not exhibit comparable corrosion protection because the combined resistance was about 50% of the value measured for the

coatings post-treated in orthophosphate solutions. The significant increase in total resistance for the orthophosphate post-treated CeCCs was likely due to the formation of the hydrated $CePO_4$ phase during the post-treatment process.

CONCLUSIONS

Post-treatment of spray deposited CeCCs on Al 2024-T3 in 2.5 wt% solutions of $NH_4H_2PO_4$, Na_3PO_4, $K_4P_2O_7$, $Na_2H_2P_2O_7$, and $Na_5P_3O_{10}$ showed that corrosion performance depends on phosphate source. Salt spray corrosion testing correlated well with electrochemical data and showed a wide range of corrosion protection, from panels with a completely salted surface (e.g., $Na_5P_3O_{10}$ solution) to panels which exhibited a few small pits with tails only visible under magnification (e.g., Na_3PO_4 and $NH_4H_2PO_4$). Electron microscopy indicated that post-treated CeCCs had less cracking than as-deposited coatings in all cases, but defects in the coatings were observed for CeCCs post-treated in solutions of $Na_5P_3O_{10}$ or $Na_2H_2P_2O_7$, resulting in poor corrosion performance, small electrochemical resistance (6 and 34 $k\Omega\text{-}cm^2$ respectively), and a smaller passivation region with lower pitting potentials (≈ -320 to -340 mV). CeCCs post-treated with a solution of orthophosphate species exhibited the least salting, showed the largest resistances (> 90 $k\Omega\text{-}cm^2$) with more noble pitting potentials (≈ -260 to -280 mV) and maintained the most noble potentials throughout the anodic sweep. The formation of hydrated $CePO_4$ was evident only after orthophosphate post-treatments and may explain why the measured total resistance of the orthophosphate post-treated CeCCs was more than two times that of the $K_4P_2O_7$ post-treated panel (> 92 $k\Omega\text{-}cm^2$ to 40 $k\Omega\text{-}cm^2$ respectively). The $K_4P_2O_7$ treated panels did not form $CePO_4{\cdot}H_2O$, but did exhibit

reduced cracking and a potentiodynamic response similar to the orthophosphate post-treated panels. The results indicate that both the crystalline phase and morphology of coatings are strong factors in determining the ability of CeCCs to inhibit corrosive attack.

ACKNOWLEDGMENTS

The support and guidance of Bruce Sartwell of the Strategic Environmental Research and Development Program (SERDP) and Donna Ballard of AFRL/MLLB was appreciated by the authors. This project was funded by SERDP under Contract W912HQ-06-C-0030. Discussion and collaboration with John DeAntoni of Boeing and Ben Curatolo of Light Curable Coatings is also acknowledged. The assistance of Eric Bohannan of the Materials Research Center at Missouri S&T was also appreciated.

REFERENCES

1. J. G. Kaufman, *ASM Handbook*, p. 95, *ASM International* (2005).

2. N. Dimitrov, J. A. Mann, and K. Sieradzki, *J. Electrochem. Soc.*, **146**(1), 98-102 (1999).

3. M. A. Jakab, F. Presuel-Moreno, and J. R. Scully, *J. Electrochem. Soc.*, **153**(7), B244-B252 (2006).

4. N. Birbilis and R. G. Buchheit, *J. Electrochem. Soc.*, **152**(4), B140-B151 (2005).

5. W. J. Clark, J. D. Ramsey, R. L. McCreery, G. S. Frankel, J. Electrochem. Soc., **149**(5), B179-B185 (2002).

6. M. Kendig and C. Yan, J. Electrochem. Soc., **151**(12), B679-B682 (2004).

7. L. Xia, E. Akiyama, G. Frankel, and R. McCreery, *J. Electrochem. Soc.*, **147**, 2556 (2000).

8. M. Kendig, S. Jeanjaquet, R. Addison, J. Waldrop, *Surf. Coat. Technol.*, **140**, 58-66 (2001).

9. J. Zhao, L. Xia, A. Sehgal, D. Lu, R. L. McCreery, G. S. Frankel, *Surf. Coat. Technol.*, **140**, 51-57 (2001).

10. Agency for Toxic Substances and Disease Registry (ATSDR), Toxicological profile for Chromium, (2008).

11. OSHA 29 CFR Part 1910.1026

12. S. M. Cohen, *Corrosion Engineering*, **51**(1), 71-78 (1995).

13. R. L. Twite and G. P. Bierwagen, *Progress in Organic Coatings*, **33**, 91-100 (1998).

14. B. R. Hinton, D. R. Arnott, and N. E. Ryan, *Met. Forum*, **7**, 211 (1984).

15. M. Bethencourt, F. J. Botana, J. J. Calvino, M. Marcos, M. A. Rodriquez-Chacoń, *Corr. Science*, **40**(11), 1803 (1998).

16. N. Mora, E. Cano, J. L. Polo, J. M. Puente, J. M. Bastidas, *Corrosion Science*, **46**, 563-578 (2004).

17. K. Aramaki, *Corr. Science*, **46**, 1565-1579 (2004).

18. A. Pardo, M. C. Merino, R. Arrabal, F. Viejo, and M. Carboneras, *J. Electrochem. Soc.*, **153**(2), B52-B60 (2006).

19. A. Kolics, A. S. Besing, P. Baradlai, and A. Wieckowski, *J. Electrochem. Soc.*, **150**(11), B512-B516 (2003).

20. B. R. Hinton, D. R. Arnott, and N. E. Ryan, *Met. Forum*, **9**, 162 (1986).

21. P. S. Jones, P. Yu, W. R. Pinc, M. J. O'Keefe, W. G. Fahrenholtz, and T. J. O'Keefe, *Int. J. Appl. Ceram. Technol.*, **5**(1), 63 (2008)

22. J. Stoffer, T. O'Keefe, S. P. Sitaram, P. Yu, X. Lin, E. L. Morris, U.S. Patent 5,932,083, issued Aug. 3, 1999.

23. W. G. Fahrenholtz, M. J. O'Keefe, H. Zhou, J. T. Grant, *Surf. Coat. Technol.*, **155**, 208 (2002).

24. W. Pinc, S. Geng, M. J. O'Keefe, W. Fahrenholtz, T. O'Keefe, *Appl. Surf. Sci.*, **255**, 4061-4065 (2009).

25. B. Y. Johnson, J. Edington, M. J. O'Keefe, *Materials Science and Engineering*, **A361**, 225-231 (2003).

26. F. H. Scholes, C. Soste, A. E. Hughes, S. G. Hardin, P. R. Curtis, *Appl. Surf. Sci.*, **253**, 1770 (2006).

27. B. F. Rivera, B. Y. Johnson, M. J. O'Keege, W. G. Fahrenholtz, *Surf. Coat. Technol.*, **176**, 349 (2003).

28. S. You, P. Jones, A. Padwal, P. Yu, M. O'Keefe, W. Fahrenholtz, T. O'Keefe, *Mat. Letters*, **61**, 3778 (2007).

29. H. Zhang, Y. Zuo, *Appl. Surf. Sci* (2008), doi:10.1016/j.apsuc.200712.066.

Table 1. Initial pH of the 2.5 wt% phosphate solutions and molar quantities of H_3PO_4 or NaOH added to adjust the solution pH to 4.4.

Phosphate Source	**Initial pH**	**H_3PO_4 (mol x10^{-3})**	**NaOH (mol x10^{-3})**
$NH_4H_2PO_4$	4.16	0	0.33
Na_3PO_4	11.83	50	0
$K_4P_2O_7$	10.11	23	0
$Na_2H_2P_2O_7$	4.15	0	0.56
$Na_5P_3O_{10}$	8.65	3.7	0

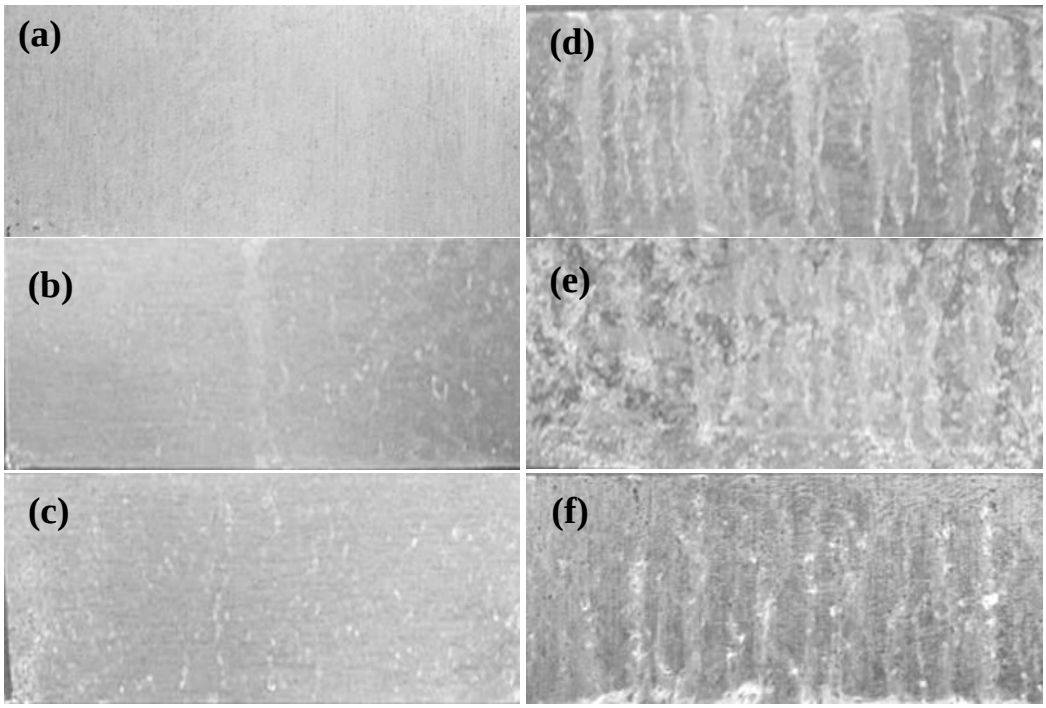

Figure 1. Optical images showing post-treated CeCCs on 3.8 cm by 7.6 cm Al 2024-T3 panels after 14 days of salt spray corrosion testing. The panels were post-treated solutions containing (a) 2.5 wt. % $NH_4H_2PO_4$, (b) 2.5 wt. % Na_3PO_4, (c) 2.5 wt. % $K_4P_2O_7$, (d) 2.5 wt. % $Na_2H_2P_2O_7$, (e) 2.5 wt. % $Na_5P_3O_{10}$, and (f) as-deposited.

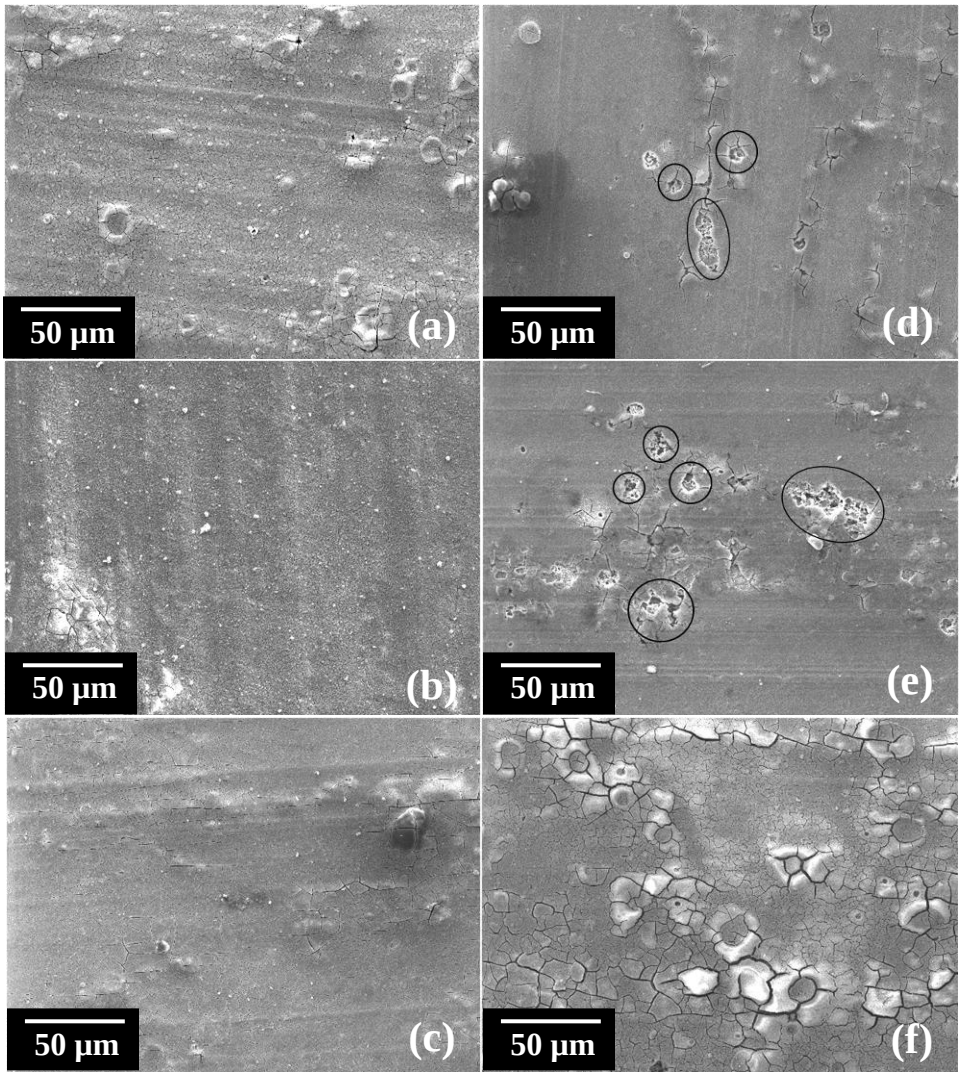

Figure 2. SEM micrographs of CeCCs on Al 2024-T3 post-treated in solutions produced from different phosphate sources, (a) 2.5 wt% $NH_4H_2PO_4$, (b) 2.5 wt% Na_3PO_4, (c) 2.5 wt% $K_4P_2O_7$, (d) 2.5 wt% $Na_2H_2P_2O_7$, (e) 2.5 wt% $Na_5P_3O_{10}$, and (f) As-deposited.

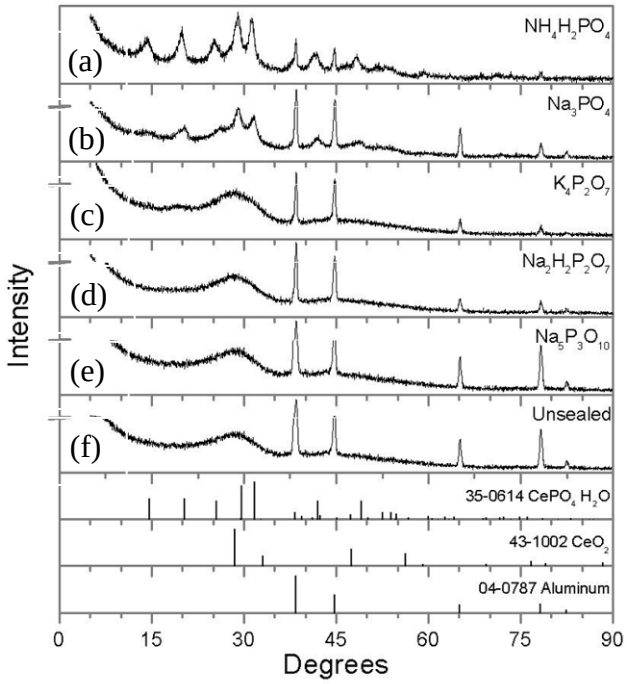

Figure 3. Grazing incidence XRD patterns for CeCCs sealed with respect to phosphate source, (a) 2.5 wt% $NH_4H_2PO_4$, (b) 2.5 wt% Na_3PO_4, (c) 2.5 wt% $K_4P_2O_7$, (d) 2.5 wt% $Na_2H_2P_2O_7$, (e) 2.5 wt% $Na_5P_3O_{10}$, and (f) As-Deposited (Unsealed).

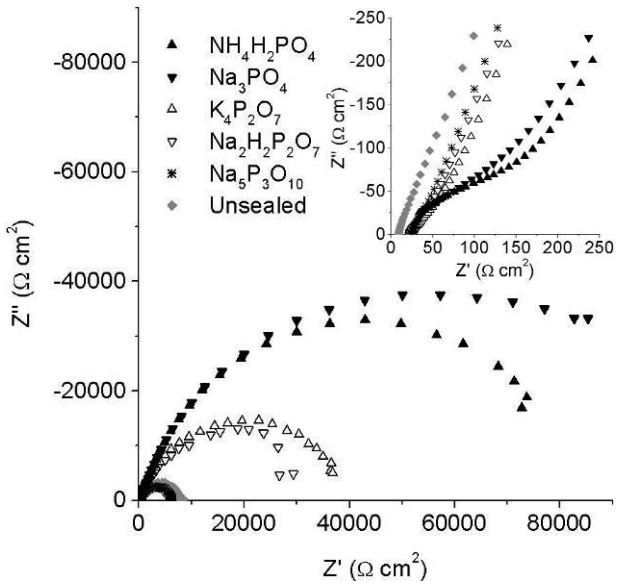

Figure 4. EIS spectra for CeCCs post-treated in heated phosphate solutions produced using different phosphate sources.

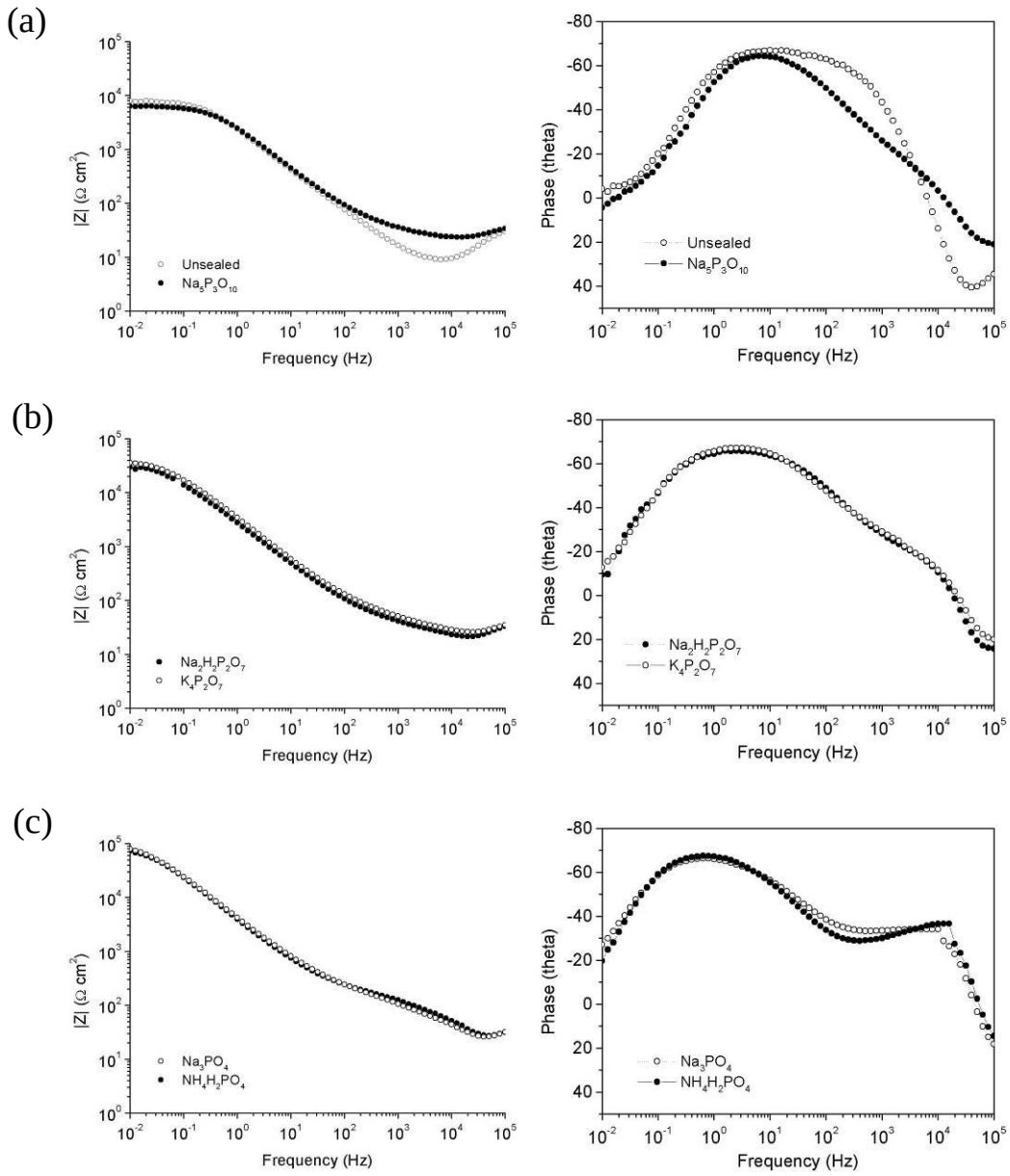

Figure 5. EIS Bode plots indicating depicting a change in coating behavior with respect to phosphate source, (a) as-deposited and polyphosphate, (b) pyrophosphates, (c) orthophosphates.

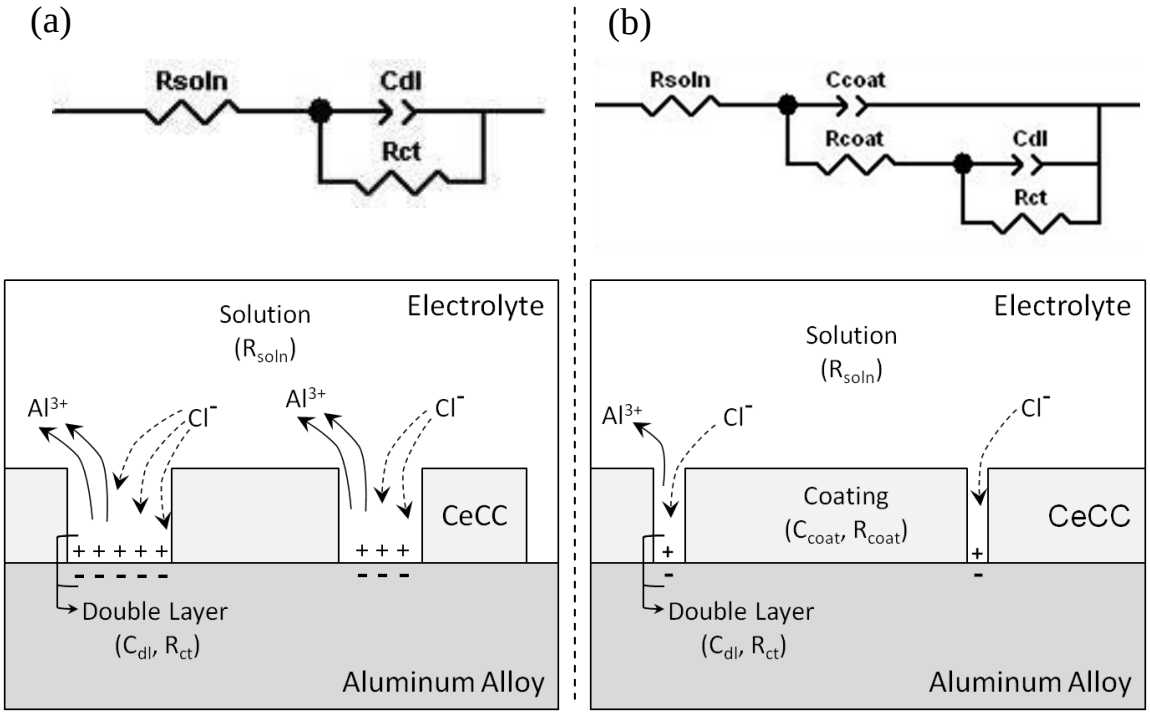

Figure 6. Equivalent circuits used to fit EIS data and associated physical representations for (a) a highly cracked coating and (b) a coating with fewer, finer cracks.

Table 2. Summary of values calculated by fitting EIS data to equivalent circuit models using ZView (R_{ct} & R_s < 5% error after fitting, R_{coat} < 20%).

Source (2.5 wt%)	**Equiv. circuit model**	R_s **(Ω-cm^2)**	R_{coat} **(Ω-cm^2)**	R_{ct} **(kΩ-cm^2)**
Unsealed	$R_s(Q_{dl}R_{ct})$	8	NA	8
$Na_5P_3O_{10}$	$R_s(Q_c(R_c(Q_{dl}R_{ct})))$	24	77	6
$Na_2H_2P_2O_7$	$R_s(Q_c(R_c(Q_{dl}R_{ct})))$	22	60	34
$K_4P_2O_7$	$R_s(Q_c(R_c(Q_{dl}R_{ct})))$	26	85	40
Na_3PO_4	$R_s(Q_c(R_c(Q_{dl}R_{ct})))$	23	203	115
$NH_4H_2PO_4$	$R_s(Q_c(R_c(Q_{dl}R_{ct})))$	23	199	92

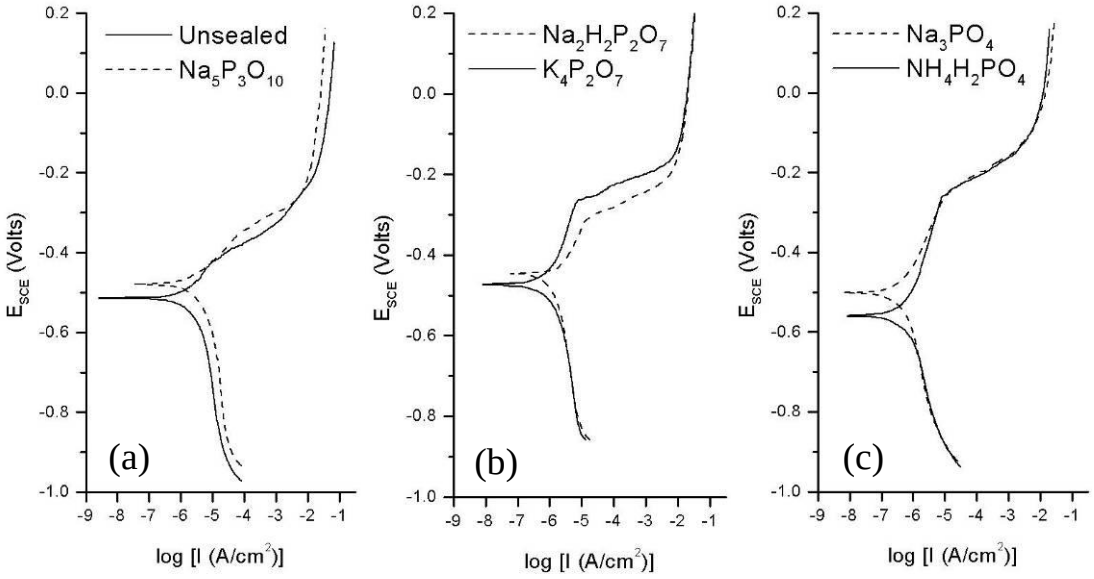

Figure 7. Potentiodynamic scans from CeCC Al 2024-T3 panels, (a) as-deposited and polyphosphate, (b) pyrophosphates, (c) orthophosphates.

Table 3. Values calculated during potentiodynamic analysis of CeCCs with respect to post-treatment.

Source (2.5 wt%)	i_{corr} **(μA/cm^2)**	E_{pit} **(mV)**
$NH_4H_2PO_4$	0.60	-261
Na_3PO_4	0.45	-280
$K_4P_2O_7$	0.74	-275
$Na_2H_2P_2O_7$	1.17	-322
$Na_5P_3O_{10}$	2.14	-343
Unsealed	1.36	-420

III. CROSS-SECTIONAL ANALYSIS OF AS-DEPOSITED AND POST-TREATED CERIUM-BASED CONVERSION COATINGS ON Al 2024-T3

Daimon K Heller, William G. Fahrenholtz, Matthew J. O'Keefe

Materials Research Center, Department of Materials Science and Engineering,

Missouri University of Science and Technology, Rolla, MO 65409, USA

ABSTRACT

As-deposited and phosphate post-treated cerium-based conversion coatings (CeCCs) deposited onto Al 2024-T3 substrates were examined in cross-section before and after exposure to neutral salt spray. Post-treated CeCCs developed an interfacial reaction layer comprised of Al, Ce, and O at the CeCC/substrate interface that was 60 – 100 nm thick after 7 days of salt spray exposure, a feature that was not observed in as-deposited CeCCs. An Al-O containing 'altered layer' also formed on the metal surface of as-deposited and post-treated specimens, presumably by attack of chloride ions at the coating/substrate interface during salt spray exposure. In the case of post-treated CeCCs, aluminum ions released from the altered layer may react with metastable cerium species to form an interfacial phase(s). Electron diffraction revealed that as-deposited and post-treated CeCCs changed structurally during salt spray exposure. Cerium hydroxy/peroxy species present in as-deposited CeCCs transitioned to $CeO_2 \cdot 2H_2O$ during salt spray exposure, and similarly, species present in post-treated CeCCs transitioned to

$CePO_4 \cdot H_2O$, indicating that the salt spray environment facilitated structural changes in the coatings. Chemical analysis did not reveal chlorine in the top half of as-deposited or post-treated CeCCs, an indication that the coatings functioned as effective barriers to the migration, or attack, of chloride ions. The structural changes that occurred in the CeCCs, and the formation of an interfacial layer in post-treated specimens, indicated that the coatings were not static, but exhibited an active response that inhibited corrosion.

1. INTRODUCTION

Cerium-based conversion coatings (CeCCs) have been recognized as a potential alternative to chromate conversion coatings for nearly a decade. The first CeCCs were produced by Hinton et al. and required immersion times beyond 100 hours to produce a continuous Ce layer capable of providing substantial corrosion resistance.[1,2] These layers were capable of reducing the measured polarization corrosion current by a factor of ten on Al 7075 substrates. Hinton's results provided the first evidence that the presence of cerium species limited the kinetics of the oxygen reduction reaction. Several authors have shown the ability of cerium-based coatings to consistently provide some electrochemical protection, predominately by slowing the kinetics of the oxygen reduction reaction occurring at local cathodes.[3,4] Since the introduction of cerium as a corrosion inhibitor in the 1980s, significant progress has been made towards developing CeCCs capable of meeting the U.S. military specification for conversion coatings, MIL-DTL-81706, in which the goal is to prevent the formation of corrosion pits and tails for two weeks (336 hours) in ASTM B117 salt spray exposure. Much of the research within

the past decade has focused on understanding and modifying the deposition process for CeCCs.

Studies on the stability of cerium species in aqueous solutions,[5] the effect of coating solution constituents,[6,7] and the importance of surface activation have been published.[8,9] The stability of cerium species is strongly dependent on pH and allows for the spontaneous precipitation of insoluble compounds when the near surface pH is increased above four. Deposition solutions are commonly acidic (pH < 2.5) and based on a soluble cerium salt, (e.g. $CeCl_3 \cdot xH_2O$ or $Ce(NO_3)_3 \cdot xH_2O$). During precipitation, Ce^{3+} ions are oxidized to form insoluble Ce^{4+} hydroxy/peroxy species, which convert to hydrated cerium oxide ($CeO_2 \cdot 2H_2O$) over time. Adding H_2O_2 to the coating solution dramatically increases the deposition rate by reducing at local cathodes to form hydroxide ions at the alloy surface. The accumulation of hydroxide ions increases the near surface pH and allows for much faster precipitation of cerium species, thereby increasing the rate of coating formation. Effective surface activation processes also increase the deposition rate, but do so by minimizing the native oxide layer. These processes expose intermetallics within the alloy matrix and facilitate electrochemical reactions that occur at local anodes and cathodes during deposition. Less effective surface activations require extended deposition times or numerous coating cycles to obtain uniform coverage. Cerium-based coatings have been demonstrated to form by the initial deposition of cerium onto local cathodic sites across the alloy matrix, eventually expanding to cover the substrate completely.[10,11]

Besides surface activation, the thickness and morphology of CeCCs can be controlled by the deposition method (i.e., spontaneous or electrolytic) and the

composition of the coating solution. For example, Johnson et al. studied the structure and morphology of CeCCs formed using spontaneous and electrolytic methods. For each method, the resulting coatings were nanocrystalline, but cross sectional transmission electron microscopy (TEM) analysis revealed that coatings deposited via an electrolytic technique had a lamellar structure not exhibited by CeCCs deposited using a spontaneous processes (i.e. immersion and spray processes), which appeared more uniform in cross section.[12] The addition of organics such as gelatin or glycerol was found to decrease the deposition rate of CeCCs and reduce cracking in the coating, contributing to improved corrosion resistance over CeCCs deposited without a similar additive.[7,13] The presence of gelatin or glycerol in the coating solution may also influence the conversion of as-deposited coatings (mainly $CeO_2 \cdot 2H_2O$) to $CePO_4 \cdot H_2O$ during phosphate post-treatment. Post-treating CeCCs is conducted by immersing the as-deposited CeCC in a heated, orthophosphate solution, typically for at least five minutes at temperatures at or above 80 °C.[14,15] Post-treatment has been shown to significantly improve the corrosion resistance of CeCCs in neutral salt spray testing performed in accordance with ASTM B117 by minimizing the formation of cracks and converting the cerium hydroxy and peroxy species present in the as-deposited coating to hydrated $CePO_4$.[16,17]

The response of CeCCs to neutral salt spray exposure has not been comprehensively examined. This work was performed to study changes in the chemical composition and microstructures of as-deposited and post-treated CeCCs in response to neutral salt spray exposure. The goal was to determine whether CeCCs provide corrosion protection by acting as an inert barrier to corrosion or if they exhibit an active response to the corrosive environment.

2. EXPERIMENTAL

Coupons measuring 3.8 cm x 7.6 cm were cut from 0.81 mm thick Al 2024-T3 sheet (AMI Metals). Prior to deposition, the substrate surfaces were cleaned with isopropyl alcohol using a standard laboratory wiper followed by rinsing with tap water. The substrates were then placed into a 5 wt. % aqueous solution of an alkaline cleaner (Turco 4215 NCLT) for 5 minutes at 55 °C and rinsed with deionized water. To complete the surface activation, the substrates were immersed in a 1 wt. % aqueous solution of H_2SO_4 for 10 minutes at 50 °C and rinsed with deionized water.

For each condition, CeCCs were spontaneously deposited from aqueous solution via a spray process using a commercially available detail spray gun operated at 35 psi. Coatings were deposited with five spray – drain cycles that consisted of misting the deposition solution onto the panel surface for ≈3 seconds and then waiting ≈30 seconds for the solution to drain from the panel. The deposition solution was prepared by dissolving 10 g $CeCl_3 \cdot 7H_2O$ (99.9 %, Alfa Aesar) into 195 g of deionized water and adjusting the pH to 2.07 with HCl. Next, 0.6 g of organic gelatin (RDH, Rousselot) was dissolved into 25 g of deionized water and added to the $CeCl_3$ solution. Finally, 20 ml of H_2O_2 (ACS 30 %, Fisher) was added < 5 min prior to coating deposition. Some CeCCs were post-treated by immersion in a 2.5 wt % NaH_2PO_4 solution for 5 min at 85 °C immediately following deposition. Coatings that were not post-treated were termed 'as-deposited' CeCCs.

Neutral salt spray tests were performed using a Q-FOG cyclic corrosion chamber (Q-Panel Lab Products) programmed in accordance with the specifications described in

ASTM B117. This test used a 5 wt. % NaCl solution and maintained a constant temperature of 35 °C.

A dual beam system (Helios NanoLab 600, FEI) equipped with a focused ion beam (FIB) milling system and a scanning electron microscopy (SEM) column was used to prepare transmission electron microscopy (TEM) specimens that were approximately 100 nm thick. The system employed a Ga ion source to selectively mill specimens so that a micromanipulator could lift out and mount TEM specimens onto Cu grids for subsequent analysis. Energy dispersive spectroscopy (EDS) was performed with a Noran EDS detector used with a Philips CM200 TEM operated at 200 kV. The EDS data were used to used to identify trends in the composition of cross-sectional specimens and not as an exact quantitative measure of the specimen composition. The balance of reported compositional data consisted predominately of Cu (from the TEM mounting grid) but also of Ga (from FIB milling) and/or Pt (deposited to protect specimen surface during FIB milling).

3. RESULTS AND DISCUSSION

3.1. As-deposited CeCCs

As-deposited CeCCs were comprised of cerium hydroxide and peroxide species that transformed into $Ce(OH)_4$ and $CeO_2{\cdot}2H_2O$ as the coating aged. These coatings exhibited regions of large cracks (>1 μm wide) on approximately 50 % of the substrate and showed visible corrosion pits and tails after one day of ASTM B117 salt spray exposure.

3.1.1. Chemical analysis. A cross-sectional TEM micrograph of the interface between an as-deposited CeCC and the alloy substrate before salt spray exposure is shown in Figure 1a. The average thickness of the interface was measured to be 10 – 20 nm. Chemical analysis performed by energy dispersive spectroscopy (EDS) revealed that the interface consisted predominately of Al and O both before and after salt spray exposure, consistent with the expected presence of native oxide/hydroxide layer on the metal surface. In each case, electron diffraction patterns collected from the interfacial region confirmed its crystallinity, but the patterns could not be indexed to a specific phase.

Prior to salt spray exposure, the lower half of the as-deposited CeCC (points 3 and 4 in Figure 2) contained Al concentrations in the range of 5 – 6 at. %, which was roughly double the concentrations of 2 – 3 at. % that were measured in the top half of the coating (points 1 and 2 in Figure 2). The increase in aluminum concentration near the coating/substrate interface is believed to be a result of the deposition process in which the combination of dissolved chloride ions and hydrogen peroxide etch the alloy substrate during coating deposition, resulting in the incorporation of aluminum into the CeCC near the substrate. Due to dissolution of aluminum from the substrate, the formation of crevices that can extend up to 10 μm into the alloy has been observed on approximately 10 % of the substrate.[18,19]

The composition of the interface did not change after 6 days of salt spray exposure but was less uniform and not as well defined. The Al-O layer on the metal surface appeared to have been altered and contained regions that were 20 – 50 nm thick and distributed unevenly across the interface. Point EDS analysis revealed a higher

concentration of Al throughout the entire thickness of the coating after salt spray exposure. Aluminum concentrations near the top and bottom of the CeCC were ≈20 at. %, with concentrations near 8 at. % throughout the middle part of the CeCC. These concentrations were three times higher than those measured prior to salt spray exposure and suggest that Al could migrate through the cerium oxide/hydroxide coating during corrosion testing. Oxygen concentrations in excess of 70 at. % were measured in the bulk of the CeCC, approximately two times higher than values measured before salt spray exposure and may be partly explained by increased coating hydration and/or the formation of aluminum hydroxide within the CeCC. If aluminum dissolution occurred at the interface during salt spray exposure, Al^{3+} ions could be introduced into the CeCC (and/or be transported to the surface via cracks), causing increased aluminum concentrations. The most likely way for this to occur is by chloride attack of aluminum oxides/hydroxides. EDS analysis consistently confirmed the presence of 1 – 2 at. % chlorine at interfacial regions, but did not detect chlorine in the upper half of the CeCC. These result suggest that the CeCCs were an effective barrier to the penetration of chloride ions, but were potentially vulnerable where the substrate was exposed by defects in the coating (i.e., cracks and subsurface crevices).

The as-deposited CeCC accumulated corrosion product during salt spray testing on more than 50 % of the panel surface. As viewed in cross section by SEM, an Al-O containing corrosion product was seen as a fibrous layer > 1 μm thick on the CeCC surface (Figure 3). Recent work by Pinc et al. has shown that an Al-O containing layer is formed on the surface of CeCCs only when subsurface crevices are present. These crevices, along with the formation of stable pits during salt spray exposure, introduce Al

ions to the coating surface where they react to form the Al-O containing regions. Explanation of the migration of aluminum ions from the substrate into the coating is more complex. Potential mechanisms for this to occur will be discussed in Section 3.3, but include dissolution of aluminum hydroxides by reaction with chlorides at the interface and/or aluminum oxidation enabled by the generation of local pH changes during corrosion. While EDS point analyses shown in Figure 3 do not indicate the presence of chlorine, concentrations up to 2 at. % were intermittently detected along the coating/substrate interface of each specimen examined in this study.

3.1.2. Structural analysis. Electron diffraction was used to collect structural data from the substrate, the coating/substrate interface, and within the CeCC. Diffuse ring patterns observed from the as-deposited CeCC were consistent with crystallites less than 10 nm in size, in agreement with previous analyses of similar CeCCs.[12]

The diffraction patterns collected from as-deposited CeCCs prior to salt spray exposure revealed several different structures and demonstrated heterogeneity within the coating. While some of the patterns could be confidently indexed to stoichiometric cerium oxide ($CeO_2 \cdot 2H_2O$), other patterns most closely corresponded to Ce-O compounds with stoichiometries between those of Ce(III) and Ce(IV) oxides (e.g., Ce_2O_3 and CeO_2) and could include cerium hydroxy and/or peroxy species for which structural reference data are unavailable, Figure 4 and Table 1. This result is consistent with previously reported XPS analysis that indicated the presence of both Ce^{3+} and Ce^{4+} oxidation states in as-deposited coatings.[20,21,22] In addition, previously reported grazing incidence XRD of analogous CeCCs showed a single, broad peak centered near 29 degrees two theta (Cu Kα radiation) that was attributed to nanocrystalline $CeO_2 \cdot 2H_2O$ or

$Ce(OH)_4$.[7,17] Heterogeneity within the CeCC could be explained by localized non-uniformity of the deposition process.[23] Cerium species deposited by a spontaneous process have been shown to first deposit at local cathodes (i.e., intermetallic compounds) on the alloy surface and then deposit on the remainder of the exposed substrate.[24] It is probable that local chemistry gradients are present during coating deposition near these sites, causing local fluctuations in the composition and rate of CeCC formation.

After 6 days of salt spray exposure, electron diffraction of the as-deposited CeCC indicated the coating had structurally changed. One of the d-spacings measured from as-deposited CeCCs, near 2.7 Å, corresponds to the (200) of CeO_2 and was only observed in coatings that were exposed to the salt spray environment. A summary of the measured interplanar spacings for as-deposited CeCCs before and after salt spray exposure is shown in Table 1. After salt spray, the coatings had become structurally more uniform and $CeO_2 \cdot 2H_2O$ was identified throughout the coating thickness (Figure 5). The more uniform CeCC structure may be a response to the aqueous environment and elevated temperatures encountered during salt spray testing, promoting the transition of cerium hydroxy and peroxy species to the more stable $CeO_2 \cdot 2H_2O$. Grazing incidence XRD did not provide conclusive evidence of structural changes because peak broadening caused by the coating's nanocrystalline structure obscured subtle changes in diffraction angle. Data from EDS analyses showed increased concentrations of aluminum and oxygen within the conversion coating after salt spray testing. The incorporation of aluminum atoms in the cerium oxide structure during deposition (or during salt spray exposure) should affect the crystalline structure and the resulting diffraction patterns. If this process had occurred, the resulting d-spacings should be shifted uniformly, corresponding to the

decreased interplanar spacing caused by substitution of smaller aluminum atoms in place of larger cerium atoms. Such evidence could not be confirmed, nor could patterns collected from the CeCC be indexed to known cerium aluminate or aluminum hydroxide species.

3.2. Post-treated CeCCs

Post-treated CeCCs provide significantly improved corrosion protection compared to as-deposited CeCCs and consistently withstood at least 7 days of salt spray exposure without exhibiting corrosion pits or salt tails. The improved corrosion resistance has previously been attributed to the improved barrier properties brought about by minimizing cracking in the coating as well as the formation of hydrated $CePO_4$.[14,15]

3.2.1. Chemical analysis. Analysis of the interface between the post-treated CeCCs and the underlying aluminum alloy substrate before salt spray exposure revealed no differences compared to the as-deposited coatings; the interfacial layer measured 10 – 20 nm in thickness and was predominately comprised of Al, Ce, and O (Figure 6a). As shown in Figure 7, EDS analyses across the thickness of the post-treated CeCC revealed a phosphorus concentration gradient through the coating thickness, ranging from 22 at. % at the CeCC surface to 12 at. % at the coating-substrate interface. Consistent with analysis of as-deposited CeCCs, the aluminum concentration in the post-treated specimen was found to increase to ≈6 at. % near the interface whereas the Al value in the center of the coating measured ≈3 at. %.

Post-treated specimens that did not have visible corrosion pits and tails after 7 days of neutral salt spray exposure responded to the corrosive environment. An

interfacial reaction layer measuring 60 – 100 nm thick and comprised of Al, Ce, and O was located between the post-treated CeCC and alloy substrate as seen in Figure 6b and Figure 8. No phosphorous was detected in the interfacial layer, indicating that it was not a phosphate phase. Electron diffraction patterns confirmed the crystallinity of the layer, but the patterns could not be indexed to $CeAlO_3$, or any other Ce-Al containing phases. The layer could also be multiphase, potentially containing a mixture of cerium and aluminum oxides and/or hydroxides. The measured Al concentration in the top and bottom 50 – 100 nm of the post-treated coating was ≈6 at. %, which was about one fourth of the ≈25 at. % that was measured in the as-deposited CeCC after six days salt spray exposure. Oxygen concentration within post-treated CeCCs was determined to be independent of salt spray exposure, with concentrations ranging from 42 – 47 at. % in each case. These results suggest that the post-treated $CePO_4 \cdot H_2O$ coating is either a more effective barrier to the movement of Al^{3+} ions through the coating during corrosion or acts in such a way as to limit aluminum dissolution.

3.2.2. Structural analysis. The d-spacings calculated from diffraction patterns of the post-treated CeCCs before salt spray exposure did not correspond to the rhabdophane phase ($CePO_4 \cdot H_2O$). Similar to as-deposited CeCCs, post-treated coatings were not structurally uniform. Prior to salt spray, some ring patterns had d-spacings comparable to those collected from as-deposited CeCCs not exposed to salt spray, providing evidence that some of the species present in as-deposited coatings may have been unaffected by the post-treatment process (Table 1 and Table 2). In other instances, the d-spacings from post-treated CeCCs were similar to a combination of species such as hydrated cerium hydrogen phosphates or phosphites (i.e., $Ce_2(PO_4)_2HPO_4H_2O$,

$CeH(HPO_3)_2(H_2O)_2$) (Figure 9). Patterns were collected throughout the thickness of the CeCC and coating structure did not appear to vary as a function of depth.

Similar to as-deposited coatings, post-treated CeCCs changed structurally during salt spray exposure. The ring patterns produced by electron diffraction in the coatings were indexed to $CePO_4 \cdot H_2O$, indicating that less stable phosphate species had transitioned to the favored rhabdophane phase during salt spray exposure (Figure 10 and Table 2). In particular, the ring patterns from post-treated CeCCs exposed to salt spray included d-spacings that were not observed for other conditions, most notably those near 2.8 Å and 2.2 Å and are in agreement with standard diffraction files for hydrated $CePO_4$ (Table 2).

The structure of as-deposited and post-treated CeCCs changed during salt spray exposure, with each coating becoming structurally more uniform. These changes may be caused by the transition of species present after coating deposition (i.e., cerium hydroxy/peroxy compounds for as-deposited coatings, cerium hydrogen phosphate compounds and/or unreacted hydroxy/peroxy species for post-treated coatings) to favored $CeO_2 \cdot 2H_2O$ or $CePO_4 \cdot H_2O$ phases respectively. The change in coating structure and formation of an interfacial reaction layer during salt spray exposure suggests that the protection mechanism of CeCCs extends beyond that of a static barrier coating and demonstrates that CeCCs can exhibit an active response to the salt spray environment.

3.3. Other Implications

The growth of an interfacial reaction layer in post-treated specimens, and its corresponding absence in as-deposited specimens, has important implications for

the processes that may be responsible for the improved corrosion performance observed from post-treated CeCCs and may help explain their improved electrochemical properties (i.e., more anodic pitting potentials and larger charge transfer resistances). Pinc et al. used electrochemical impedance spectroscopy to evaluate the electrochemical response of CeCCs as a function of salt spray exposure time and reported an increase in charge transfer resistance with salt spray exposure time up to 336 hours of exposure for post-treated specimens.[25] Upon reaching 336 hours, the charge transfer resistance of post-treated CeCCs was found to decrease, corresponding to the observed formation of corrosion pits. The increased resistance before 336 hours was attributed to the development of a surface layer on top of the CeCC that was rich in aluminum and oxygen. The surface layer was detected by Auger electron spectroscopy (AES) depth profiles. As-deposited specimens were also found to exhibit an increased aluminum concentration near the surface during salt spray testing, but did not exhibit an impedance increase. As a result, it was hypothesized that the $CePO_4 \cdot H_2O$ phase facilitated the formation of a protective alumina layer on the outer surface of the CeCC. The present study confirmed the higher aluminum concentrations near the surface of as-deposited and post-treated CeCCs after salt spray exposure, but, in contrast, proposes the increased impedance is a result of the interfacial reaction layer that forms between the CeCC and substrate.

Analysis after salt spray provided no evidence that chloride ions had migrated through either as-deposited or post-treated CeCCs. The EDS analyses performed on as-deposited or post-treated CeCCs did not reveal the presence of chlorine in the top half of the CeCC after one week of salt spray exposure and indicated that the coating was an

effective barrier to chloride ions. Chlorine was only detected in the corrosion product on the surface of as-deposited CeCCs and intermittently detected at the coating/substrate interface in both as-deposited and post-treated CeCCs. This analysis also supports the hypothesis that pitting corrosion initiates from sites that are presumably more electrochemically active (i.e., regions containing subsurface crevices) and not by attack/penetration of the CeCC by chloride ions. Prior to salt spray exposure, the presence of chlorine at the interface is believed to be a result of the deposition process in which chloride ions were trapped at or near the interface during the initial rapid formation of the coating. However, additional chloride ions may be introduced to the interface during salt spray exposure (where cracks in the CeCC extend to the substrate). An altered region consisting of aluminum, oxygen, and ≈1 at. % chlorine was detected just above the alloy substrate in as-deposited and post-treated specimens after salt spray exposure (labeled in Figures 3 and 6). This layer is believed to be a form of aluminum hydroxide that may not be stable in the presence of chloride ions. The presence of cracks and other defects enable chloride ions to react with the aluminum hydroxide or hydrated oxides at the coating/substrate interface and take up positions on oxygen vacancy sites and/or lead to formation of soluble aluminum chloride species.[26] Such a reaction could produce additional oxygen vacancies at the interface, potentially allowing for the migration of chloride ions along the interface, leading to the formation of the altered layer, shown schematically in Figure 11a. Attack of the aluminum hydroxide could facilitate a reaction with neighboring Ce species, potentially forming a non-stoichiometric cerium aluminate at the interface. A change in pH near the interface may also influence the stability of cerium or aluminum species, which could facilitate species

migration and the formation of a more stable phase(s) (Figure 11b). Continued introduction of chloride ions would increase aluminum dissolution, providing a mechanism by which aluminum ions are continually generated and either incorporated into the interfacial reaction layer (for post-treated CeCCs), transported into the CeCC, or released to the surface via cracks. The formation of corrosion pits was not observed at crack/substrate interfaces, nor was the interfacial layer determined to bridge this gap, indicating that post-treated CeCCs provided limited electrochemical protection of the alloy substrate exposed by coating defects.

4. CONCLUSIONS

Post-treated CeCCs exhibited an active response to the salt spray environment by forming an interfacial reaction layer comprised of Ce, Al, and O that was 60 – 100 nm thick after 7 days of exposure. Post-treated specimens did not exhibit visible corrosion pits or tails during this time; however, as-deposited CeCCs contained pits and salt tails distributed across the majority of the specimen surface after 6 days of salt spray exposure and did not form a similar interfacial layer. No chlorine was detected by EDS in the top half of as-deposited or post-treated CeCCs, indicating that each of the coatings was an effective barrier to chloride ions and were not degraded by chloride attack. Because CeCCs contain defects, (e.g. cracks in the coating and subsurface crevices in the substrate beneath the coating), this result suggests that one mechanism of coating failure may be chloride ion attack of the aluminum oxide/hydroxide layer present on the metal surface. The introduction of chloride ions, and their movement along the interface, would

facilitate aluminum dissolution by promoting cyclic formation and destabilization of aluminum oxides/hydroxides.

The presence of chloride ions at the coating/substrate interface may lead to the formation of the 'altered layer' that was observed for both as-deposited and post-treated CeCCs after salt spray exposure. During corrosion, this layer may act as a source of aluminum ions, which, in the case of as-deposited CeCCs, migrate into the CeCC, causing the aluminum concentration in the CeCC near the substrate to increase from 6 at. % to > 20 at. % after salt spray exposure. Post-treated CeCCs did not show an increase in Al content despite the presence of the altered layer, suggesting that the $CePO_4 \cdot H_2O$ based coating was an improved barrier to the migration of Al^{3+} ions, effectively trapping them near the interface, and/or establishing an environment conducive to their reaction with neighboring Ce species. Electron diffraction patterns from as-deposited and post-treated CeCCs indicated that the coatings changed structurally during exposure to the salt spray environment. In particular, ring patterns from as-deposited and post-treated CeCCs exposed to salt spray corresponded to d-spacings near 2.7 Å and 2.8 Å respectively, and were not present in the as-coated (i.e., no salt spray exposure) specimens. These results indicate that at least some of the compounds comprising the CeCCs were not stable during corrosion testing and transitioned to the favored $CeO_2 \cdot 2H_2O$ or $CePO_4 \cdot H_2O$ phases for as-deposited or post-treated coatings, respectively. These changes demonstrate that CeCCs are not inert barriers and are capable of reacting to a corrosive environment. Accordingly, Ce species near the interface may be available to react with free Al^{3+} ions or aluminum hydroxides destabilized by chloride ions. Since as-deposited CeCCs did not form an interfacial reaction layer, phosphate post-treatment may influence the chemical

activity of available Ce species or the local pH environment adjacent to the interface in a manner conducive to the formation of a reaction layer phase(s).

While the mechanism of interfacial layer formation is unclear, the corrosion protection provided by post-treated conversion coatings extended beyond that of a static, inert barrier. Post-treated CeCCs responded actively to the salt spray environment by forming an interfacial reaction layer that appears to play a vital role in corrosion protection.

ACKNOWLEDGMENTS

The authors appreciate conversations with Geoff Fair and assistance with TEM analysis by Randall Hay at the Air Force Research Laboratory at Wright Patterson Air Force Base. The technical assistance of Ming Zhang and Elizabeth Kulp at the Missouri University of Science and Technology is also acknowledged. The authors also acknowledge the technical guidance and support of Bruce Sartwell at the Strategic Environmental Research and Development Program (SERDP). This work was funded through SERDP under contract W912HQ-08-C-0008.

REFERENCES

1. B.R.W. Hinton, D.R. Arnott, N.E. Ryan, "Cerium Conversion Coatings for the Corrosion Protection of Aluminium," *Mat. Forum*, **9** (3), 162-173 (1986).
2. B.R.W. Hinton, D.R. Arnott, N.E. Ryan, "The Inhibition of Aluminium Alloy Corrosion by Cerous Cations," *Met. Forum*, **7** (4), 211-217 (1984).
3. M. Kendig and C. Yan, *J. Electrochem. Soc.*, "Critical Concentration for Selected Oxygen Reduction Reaction Inhibitors," **151** (12) B679-B682 (2004).

4. M.A. Jakab, F. Presuel-Moreno, J.R. Scully, "Effect of Molybdate, Cerium, and Cobalt Ions on the Oxygen Reduction Reaction on AA2024-T3 and Selected Intermetallics," *J. Electrochem. Soc.*, **153** (7) B244-B252 (2006).

5. P. Yu, S.A. Hayes, T.J. O'Keefe, M.J. O'Keefe, J.O. Stoffer, "The Phase Stability of Cerium Species in Aqueous Systems II," *J. Electrochem. Soc.*, **153** (1) C74-C79 (2006).

6. F.H. Scholes, C. Soste, A.E. Hughes, S.G. Hardin, P.R. Curtis, "The Role of Hydrogen Peroxide in the Deposition of Cerium-based Conversion Coatings," *App. Surf. Sci.*, **253**, 1770-1780 (2006).

7. W. Pinc, P. Yu, M. O'Keefe, W. Fahrenholtz, "Effect of Gelatin Additions on the Corrosion Resistance of Cerium Based Conversion Coatings Spray Deposited on Al 2024-T3," *Surf. Coat. Tech.*, **203**, 3533-3540 (2009).

8. W. Pinc, S. Geng, M. O'Keefe, W. Fahrenholtz, T. O'Keefe, "Effects of Acid and Alkaline Based Surface Preparations on Spray Deposited Cerium Based Conversion Coatings on Al 2024-T3," *App. Surf. Sci.*, **255**, 4061-4065 (2009).

9. A. de Frutos, M.A. Arenas, Y. Liu, P. Skeldon, G.E. Thompson, J. de Damborenea, A. Conde, "Influence of Pre-treatments in Cerium Conversion Treatment of AA2024-T3 and 7075-T6 alloys," *Surf. Coat. Tech.*, **202**, 3797-3807 (2008).

10. A.E. Hughes, J.D. Gorman, P.R. Miller, B.A. Sexton, P.J.K. Paterson, R.J. Taylor, "Development of Cerium-based Conversion Coatings on 2024-T3 Al Alloy After Rare-eath Desmutting," *Surf. Interface Anal.*, **36**, 290-303, (2004).

11. P. Campestrini, H. Terryn, A. Hovestad, J.H.W. de Wit, "Formation of a Cerium-based Conversion Coatings on AA2024: Relationship with the Microstructure," *Surf. Coat. Tech.*, **176**, 365-381 (2004).

12. B.Y. Johnson, J. Eddington, A. Williams, M.J. O'Keefe, "Microstructural Characteristics of Cerium Oxide Conversion Coatings Obtained by Various Aqueous Deposition Methods," *Mat. Char.*, **54**, 41-28 (2005).

13. B.Y. Johnson, J. Eddington, M.J. O'Keefe, "Effect of Coating Parameters on the Microstructure of Cerium Oxide Conversion Coatings," *Mat. Sci. Eng.*, **A361**, 225-231 (2003).

14. H. Zhang, Y. Zuo, "The Improvement of Corrosion Resistance of Ce Conversion Films on Aluminum Alloy by Phosphate Post-treatment," *Appl. Surf. Sci.*, **254**, 4930-4936 (2008).

15. D.K Heller, W.G. Fahrenholtz, M.J. O'Keefe, "The Effect of Post-Treatment Time and Temperature on Cerium Based Conversion Coatings on Al 2024-T3," *Corr. Science*, **52** (2), 360-368, (2009).

16. Standard Practice for Operating Salt Spray (Fog) Apparatus, ASTM B117-97, American Society for Testing and materials, West Conshohocken, PA, 1997.

17. D.K Heller, W.G. Fahrenholtz, M.J. O'Keefe, "Effect of Phosphate Source on Post-treatment of Cerium Based Conversion Coatings on Al 2024-T3," *J. Electrochem. Soc.*, **156** (11), C400 - C406 (2009).

18. W. Pinc, S. Maddela, M. O'Keefe, W. Fahrenholtz, "Formation of Subsurface Voids in Aluminum Alloy 2024-T3 During Deposition of Cerium-based Conversion Coatings," submitted to *Surf. Coat. Tech.* on Feb. 8, 2010.

19. D.K. Heller, W.G. Fahrenholtz, M.J. O'Keefe, "Crevice TEM Paper," to be submitted to *Materials Letters*.

20. X. Yu, G. Li, "XPS Study of Cerium Conversion Coating on the Anodized 2024 Aluminum Alloy," *J. Alloy Compd.*, **364**, 193-198 (2004).

21. M. Dabalà, L. Armelao, A. Buchberger, I. Calliari, "Cerium-based Conversion Layers on Aluminum Alloys," *Appl. Surf. Sci.*, **172**, 312-322 (2001).

22. W.G. Fahrenholtz, M.J. O'Keefe, H. Zhou, J.T. Grant, "Characterization of Cerium-based Conversion Coatings for Corrosion Protection of Aluminum Alloys," *Surf. Coat. Tech.*, **155**, 208-213 (2002).

23. M. Bethencourt, F.J. Botana, M.J. Cano, M. Marcos, "High Protection, Environmental Friendly and Short-time Developed Conversion Coatings for Aluminium Alloys," *Appl. Surf. Sci.*, **189**, 162-173 (2002).

24. B.R.W. Hinton, "Corrosion Inhibition with Rare Earth Metals Salts," *J. Alloys Compd.*, **180**, 15-25 (1992).

25. W. Pinc, D. Heller, W. Fahrenholtz, M. O'Keefe, "Electrochemical and Structural Changes in Cerium Based Conversion Coatings During Exposure to Salt Spray," *ECS Trans.*, **25** (29), 3-17 (2010).

26. Z. Szklarska-Smialowska, "Pitting Corrosion of Aluminum," *Corr. Sci.*, **41**, 1743-1767 (1999).

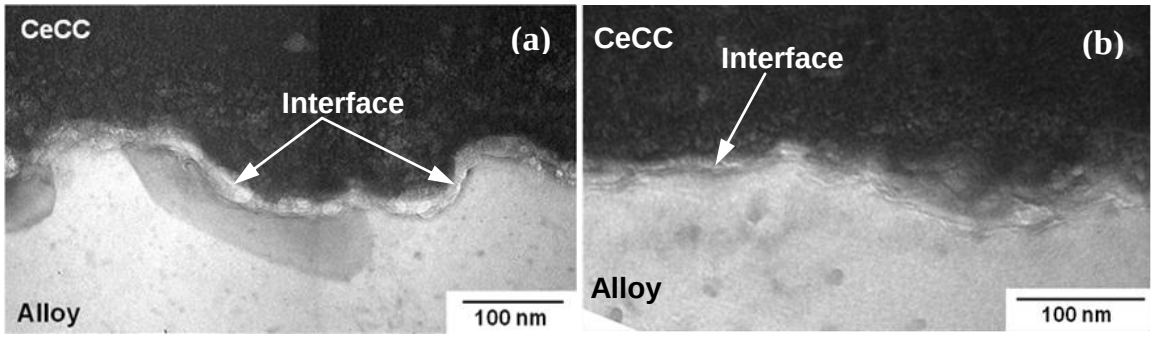

Figure 1. TEM micrographs of the interface between the as-deposited CeCC and Al 2024-T3 substrate, (a) before salt spray exposure (montage), (b) after 6 days salt spray exposure.

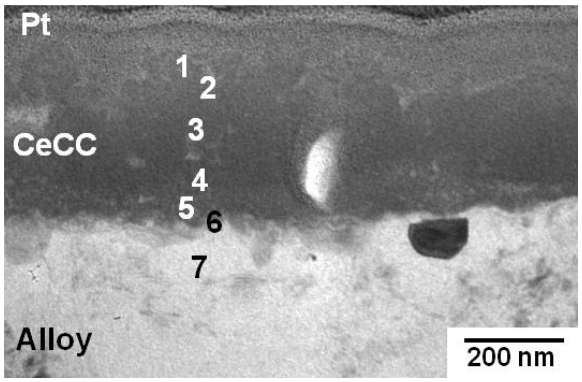

EDS Data (at. %)					
Spot	Ce	Al	O	Cl	Pt
1	15	2.5	22	-	5.7
2	16	2.2	27	-	3.9
3	18	4.8	39	-	-
4	19	5.9	36	-	-
5	6.7	48	26	0.6	-
6	-	64	22	0.3	-
7	-	91	2.0	-	-

Figure 2. Cross-sectional TEM with corresponding EDS analysis for as-deposited CeCCs prior to salt spray exposure (balance Cu).

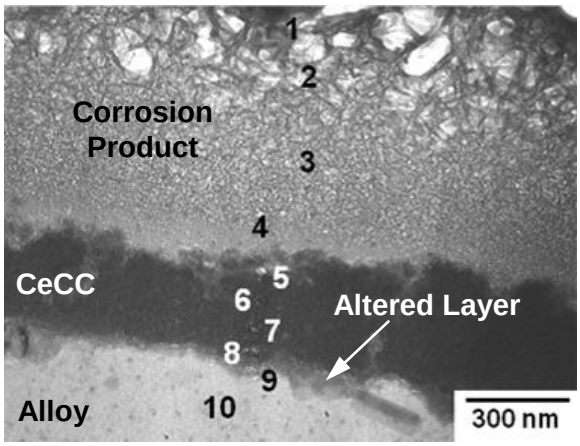

EDS Data (at. %)					
Spot	Ce	Al	O	Cl	Pt
1	-	7.6	-	-	64
2	-	54	22	1.1	12
3	-	62	26	0.6	5.1
4	-	64	26	0.9	4.6
5	8.0	20	50	-	-
6	9.0	8.0	76	-	-
7	8.8	8.2	74	-	-
8	6.1	27	62	-	-
9	0	88	10	-	-
10	-	95	1.5	-	-

Figure 3. Cross-sectional TEM with corresponding EDS analysis for as-deposited CeCCs after 6 days of salt spray exposure (balance Cu).

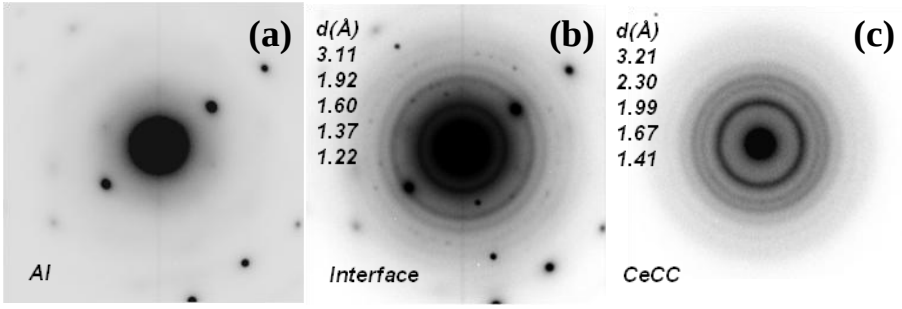

Figure 4. Electron diffraction patterns from as-deposited CeCCs before salt spray exposure, (a) aluminum matrix, (b) interface, and (c) CeCC (L = 500 mm).

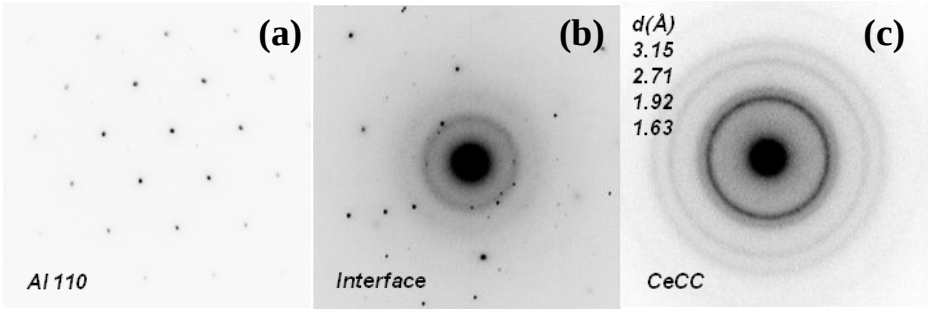

Figure 5. Electron diffraction patterns from as-deposited CeCCs after 6 days salt spray exposure, (a) aluminum matrix, (b) coating/substrate interface, and (c) CeCC.

Table 1. Measured d-spacings (Å) from electron diffraction ring patterns of as-deposited CeCCs before and after salt spray exposure.

Ce_2O_3 PDF 78-0484	CeO_2 PDF 81-0792	As-dep. Before	As-dep. After
3.37	3.12	3.21	3.15
3.03	2.70	2.30	2.71
2.25	1.91	1.99	1.92
1.95	1.63	1.67	1.63
1.68	1.56	1.41	
	1.35		

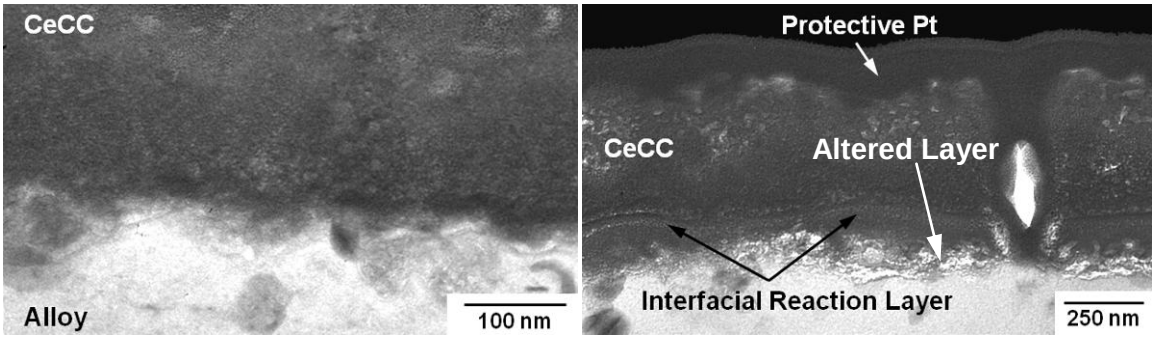

Figure 6. TEM micrographs of the interface between post-treated CeCCs and Al 2024-T3 substrate, (a) before salt spray exposure (montage), (b) after 7 days salt spray exposure.

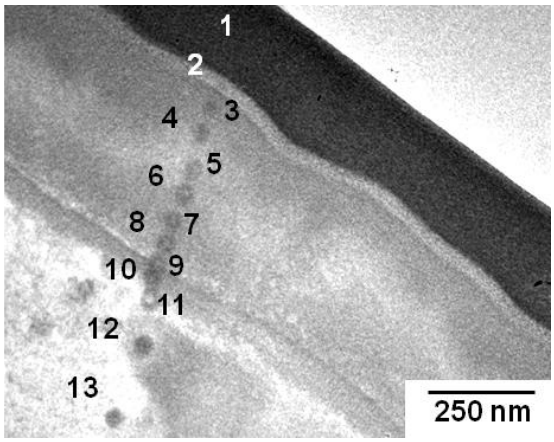

EDS Data (at. %)						
Spot	Ce	P	Al	O	Cl	Pt
1	-	-	-	-	-	37
2	-	-	-	-	-	42
3	-	-	-	-	-	51
4	5.1	-	-	-	-	49
5	13	15	4.0	41	-	9.7
6	13	22	2.0	47	0.6	2.3
7	12	19	3.6	46	0.5	-
8	11	15	5.6	46	1.1	-
9	10	11	11	46	1.0	-
10	8.9	0.9	23	47	1.9	-
11	2.7	-	32	42	2.1	-
12	-	-	60	10	-	-
13	-	-	92	2.4	-	-

Figure 7. Cross-sectional TEM with corresponding EDS analysis for post-treated CeCCs prior to salt spray exposure (balance Cu).

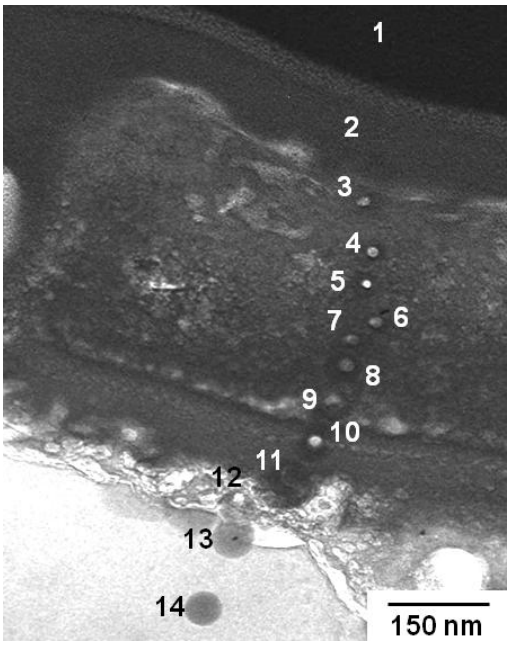

EDS Data (at. %)						
Spot	Ce	P	Al	O	Cl	Pt
1	-	-	-	-	-	40
2	-	-	-	-	-	43
3	6.4	-	14	21	-	21
4	9.4	14	5.6	38	-	6.0
5	9.1	23	0.9	42	-	-
6	10	19	0.8	44	-	-
7	11	19	1.7	42	-	-
8	11	14	5.8	44	-	-
9	9.4	16	5.8	46	-	-
10	8.2	-	19	51	0.8	-
11	9.0	-	25	45	2.1	-
12	-	-	57	29	-	-
13	-	-	87	5.7	-	-
14	-	-	91	1.8	-	-

Figure 8. Cross-sectional TEM with corresponding EDS analysis for post-treated CeCCs after 7 days salt spray exposure (balance Cu).

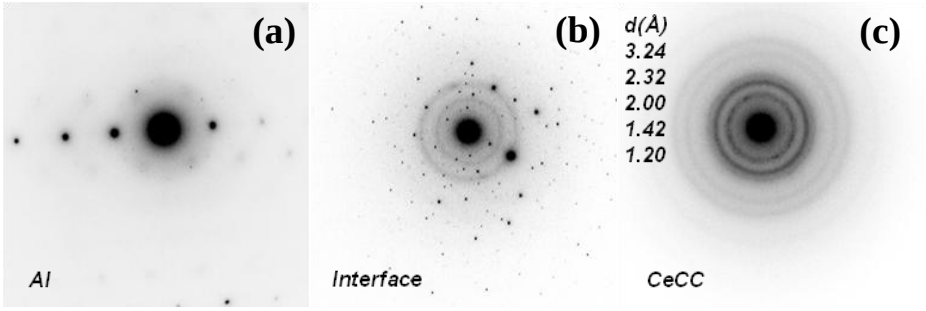

Figure 9. Electron diffraction patterns from post-treated CeCCs before salt spray exposure, (a) aluminum matrix, (b) coating/substrate interface, and (c) CeCC (L = 360 mm).

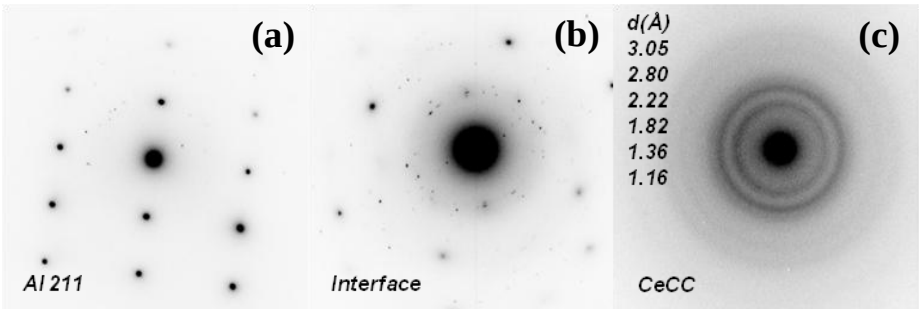

Figure 10. Electron diffraction patterns from post-treated CeCCs after 7 days exposure to neutral salt spray, (a) aluminum matrix, (b) coating/substrate interface, and (c) CeCC (L = 500mm).

Table 2. Measured d-spacings (Å) from electron diffraction ring patterns of post-treated CeCCs before and after salt spray exposure.

$CePO_4 \cdot H_2O$ PDF 35-0614	Post-treated Before	Post-treated After
3.01	3.24	3.05
2.82	2.32	2.80
2.19	2.00	2.22
1.85	1.42	1.82
1.36	1.20	1.36
1.16		1.16

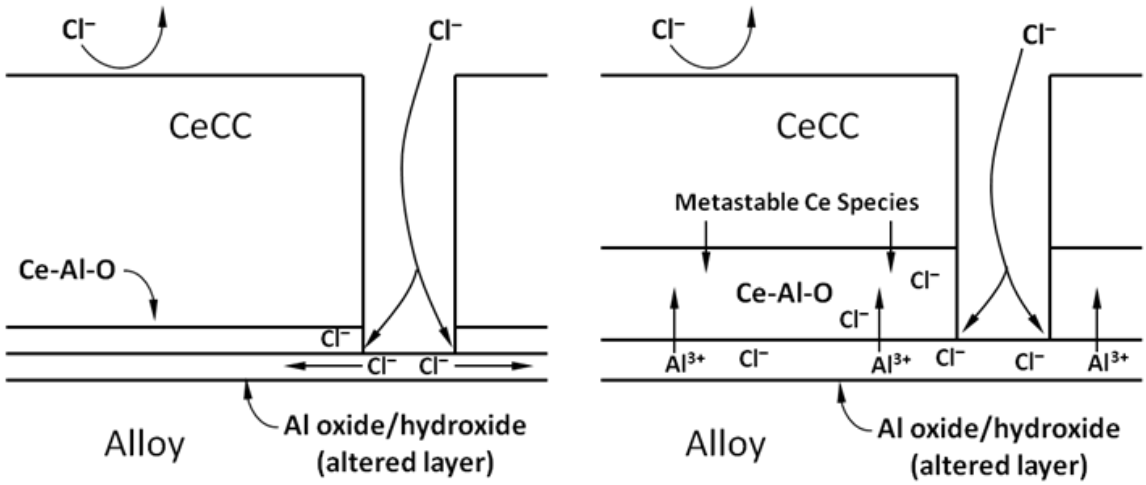

(a) **(b)**

Figure 11. Potential mechanism of interfacial reaction layer formation for post-treated CeCCs during (a) initial formation of altered layer by chloride ion attack and migration at the interface, and (b) after continued chloride exposure, chloride facilitates aluminum dissolution from the altered layer, releasing it towards the CeCC where it reacts with metastable cerium compounds to form the interfacial phase(s).

IV. DIRECTLY DEPOSITED CERIUM PHOSPHATE COATINGS FOR THE CORROSION PROTECTION OF Al 2024-T3

Daimon K Heller[a], William G. Fahrenholtz[a], Geoff E. Fair[b], Matthew J. O'Keefe[a]

[a]Materials Research Center, Department of Materials Science and Engineering, Missouri University of Science and Technology, Rolla, MO 65409, USA

[b]Air Force Research Laboratory, Wright-Patterson Air Force Base, Dayton, OH 45433, USA

ABSTRACT

Cerium phosphate coatings were directly deposited onto Al 2024-T3 substrates by precipitation from aqueous solution containing cerium citrate and phosphoric acid. These coatings were characterized and compared to post-treated, cerium-based conversion coatings (CeCCs). Directly deposited $CePO_4$ coatings exhibited corrosion current densities of 2 – 4 $\mu A/cm^2$, compared to ≈0.45 $\mu A/cm^2$ for CeCCs. Analysis revealed that directly deposited $CePO_4$ coatings did not significantly impact the electrochemical properties of bare Al 2024-T3, an indication that deposition was independent of the local galvanic activity utilized to deposit CeCCs. After salt spray exposure, cross-sectional analyses showed that directly deposited coatings acted as a static barrier to corrosion, allowing the formation of pits at crack/substrate interfaces, which were not observed in similar regions of post-treated CeCCs. Instead, an interfacial reaction layer had formed

at the CeCC/substrate interface, revealing that the CeCC exhibited an active response to the salt spray environment that influenced corrosion protection.

1. INTRODUCTION

Conversion coatings based on rare-earth elements, such as environmentally friendly cerium compounds, have been shown to provide corrosion protection to high strength aluminum alloys 2024-T3 and 7075-T6 that are used throughout the aerospace industry. These rare-earth-based coatings are a potential alternative to Cr^{6+} containing chromate conversion coatings (CCCs) that have been used successfully for decades. While more stringent regulation of hexavalent chromium, a known toxin and carcinogen, has been anticipated for years, new policies restricting its use were recently enacted and have further motivated the development of environmentally benign alternatives to CCCs.[1]

The use of cerium to inhibit the corrosion of high strength aluminum alloys was first reported in the 1980s. Hinton et al. exposed Al 7075-T6 substrates to aqueous saline solutions containing Ce^{3+} ions and observed a shift in polarization curves consistent with inhibition of the oxygen reduction reaction.[2] Exposing Al 7075-T6 substrates to aqueous Ce^{3+} solutions for times up to 160 hrs at open circuit potential reduced the corrosion current, increased the pitting potential, and produced a yellow cerium oxide film across the substrate surface.[3] Coating deposition was believed to proceed by the precipitation of cerium compounds onto cathodic sites (i.e., intermetallic compounds) because of an increase in the near-surface pH caused by oxygen reduction, hydrogen generation, and/or reduction of hydrogen peroxide. In particular, the presence of hydrogen peroxide in the coating solutions has been shown to dramatically increase the deposition rate of cerium-

based conversion coatings (CeCCs).[4,5] In addition to spontaneous spray and immersion techniques, CeCCs can also be deposited with current driven (i.e., electrolytic) methods.[3,6]

The performance of CeCCs depends on the processes used to deposit and modify the coating, such as surface activation prior to coating, [7] composition of the coating solution, [8] and post-treatment.[9,10] Acid and alkaline surface activations minimize the native oxide and expose intermetallic particles, facilitating interaction between the coating solution and the alloy substrate. By altering the chemistry at the alloy surface, the morphology, deposition rate, and performance of the coating is affected.[11] CeCCs are typically deposited from acidified, aqueous solutions that contain cerium chloride or cerium nitrate in combination with organic additives (e.g., gelatin) and/or hydrogen peroxide. The presence of gelatin has been shown to slow the deposition rate, producing a more uniform coating than when no gelatin is used.[12] In some cases, CeCCs are post-treated in an aqueous phosphate solution to improve the corrosion performance. This process has typically been performed by immersing the sample for 5 to 20 min in a solution of 2.5 to 3.0 wt% Na_3PO_4 heated to at least 80 °C.[13,14,15,16] The results indicated that phosphate post-treatment can convert the as-deposited nanocrystalline cerium species, (i.e., cerium hydroxides/peroxides), to hydrated $CePO_4$, which improved the corrosion resistance of the coating. Post-treated coatings in which hydrated $CePO_4$ formed were observed to have less cracking, lower corrosion currents (i_{corr}) and higher pitting potentials (E_{pit}).[9,10]

The present study uses an aqueous deposition method developed by Fair et al. to deposit hydrated $CePO_4$ directly onto Al 2024-T3 substrates.[17,18] The process combines

cerium citrate and phosphoric acid precursor solutions to precipitate the desired $CePO_4$ phase. The deposition conditions were varied in an attempt to alter the morphology and thickness of the coatings to mimic the characteristics of post-treated CeCCs, for which the $CePO_4 \cdot H_2O$ phase was formed via a phosphate post-treatment. The purpose of this study was to directly deposit $CePO_4$ coatings onto Al 2024-T3, evaluate their efficacy, and analyze the observed performance for comparison to post-treated, spray deposited CeCCs.

2. EXPERIMENTAL

2.1. Surface Cleaning and Activation

Prior to coating deposition, coupons of Al 2024-T3 (AMI Metals) measuring 3.8 cm x 7.6 cm coupons were cut from a larger sheet that was 0.81 mm thick. Alloy substrates were cleaned by wiping the surface with isopropyl alcohol, immersing the panel in a 5 wt. % solution of Turco 4215 NCLT for 5 minutes at 55 °C followed by a 25 second immersion in room temperature 0.5 wt. % HBF_4. For cerium-based conversion coatings (CeCCs), acid activation was performed with a 10 min immersion in a 50 °C solution of 1.0 wt. % H_2SO_4 in addition to isopropyl alcohol and Turco cleaning processes. The substrates were rinsed with deionized water after each step.

2.2. Directly Deposited $CePO_4$ Coatings

The solution used to prepare the directly deposited $CePO_4$ coatings consisted of two precursor solutions that were chilled to ≤ 5 °C before being mixed immediately prior to coating deposition. The first solution was comprised of a mixture of

$Ce(NO_3)_3 \cdot 6H_2O$ (Alfa Aesar, 99.5 %) and citric acid (Alfa Aesar, 99%), forming a cerium citrate complex, and the second was an aqueous solution of H_3PO_4. The concentrations and ratios of individual species were varied experimentally according to Table 1 to optimize the morphology and corrosion performance of the coatings. Precursor concentrations designed to yield 60 g/L $CePO_4$ were chosen for these experiments because the thickness of the resulting coating was 400 – 450 nm and most closely matched thicknesses of spontaneously spray deposited CeCCs.[11] The direct deposition process consisted of mixing equal parts of the precursors solutions, distributing a continuous film of coating solution across the substrate with a transfer pipette, and immersing the panel in a 50 °C water bath for ≈10 sec. Following deposition, coated surfaces were gently wiped to remove loosely bound precipitates and rinsed with deionized water. This process was repeated five times, after which specimens were allowed to dry in the ambient prior to analysis.

2.3. Cerium-based Conversion Coatings

Cerium-based conversion coatings were spontaneously deposited from aqueous solution via a spray technique that has been described previously.[11,19] The deposition solution was comprised of 220 g of deionized H_2O, 20 ml of H_2O_2, 10 g $CeCl_3 \cdot 7H_2O$, and 0.6 g of an organic gelatin (RDH, Rousselot). The solution was misted onto the panel surface for ≈3 seconds using a commercially available detail spray gun operated at ≈35 psi. Panels were allowed to drain for ≈30 seconds. The spray-drain process was repeated five times and then the specimens were rinsed using deionized water. The coated panels were then immediately post-treated by immersion in an 85 °C solution containing 2.5 wt.

% NaH_2PO_4 for 5 minutes. The specimens were again rinsed with deionized water and allowed to dry in the ambient.

2.4. Characterization

A Q-FOG cyclic corrosion tester (Q-Panel Lab Products) was used to test the corrosion resistance of the coatings according to ASTM B117. This test was conducted at 35 °C using a 5 wt. % NaCl solution. Polarization scans were performed using a model 273A potentiostat from Princeton Applied Research. Scans were conducted from -0.4 to +0.7 V with respect to open circuit potential using a scan rate of 1.5 mV/s. Electrochemical impedance spectroscopy (EIS) measurements were collected using a Schlumberger model SI1255 frequency response analyzer. Impedance spectra were collected from $1x10^{-2}$ to $1x10^{5}$ Hz using an AC amplitude of 10 mV. A Prince Applied Research model K0235 flat cell with an exposed specimen area of 1.0 cm^2 was used for all corrosion tests. The cell was allowed to stabilize for 750 seconds prior to the start of data collection. Each test was performed in a 1.5 wt. % NaCl electrolyte and used a saturated calomel electrode (SCE). Data fitting and analysis was performed using CView and ZView software (Scribner Associates).

A Helios NanoLab 600 dual beam system consisting of a focused ion beam (FIB) for selective material removal and a field emission scanning electron microscopy (FESEM) for imaging was used for analysis. A gallium ion source was used to used to selectively remove materials and produce cross section specimens. A Hitachi S570 SEM equipped with a LaB_6 electron source was used to perform routine analysis of coatings

morphology. Transmission electron microscopy was performed using a Philips CM200 operated at 200kV.

3. RESULTS AND DISCUSSION

Based on the conditions initially used by Fair et al., cerium phosphate coatings were deposited directly on Al 2024-T3 substrates from solutions designed to yield 5, 15, 30, or 60 g/L $CePO_4$ with a Ce:P:citrate ratio of 1:1:2.[17] Coatings deposited with the 5 g/L solution appeared to deposit slowly, with visible deposition only observed after multiple coatings cycles had been performed. Visual examination of coatings deposited from solutions designed to yield 15, 30, or 60 g/L $CePO_4$ indicated that the coating thickness increased with increasing $CePO_4$ in the deposition solution. Since the deposition times were the same for each coating, the thicker coatings corresponded to faster deposition rates. Deposition from the 5 g/L solution resulted in coatings with the least cracking as shown in Figure 1a. Coatings deposited from the 15, 30, and 60 g/L solutions exhibited similar morphologies and did not change significantly as a function of precursor concentration (Figure 1b – 1d). When the deposition solution was heated, precipitation appeared to occur uniformly throughout the solution and was not observed to preferentially precipitate on the alloy surface. Hence, the adhered coating was formed by precipitation of species in close proximity to the substrate with the majority of the remaining precipitate being removed during subsequent rinsing steps. Electron diffraction of the resulting coatings, Figure, indicated that hydrated $CePO_4$, rhabdophane or $CePO_4 \cdot H_2O$, was present. After 18 hours of salt spray exposure, corrosion pits and tails were evident across the panel surface for each of the directly deposited coatings as

shown in Figure. Coatings deposited from 5 g/L solutions exhibited less corrosion than coatings deposited with higher concentration solutions because they contained fewer cracks, thereby functioning as a better barrier coating.

The ratio of Ce, P, and citrate present in the precursors solutions was varied in an attempt to alter the deposition rate and/or morphology of the resulting coatings. These permutations did not have a significant effect on coating morphology (Figure) or corrosion performance (Figure). Coating solutions containing higher amounts of Ce and P were believed to have higher deposition rates based on visual observations of thicker $CePO_4 \cdot H_2O$ layers per coating cycle. Also, solutions with less citric acid exhibited faster precipitation compared to those with higher concentrations of citric acid, indicating that the $CePO_4 \cdot H_2O$ formation was slower from solutions containing the cerium citrate complex as compared to free Ce^{3+} ions. To some extent this allows control of the precipitation rate, which can be used to slow deposition and produce coatings with less noticeable cracking as citrate concentration is increased, Figurea – 4c. Changing the relative concentrations of cerium and phosphate in the solution influenced the observed deposition rate more strongly than citrate concentration, with higher concentration of phosphoric acid resulting in significantly faster (and less controlled) precipitation. In addition, higher phosphate contents resulted in coating morphologies that exhibited larger cracks and even some spalling of the coating, Figuref. These changes in morphology did not have a significant impact on the corrosion performance of the directly deposited $CePO_4$ coatings. Despite their poor corrosion performance, the $CePO_4 \cdot H_2O$ coatings had uniform morphology across the alloy substrate surfaces.

The morphology of spontaneously spray deposited CeCCs was less uniform than the directly deposited coatings. Approximately 90 % of the surface of phosphate post-treated conversion coatings contained fine (< 150 nm wide), or no, cracks whereas the remaining 10 % exhibits larger cracks that had widths > 1 μm. However, these CeCCs provide significant corrosion protection. Previous studies have shown that CeCCs prepared using similar conditions can withstand up to 336 hours of salt spray exposure without exhibiting significant corrosion pits or tails.

Polarization and EIS data were collected from directly deposited coatings, bare Al 2024-T3, and a post-treated CeCC. Representative polarization scans are shown in Figure 6 and a summary of values measured by fitting polarization and impedance data is included as Table 2. Just as varying the direct deposition process parameters had little effect on corrosion performance, no large differences in total resistance, corrosion current, or pitting potential were observed among the directly deposited specimens. Compared to the bare Al 2024-T3 substrate, directly deposited $CePO_4$ coatings had a small influence on electrochemical properties, increasing the total resistance by only 2 – 6 times, from 1.1 kΩ cm^2 to 2.1 – 6.9 kΩ cm^2. However, neither the measured corrosion current densities (≈2 μA/cm^2 to ≈4 μA/cm^2) nor the pitting potentials (≈-570 mV) changed significantly. The increased total resistance may correspond to partial coverage of the substrate or fewer defects in the coating, but the changes did not have a significant effect on corrosion performance. For comparison, parallel measurements collected from CeCCs showed a six-fold increase in total resistance compared to directly deposited $CePO_4$ coatings on average (from ≈4 kΩ cm^2 to ≈24 kΩ cm^2), a corresponding decrease in the corrosion current (≈2.5 μA/cm^2 to ≈0.45 μA/cm^2), and pitting potentials that were

approximately 30 mV more anodic. The improved electrochemical properties of CeCCs correlate to improved corrosion performance such as during ASTM B117 salt spray corrosion testing used in this study. Post-treated CeCCs are consistently able to withstand at least 168 hours of salt spray exposure without exhibiting corrosion pits or tails, whereas directly deposited $CePO_4$ coatings show extensive corrosion after only 18 hours.

The lack of corrosion inhibition of directly deposited $CePO_4$ coatings is attributed to the deposition mechanism, which is primarily driven by a change in temperature rather than pH or surface chemistry as is the case with CeCCs. The temperature driven mechanism operates independently of localized chemical or electrochemical gradients and, therefore, does not exhibit preferential deposition near active sites. As a consequence, local cathodes distributed throughout the alloy matrix may, or may not, have been adequately covered during coating deposition. In contrast, deposition of CeCCs relies on electrochemical interactions with the substrate to precipitate cerium compounds. Initial deposition of CeCCs occurs on or near intermetallic particles (serving as local cathodes) before spreading to cover the remaining substrate.[20,21] In part, the corrosion protection provided by CeCCs is via a barrier mechanism in which the oxygen reduction reaction is inhibited by the selective deposition of cerium compounds onto local cathodes. However, CeCCs commonly have defects such as surface cracking and subsurface crevices.[22] These features expose localized areas of the substrate that should be susceptible to corrosion, similar to a directly deposited coating that only partially covers a localized, electrochemically active area.

Cross-sectional analysis of directly deposited $CePO_4$ coatings and post-treated CeCCs after salt spray exposure revealed that the two coatings exhibited significantly different responses to corrosive environments, Figure and 8. For directly deposited coatings, exposed areas at the base of cracks that extended to the substrate showed evidence of pit initiation at the crack/substrate interface as well as the formation of corrosion product beneath the coating adjacent to the cracks. Corrosion products were also evident on the surface of the coatings as a highly porous, fibrous layer rich in aluminum and oxygen. The coating/substrate interface farthest from the cracks remained unchanged, suggesting that the directly deposited coatings functioned as barriers. While cracks in the post-treated CeCC also extended to the substrate, no signs of pitting corrosion were observed at the crack/substrate interface after seven days of salt spray exposure and no visible evidence of corrosion was evident on the specimen surface. Furthermore, a 60 – 100 nm thick layer had formed at the CeCC/substrate interface. The CeCCs appear to be capable of providing protection by reacting to the corrosive environment and protecting areas of the substrate exposed by defects in the coating. Likewise, chromate based conversion coatings provide excellent protection and release hexavalent chromium ions that reduce to form a hydrated Cr(III) oxide on electrochemically active sites, thereby protecting limited areas of exposed substrate. This interfacial reaction layer is believed to improve the corrosion performance of CeCCs and demonstrates that post-treated CeCCs are not acting solely as inert barriers, but respond to the salt spray environment.

Analysis of the interfacial reaction layer by EDS did not reveal the presence of phosphorous, but rather showed its composition to consist predominately of Ce, Al,

and O. The mechanism by which the interfacial layer formed during corrosion testing is not understood, but the layer has been observed only in CeCCs subjected to a phosphate post-treatment. It is theorized that the formation process may be sensitive to changes in the local pH, facilitating the reaction between cerium and aluminum hydroxide species to potentially form a thermodynamically favorable cerium aluminate phase. Analysis by EDS also suggests that chloride ions from the deposition process may have been trapped at the CeCC/substrate interface during the initial stages of coating formation. The residual chloride ions, or the introduction of chloride ions at the coating/substrate interface during salt spray exposure, may act to destabilize the aluminum oxides and/or hydroxides present near the interface, facilitating reaction with neighboring cerium species. Post-treatment transforms many of the cerium hydroxy/peroxy species present after coating deposition to $CePO_4 \cdot H_2O$, and prior analysis has suggested nearly complete reduction of Ce(IV) species to hydrated Ce(III) phosphate at the surface.[10] However, post-treated CeCCs did not exhibit a uniform rhabdophane phase throughout the coating thickness, but rather exhibited heterogeneity of structures and compounds (e.g., unconverted cerium hydroxy/peroxy species and cerium hydrogen phosphate species) that may be metastable.[23] These compounds may be predisposed to react with neighboring species during salt spray exposure, acting to protect exposed areas of the substrate, whereas a uniform $CePO_4 \cdot H_2O$ coating containing only the rhabdophane phase (i.e., directly deposited $CePO_4$ coatings) would remain unchanged under the same conditions, responding like a static barrier coating by only protecting areas of the substrate that were coated.

4. CONCLUSIONS

Cerium phosphate coatings were deposited onto Al 2024-T3 substrates from aqueous solutions. The morphology and corrosion performance of the coatings was not influenced by the composition of the precursor solutions. After 18 hours of salt spray exposure, directly deposited $CePO_4$ coatings exhibited corrosion pits and tails across much of the specimen surface for all deposition conditions. Electrochemical analysis corresponded to observed performance after salt spray corrosion testing and revealed that the coatings did not significantly alter the electrochemical properties of the substrate. The average impedance of directly deposited coatings was ≈4 kΩ cm^2, six times smaller than that for post-treated CeCCs (≈24 kΩ cm^2). CeCCs also exhibited correspondingly lower corrosion current densities and pitting potentials that were ≈30 mV more anodic than measured from the directly deposited coatings. Analysis in cross-section revealed that corrosion pits had formed at crack/substrate interfaces in directly deposited specimens after 3 days of salt spray exposure, which suggested that the coating functioned as an inert barriers by providing corrosion protection only to areas of the substrate that were covered by the coating. CeCCs, however, were able to protect areas of the substrate that were exposed by cracks through the coating from pit formation for at least seven days of salt spray exposure.

An interfacial reaction layer comprised of Ce, Al, and O formed between the CeCC and substrate during corrosion testing. The formation or growth of this layer during corrosion testing demonstrates that post-treated CeCCs exhibit an active response to corrosion that may control corrosion protection. Furthermore, the presence of the $CePO_4 \cdot H_2O$ phase does not guarantee corrosion protection. Instead, the heterogeneity of

species/compounds believed to be present in the CeCC (e.g., cerium hydroxides/peroxides or potentially metastable cerium hydrogen phosphate species), may be more conducive to react with neighboring aluminum containing species to generate an interfacial region that provides corrosion protection. A homogeneous, stable, $CePO_4 \cdot H_2O$ coating like that generated during the direct deposition process is unlikely to exhibit this type of response.

ACKNOWLEDGMENTS

The authors acknowledge the technical assistance of Ming Zhang and Elizabeth Kulp at the Missouri University of Science and Technology. Assistance with TEM analysis by Randall Hay at the Air Force Research Laboratory at Wright Patterson Air Force Base was also appreciated. The authors also acknowledge the technical guidance and support of Bruce Sartwell at the Strategic Environmental Research and Development Program (SERDP). This work was funded through SERDP under contract W912HQ-08-C-0008.

REFERENCES

1. OSHA 29 CFR Part 1910.1026, available from http://www.osha.gov/, 6 July 2010.
2. B.R.W. Hinton, D.R. Arnott, and N.E. Ryan, *Met. Forum*, **7**(4), 211-217 (1984).
3. B.R.W. Hinton, D.R. Arnott, and N.E. Ryan, *Mat. Forum*, **9**(3), 162-173 (1986).
4. A.E. Hughes, R.J. Taylor, B.R.W. Hinton, and L. Wilson, *Surf. Interface Anal.*, **23**, 540-550 (1995).
5. F.H. Scholes, C. Soste, A.E. Hughes, S.G. Hardin, P.R. Curtis, *Appl. Surf. Sci.*, **253**(4), 1770-1780 (2006).

6. J. Stoffer, T. O'Keefe, S. P. Sitaram, P. Yu, X. Lin, E. L. Morris, U.S. Patent 5,932,083, issued Aug. 3, 1999.

7. B. Hinton, A. Hughes, R. Taylor, M. Henderson, K. Nelson, and L. Wilson, *ATM Metallurgie*, **37**(2), (1997).

8. S. Geng, P. Yu, M.J. O'Keefe, W.G. Fahrenholtz, and T.J. O'Keefe, *J. Appl. Electrochem.*, **40**(3) 551-559 (2010).

9. D.K Heller, W.G. Fahrenholtz, M.J. O'Keefe, *J. Electrochem. Soc.*, **156**(11), C400 - C406 (2009).

10. D.K Heller, W.G. Fahrenholtz, M.J. O'Keefe, *Corr. Science*, **52**(2), 360-368, (2009).

11. W. Pinc, S. Geng, M. O'Keefe, W. Fahrenholtz, T. O'Keefe, *App. Surf. Sci.*, **255**, 4061-4065 (2009).

12. W. Pinc, P. Yu, M. O'Keefe, W. Fahrenholtz, *Surf. Coat. Tech.*, **203**, 3533-3540 (2009).

13. B.Y. Johnson, J. Edington, M.J. O'Keefe, *Mat. Sci. and Engr.*, **A361**, 225-231 (2003).

14. B. F. Rivera, B.Y. Johnson, M.J. O'Keefe, W.G. Fahrenholtz, *Surf. Coat. Technol.*, **176**, 349-356 (2004).

15. H. Zhang, Y. Zuo, *Appl. Surf. Sci.*, **254**, 4930 (2008).

16. S. You, P. Jones, A. Padwal, P. Yu, M. O'Keefe, W. Fahrenholtz, T. O'Keefe, *Mat. Letters*, **61**, 3778-3782 (2007).

17. G.E. Fair, R.S. Hay, E.E. Boakye, *J. Am. Ceram. Soc.*, **91**(7), 2117-2123 (2008).

18. G.E. Fair, R.S. Hay, E.E. Boakye, *J. Am. Ceram. Soc.*, **91**(5), 1508-1516 (2008).

19. B.Y. Johnson, J. Eddington, A. Williams, M.J. O'Keefe, *Mat. Char.*, **54**, 41-28 (2005).

20. A.E. Hughes, J.D. Gorman, P.R. Miller, B.A. Sexton, P.J.K. Paterson, R.J. Taylor, *Surf. Interface Anal.*, **36**, 290-303, (2004).

21. P. Campestrini, H. Terryn, A. Hovestad, J.H.W. de Wit, *Surf. Coat. Tech.*, **176**, 365-381 (2004).

22. W. Pinc, S. Maddela, M. O'Keefe, W. Fahrenholtz, accepted for publication in *Surf. Coat. Tech.* on 24 May 2010.

23. D.K Heller, W.G. Fahrenholtz, G.E. Fair, M.J. O'Keefe, to be submitted to *Surf. Coat. Tech.*

Table 1. Composition of solutions for directly deposited $CePO_4$ coatings.

Concentration (g/L), (Ce:P:Citrate)	**Solution 1**		**Solution 2**
	$Ce(NO_3)_3 \cdot 6H_2O$ (g)	**Citric Acid (g)**	**H_3PO_4 (g)**
5, (1:1:2)	0.924	0.817	0.245
15, (1:1:2)	2.771	2.452	0.735
30, (1:1:2)	5.541	4.903	1.470
60, (1:1:2)	11.082	9.807	2.940
60, (1:0.5:0.5)	11.082	2.452	1.470
60, (1:0.5:2)	11.082	9.807	1.470
60, (1:1:1)	11.082	4.903	2.940
60, (1:1:0.5)	11.082	2.452	2.940
60, (1:2:2)	11.082	9.807	5.881

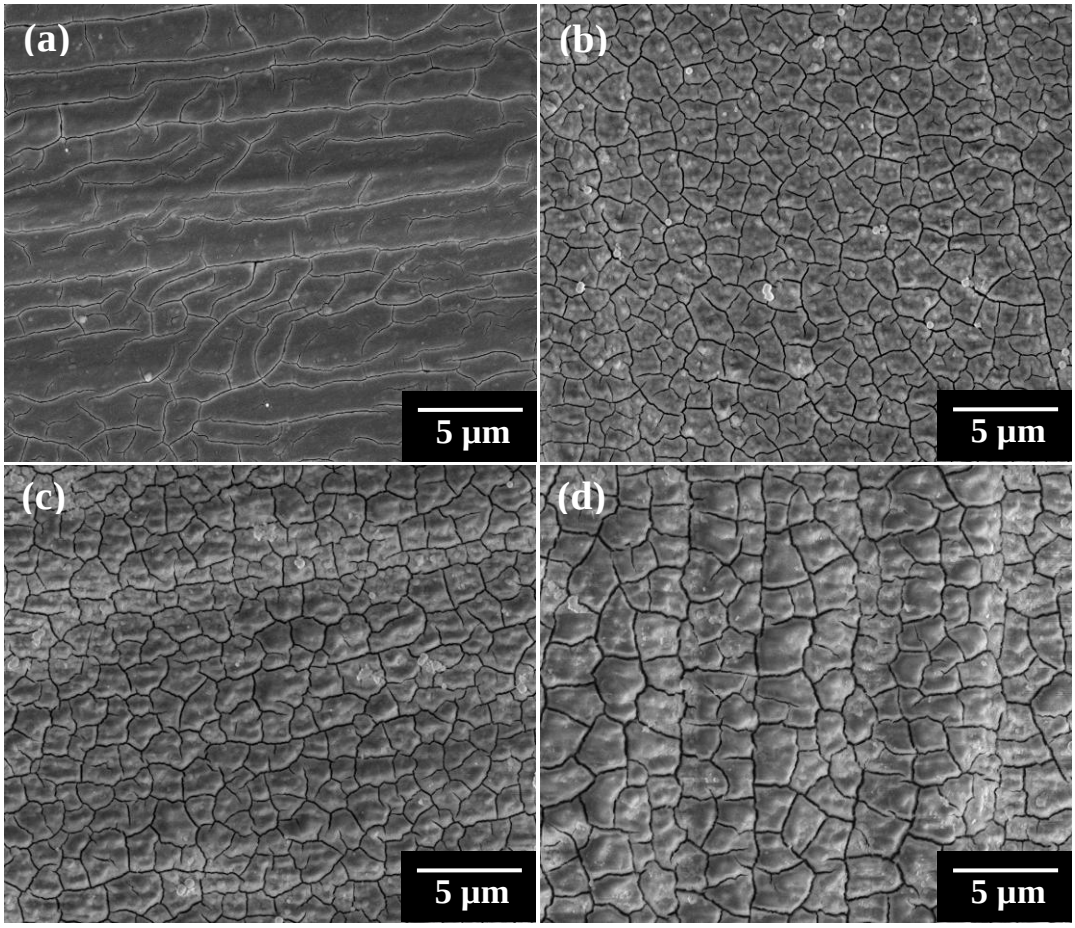

Figure 1. Surface morphology of directly deposited $CePO_4$ coatings produced using precursor solutions designed to yield (a) 5, (b) 15, (c) 30, and (d) 60 g/L $CePO_4$.

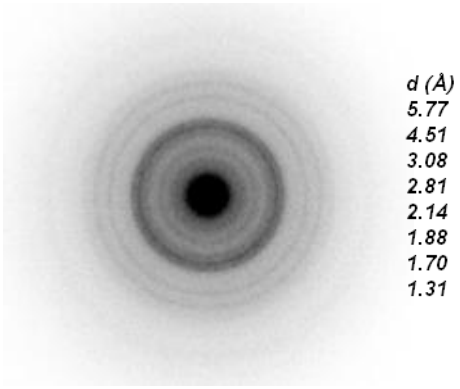

Figure 2. Electron diffraction ring pattern observed from a directly deposited $CePO_4$ coating. The ring pattern is indicative of hydrated $CePO_4 \cdot H_2O$, rhabdophane (PDF 35-0614).

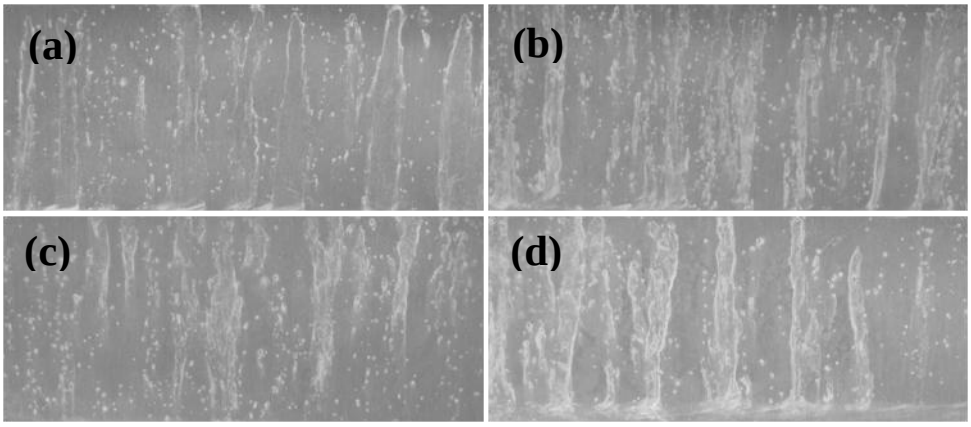

Figure 3. Directly deposited $CePO_4$ coatings after 18 hours of salt spray exposure, (a) 5 g/L, (b) 15 g/L, (c) 30 g/L, (d) 60 g/L. The tested areas shown for the panels measure about 2.5 cm x 6.5 cm.

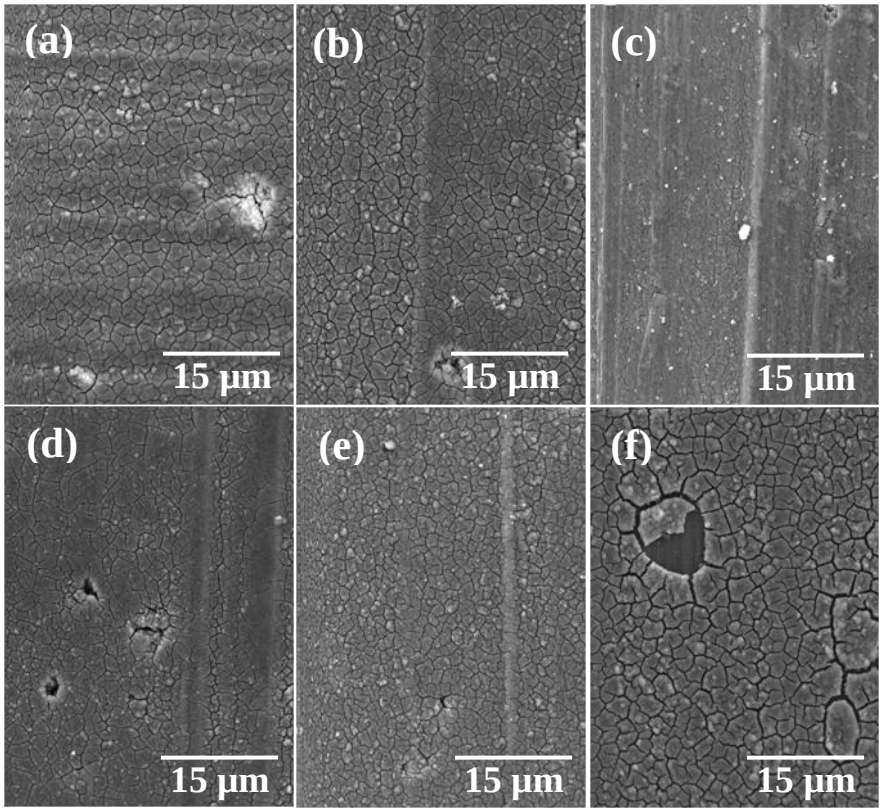

Figure 4. Surface morphology of directly deposited $CePO_4$ coatings deposited with different ratios of Ce:P:citrate in the precursor solutions, (a) 1:1:0.5, (b) 1:1:1, (c) 1:1:2, (d) 1:0.5:2, (e) 1:0.5:0.5, and (f) 1:2:2

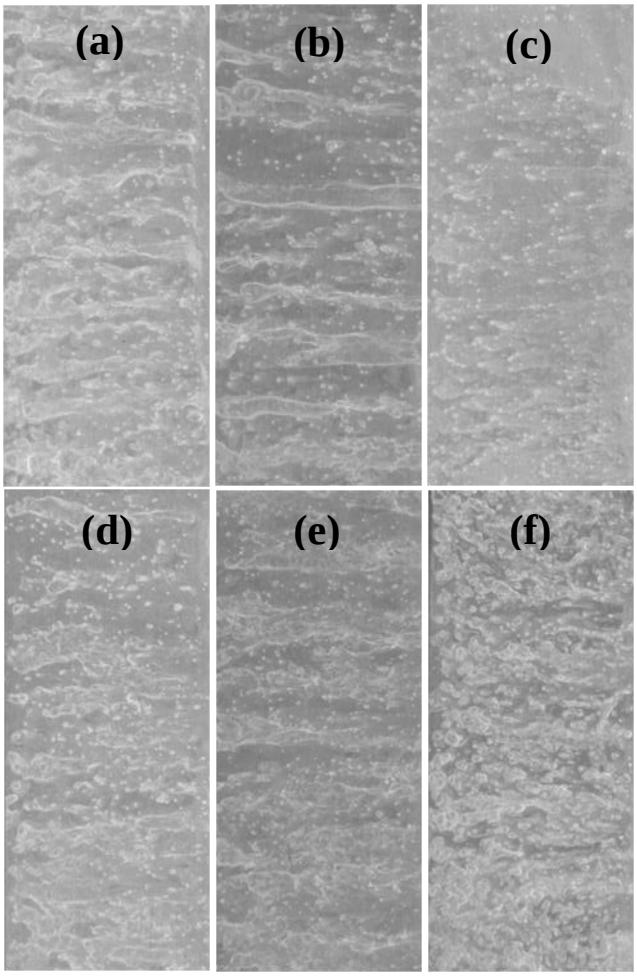

Figure 5. Directly deposited coatings (60 g/L $CePO_4$) after 18 hours of salt spray exposure, (a) 1:1:0.5 (Ce:P:citrate), (b) 1:1:1, (c) 1:1:2, (d) 1:0.5:2, (e) 1:0.5:0.5, (f) 1:2:2. The tested areas shown for the panels measure about 2.5 cm x 6.5 cm.

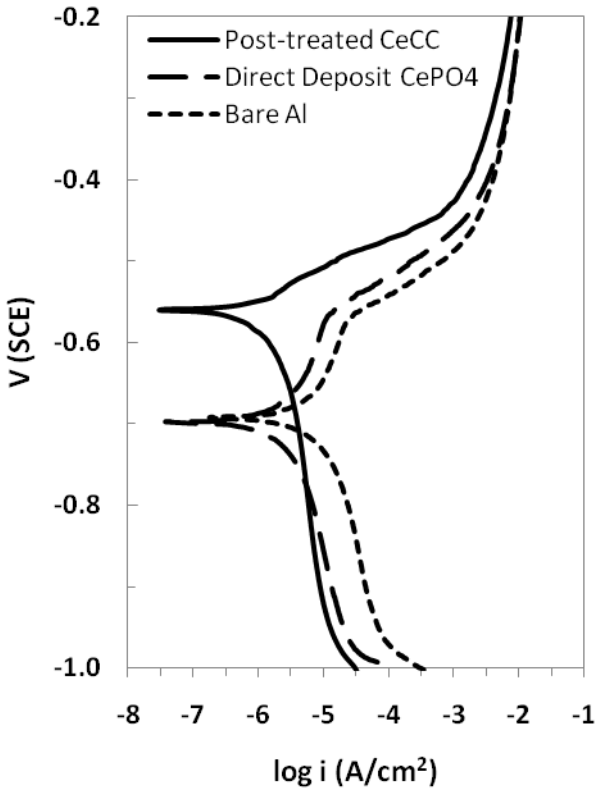

Figure 6. Representative polarization scans of bare Al 2024-T3, directly deposited $CePO_4$, and post-treated CeCC.

Table 2. Summary of electrochemical properties measured from bare Al 2024-T3, directly deposited $CePO_4$ coatings, and post-treated CeCCs.

	R_p (kΩ cm^2)	E_{corr}, mV(SCE)	i_{corr} (μA/cm^2)	E_{pit}, mV(SCE)
Bare	1.16	-695	3.93	-573
5 g/L	2.45	-697	3.36	-583
15 g/L	5.55	-727	4.07	-568
30 g/L	5.66	-709	2.72	-578
60 g/L	6.93	-693	1.53	-565
1:0.5:0.5	6.94	-711	1.19	-575
1:0.5:2	2.13	-716	3.66	-577
1:1:1	4.82	-716	2.65	-573
1:1:0.5	3.59	-693	2.76	-585
CeCC	24.4	-567	0.466	-548

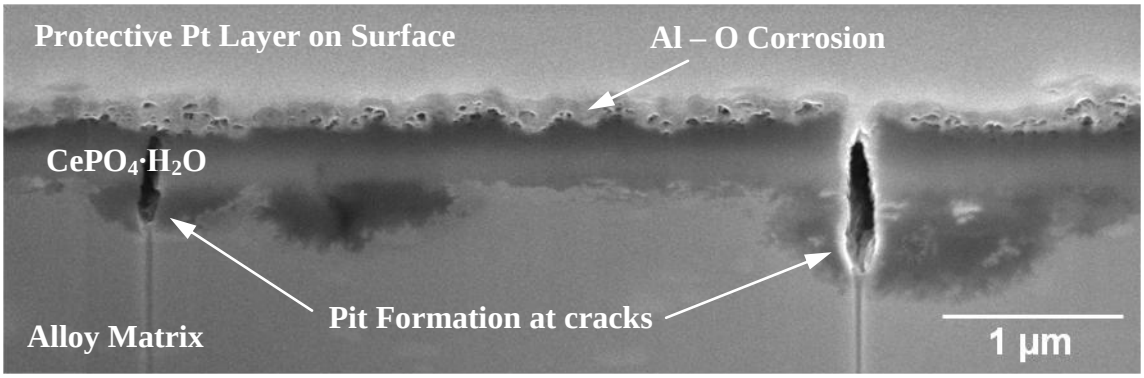

Figure 7. Cross-sectional montage of a directly deposited $CePO_4$ coating after 3 days of salt spray exposure. Image is a cross-section of a bulk specimen viewed 45° from the sample surface.

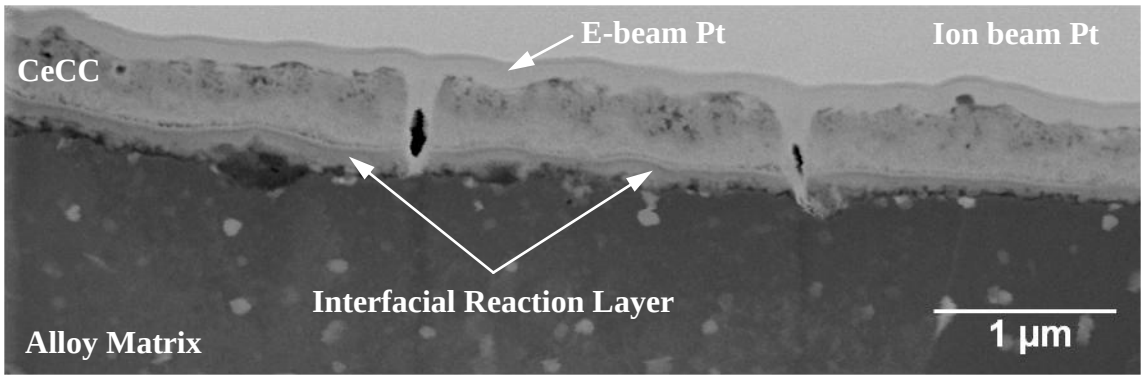

Figure 8. Cross-sectional montage of a phosphate post-treated CeCC after 7 days of salt spray exposure imaged in STEM/HAADF mode.

V. CHEMICAL AND STRUCTURAL ANALYSIS OF SUBSURFACE CREVICES FORMED DURING SPONTANEOUS DEPOSITION OF CERIUM-BASED CONVERSION COATINGS

Daimon K Heller, William G. Fahrenholtz, Matthew J. O'Keefe

[a]Materials Research Center, Department of Materials Science and Engineering, Missouri University of Science and Technology, Rolla, MO 65409, USA

ABSTRACT

Subsurface crevices formed during the deposition of cerium-based conversion coatings (CeCCs) were analyzed in cross-section to assess the effect of deposition and post-treatment on the structure and chemistry of phases present. An Al-O containing phase, believed to be amorphous $Al(OH)_3$, was formed in as-deposited CeCC specimens during coating deposition. Analysis by energy dispersive spectroscopy (EDS) revealed the presence of up to 1.6 at. % chlorine within this phase, a product of soluble chlorides that were present in the CeCC coating solution. Cerium was not detected within crevices. After post-treatment in an 85 °C aqueous phosphate solution, the chloride concentration was reduced to 0.15 – 0.30 at. % and electron diffraction in the $Al(OH)_3$ phase produced ring patterns, indicating the phase had crystallized. Some patterns could be indexed to gibbsite ($Al(OH)_3$), but others are believed to be a combination of hydrated aluminum hydroxides and/or oxides. An aluminum phosphate phase was not identified. Separately

from its affect on CeCCs, phosphate post-treatment improved the corrosion resistance of CeCC specimens by acting to crystallize an $Al(OH)_3$ phase present on crevice surfaces and by reducing the chloride concentration.

INTRODUCTION

Significant advances in cerium-based conversation coating (CeCC) technology have been made over the past 25 years. The initial CeCCs deposited by Hinton et al. were based on $Ce(NO_3)_3$ solutions and required immersion times in excess of 160 hrs to establish complete coverage of the substrate and provide significant corrosion protection to Al 7075-T6.[1,2] The stability of cerium species in aqueous solution is strongly dependent on pH. Above a pH threshold near 6, Ce^{3+} ions oxidize and precipitate as $Ce(OH)_4$, a dark orange species which transitions over time to $CeO_2 \cdot 2H_2O$, a pale yellow species.[3] The mechanism of CeCC deposition has been shown to proceed by the precipitation of cerium compounds onto local cathodes (i.e., intermetallic particles), where it spreads to cover the alloy matrix.[4] Galvanic potentials between Cu-containing intermetallic particles and the aluminum alloy matrix drive the electrochemical oxidation of aluminum in the presence of an electrolyte, releasing electrons to local cathodes where they reduce water to form hydroxide ions and hydrogen gas. This reaction causes the local pH increase that drives the precipitation of cerium compounds. More modern deposition solutions contain hydrogen peroxide, which has been shown to significantly increase the deposition rate of CeCCs.[5] Since H_2O_2 is easily reduced to form hydroxide ions and oxygen gas, it facilitates the creation of a local pH gradient and acts to oxidize Ce^{3+} ions.

The deposition rate is also dependent on the type of cerium salt.[6] In the presence of a non-aggressive electrolyte (e.g., solutions based on $Ce(NO_3)_3$), deposition is effectively limited by the rate of aluminum oxidation and may require several hours to form a coating capable of providing corrosion protection even when H_2O_2 is present. However, using $CeCl_3$ based solutions in conjunction with H_2O_2 provides complete coverage of an Al 2024-T3 substrate in less than one minute. In this case, chloride ion attack causes increased aluminum dissolution, thereby increasing the amount of H_2O_2 that is reduced to form hydroxide ions, and quickly establishes the pH gradient necessary for deposition to occur. The aggressive dissolution of aluminum during CeCC deposition from solutions containing both soluble chlorides and hydrogen peroxide produces crevices in the aluminum alloy that can penetrate up to 10 μm into the substrate.[7] These features typically occur on approximately 10 % of the substrate and are consistently located beneath regions of CeCCs that exhibit cracks > 1 μm wide. The remaining 90 % of the coating exhibits fine cracks < 150 nm wide and do not have subsurface crevices.

Immediately following deposition, CeCCs are commonly post-treated in a heated phosphate solution to improve their corrosion resistance. Post-treated CeCCs consistently withstand at least one week of salt spray exposure without exhibiting corrosion pits or tails, whereas as-deposited CeCCs with less than 3 days of exposure exhibit extensive corrosion across the panel surface. Post-treatment has been shown to minimize the formation of cracks in the coating and transform the as-deposited cerium hydroxy and peroxy species to hydrated $CePO_4$. A reduction of cracks in the coating and the formation of the $CePO_4 \cdot H_2O$ phase improves the barrier properties of the coating.[8] More recent results demonstrate that post-treated CeCCs exhibit an active response to

corrosion through structural transitions and the formation of an interfacial reaction layer during salt spray exposure.[9]

Aside from the spontaneous deposition process described above, CeCCs can also be deposited by electrolytic methods. Since these processes are current driven, extensive aluminum dissolution did not occur during deposition and subsurface crevices were not observed. In work performed by Pinc et al., subsurface crevices were introduced separately from coating deposition to determine how their presence affected corrosion performance.[10] This was accomplished by spraying an Al 2024-T3 substrate, to which an electrodeposited CeCC had been applied and post-treated, with a solution of NaCl and H_2O_2. The solution attacked the alloy in localized regions that were exposed by cracks in the CeCC and formed crevices similar to those that were formed during spontaneous deposition processes from $CeCl_3$ and H_2O_2. Specimens treated with the NaCl and H_2O_2 solution exhibited visible corrosion after 3 days of salt spray exposure. However, if the specimens were subjected to a second post-treatment (after the introduction of crevices), the corrosion resistance was fully restored.

This study examines how phosphate post-treatment affects the chemistry and structure of subsurface crevices by analyzing as-deposited and post-treated CeCCs in cross-section.

EXPERIMENTAL

CeCCs were deposited onto Al 2024-T3 (AMI Metals) substrates cut to 3.8 cm by 7.6 cm from a larger sheet that was 0.81 mm thick. Prior to deposition, the substrate surfaces underwent cleaning and activation process. A laboratory wiper soaked in

isopropyl alcohol was used to remove contaminants from the surface. Afterwards, the panels were then rinsed in tap water and immersed in a 55 °C aqueous solution of a commercial alkaline cleaning agent (Turco 4215 NCLT). After rinsing with deionized water, the substrates were acid activated in a 1.0 wt. % aqueous solution of H_2SO_4 for 10 min, rinsed with deionized water, and set aside for coating deposition.

The coating solution was prepared by dissolving 10 g $CeCl_3 \cdot 7H_2O$ (99.9 %, Alfa Aesar) into 195 g of deionized water and adjusting the pH to 2.1 with HCl. Then, 0.6 g of gelatin (RDH, Rousselot) was dissolved in 25 g of deionized water and added the $CeCl_3$ solution. Just prior to deposition, 20 ml of H_2O_2 (ACS 30 %, Fisher) was added. The panels were coated with a spray process using a commercially available detail spray gun operated at 35 psi. The CeCCs were deposited with five spray – drain cycles. Each cycle consisted of misting the coating solution onto the panel surface for several seconds and allowing 30 seconds for it to drain. Post-treatment was performed by immediately immersing the CeCC specimen into an 85 °C aqueous solution of 2.5 wt. % NaH_2PO_4 for 5 minutes.

Transmission electron microscopy (TEM) specimens were prepared with a dual beam system (Helios NanoLab 600, FEI) equipped with a focused ion beam (FIB) milling system and a scanning electron microscopy (SEM) column. Using a Ga ion source, areas of the specimen were selectively milled to enable a micromanipulator to lift out and mount TEM specimens onto Cu grids for subsequent analysis. The Ga rich layer indicated on the surface of crevices is an artifact caused by ion milling during specimen preparation. An Oxford X-Max Silicon Drift Detector was used to perform energy

dispersive spectroscopy at an accelerating voltage of 30 kV. Electron diffraction patterns were collected with a Philips CM200 TEM operated at 200 keV.

RESULTS AND DISCUSSION

The spontaneous deposition of CeCCs from coating solutions containing soluble chlorides and H_2O_2 formed subsurface crevices in the alloy substrate. Cross-section microscopy showed that these areas are exposed to the surface through cracks in the CeCCs. Additional EDS analyses indicated that no cerium was present on crevice surfaces, consistent with previous analyses.[7] Since these regions were not protected by CeCCs, areas containing crevices should be more susceptible to the formation of stable pits, which would lead to visible corrosion of the specimen. Because subsurface crevices are formed during CeCC deposition, they were present in as-deposited and post-treated CeCCs. As-deposited coatings contained visible corrosion pits and salt tails after 3 days of salt spray exposure, but post-treated CeCCs have been shown to withstand up to 14 days of salt spray exposure without exhibiting visible corrosion. The significant improvement in the corrosion resistance of CeCCs after phosphate post-treatment has been attributed to factors that affect barrier properties (i.e., minimization of cracks and the formation of $CePO_4 \cdot H_2O$ within the coating) as well as characteristics that indicated active corrosion inhibition (i.e., structural changes and interfacial layer formation) during salt spray exposure.[8,9] Cross-sectional analyses of as-deposited and post-treated CeCC specimens indicated that post-treatment also affects subsurface crevices, increasing the corrosion resistance of crevices separately of its affect on CeCCs.

Localized subsurface crevices in an as-deposited CeCC specimen are shown below as Figure 1. A FESEM/FIB equipped with a STEM detector was used to collect cross-sectional images and perform chemical mapping. As labeled in the figure, an Al-O containing phase was present on the crevice surface. In as-deposited specimens, electron diffraction patterns from this phase did not exhibit diffracted spots or rings (Figure 2a), indicating it was structurally amorphous. A previous investigation has shown that the combination of soluble chlorides and hydrogen peroxide species aggressively etches the aluminum alloy substrate during coating formation.[7] This etching introduces Al^{3+} ions into the near surface environment where the estimated pH is > 5 based on the precipitation of Ce species. Under these conditions, the formation of an $Al(OH)_3$ gel-like phase is favored.[11,12] The amorphous $Al(OH)_3$ phase present in regions containing subsurface crevices in as-deposited specimens was also found to contain up to 1.6 at. % Cl. In an aqueous environment, chloride ions will act to destabilize the aluminum hydroxide structure, providing a plausible explanation for the accumulation of aluminum corrosion product on the coating surface that has been reported elsewhere.[13] Earlier studies examining the corrosion of nominally pure aluminum by water reported that amorphous aluminum hydroxide exhibited the highest solubility in water compared to other crystalline forms of hydrated aluminum oxides/hydroxides such as boehmite, bayerite, or gibbsite.[12] A detailed study of the hydration of passive oxide films on aluminum is available elsewhere.[14]

Analysis of the Al-O phase inside crevices of specimens that were post-treated in an orthophosphate solution at 85 °C for 5 min revealed several differences. For post-treated specimens, electron diffraction within the $Al(OH)_3$ phase produced ring patterns

(Figures 2b and 2c), indicating this phase crystallized during post-treatment. Analysis by EDS, shown in Figure 3, suggested that processes active during post-treatment removed the majority of chlorine from these regions, reducing the detected concentration to 0.15 – 0.30 at. %. Since as-deposited and post-treated specimens were cross-sectioned in the same manner (i.e., FIB milling), the difference in chlorine concentration was not an artifact of sample preparation. The reduced chlorine concentration may help explain the increased pitting potentials observed from post-treated coatings since the concentration of chlorine in aluminum oxide/hydroxide films is inversely proportional to pitting potential (i.e., lower chloride concentrations correspond to more anodic pitting potentials).[15,16] Some of the diffraction patterns of the crystallized phase match closely to that of gibbsite, a crystallized form of $Al(OH)_3$. However, the structure of the phase located on crevices surfaces was not uniform, and probably consists of various forms of hydrated aluminum hydroxides and/or oxides. None of the diffraction patterns matched aluminum phosphate phases, nor did EDS analysis indicate the presence of phosphorus. The structural transition of amorphous $Al(OH)_3$ to transition aluminas upon exposure to aqueous environment appears to be consistent with other data reported in literature.[17,18] Hart investigated the phase of films formed on aluminum after exposure to pure water at temperatures of 25 – 100 °C. A critical temperature near 65 °C was defined, above which, the developed films consisted only of boehmite and below which growth of the oxide film was believed to progress from an amorphous film, to boehmite, and finally bayerite. Therefore, it appears reasonable for amorphous aluminum hydroxide that formed during CeCC deposition to be at least partially crystallized during exposure to 85 °C aqueous phosphate solution. During extended exposure to salt spray environment

this phase may slowly transform to the boehmite or bayerite structure. Compared to an amorphous $Al(OH)_3$ layer, a crystalline layer should have fewer defects and function as an improved barrier coating, thus improving corrosion resistance.

When analyzed in conjunction with the data reported by Pinc et al. that was described earlier,[10] it can be concluded that the effect of post-treatment on subsurface crevices has a significant impact on corrosion resistance that is separate of its affect on the CeCC. By introducing crevices into an electrodeposited CeCC specimen (which does not form crevices during deposition), the corrosion performance is adversely affected by the formation of an amorphous $Al(OH)_3$ phase that containing chlorine. This effectively generates regions that are more susceptible to corrosion, significantly reducing the corrosion resistance of the specimen. Since phosphate post-treatment restores the corrosion resistance of these specimens, the mechanism of restoration appears to be a result of the reduced chloride concentrations and $Al(OH)_3$ crystallization observed within crevices after post-treatment.

CONCLUSIONS

Cross-sectional analyses of subsurface crevices formed during the spontaneous deposition of CeCCs revealed that post-treatment affected the composition and structure of regions within crevices. As-deposited specimens contained an Al-O layer on crevice surfaces, believed to be an amorphous, gel-like $Al(OH)_3$ that formed when Al ions were introduced to the near surface alkaline environment present during coating deposition. While comprised predominately of Al and O, this phase also contained up to 1.6 at. % chlorine. After post-treatment, the concentration of chlorine decreased to 0.15 –

0.30 at. % and electron diffraction in the $Al(OH)_3$ phase revealed that the Al-O layer had at least partially crystallized into gibbsite and/or other hydrated aluminum oxides or hydroxides. These changes are believed to have improved the corrosion protection of CeCC specimens in two ways. First, the crystallized $Al(OH)_3$ phase should act as a more effective barrier to corrosive species, and second, the reduced chloride concentrations should shift the pitting potential to more anodic values.

ACKNOWLEDGMENTS

The authors appreciate conversations with Geoff Fair and assistance with TEM analysis by Randall Hay at the Air Force Research Laboratory at Wright Patterson Air Force Base. The technical assistance of Ming Zhang and Elizabeth Kulp at the Missouri University of Science and Technology is also acknowledged. The authors also acknowledge the technical guidance and support of Bruce Sartwell at the Strategic Environmental Research and Development Program (SERDP). This work was funded through SERDP under contract W912HQ-08-C-0008.

REFERENCES

1. B.R.W. Hinton, D.R. Arnott, N.E. Ryan, "The Inhibition of Aluminium Alloy Corrosion by Cerous Cations," *Met. Forum*, **7**(4), 211-217 (1984).

2. B.R.W. Hinton, D.R. Arnott, N.E. Ryan, "Cerium Conversion Coatings for the Corrosion Protection of Aluminium," *Mat. Forum*, **9**(3), 162-173 (1986).

3. P. Yu, S.A. Hayes, T.J. O'Keefe, M.J. O'Keefe, J.O. Stoffer, "The Phase Stability of Cerium Species in Aqueous Systems," *J. Electrochem. Soc.*, **153**(1), C74-C79 (2006).

4. P. Campestrini, H. Terryn, A. Hovestad, J.H.W. de Wit, "Formation of a Cerium-based Conversion Coatings on AA2024: Relationship with the Microstructure," *Surf. Coat. Tech.*, **176**, 365-381 (2004).

5. F.H. Scholes, C. Soste, A.E. Hughes, S.G. Hardin, P.R. Curtis, "The Role of Hydrogen Peroxide in the Deposition of Cerium-based Conversion Coatings," *App. Surf. Sci.*, **253**, 1770-1780 (2006).

6. B. Treu, S. Joshi, W. Pinc, M. O'Keefe, W. Fahrenholtz, "Sub-surface Electrochemical Effects on the Spontaneous Deposition of Cerium Conversion Coatings on Aluminum Alloys," *ECS Trans.*, **19**(29), 101-113 (2009).

7. W. Pinc, S. Maddela, M. O'Keefe, W. Fahrenholtz, "Formation of Subsurface Voids in Aluminum Alloy 2024-T3 During Deposition of Cerium-based Conversion Coatings," accepted for publication in *Surf. Coat. Tech.* on 24 May 2010.

8. H. Zhang, Y. Zuo, "The Improvement of Corrosion Resistance of Ce Conversion Films on Aluminum Alloy by Phosphate Post-treatment," *Appl. Surf. Sci.*, **254**, 4930-4936 (2008).

9. D.K Heller, W.G. Fahrenholtz, M.J. O'Keefe, "Cross-sectional Analysis of As-deposited and Post-treated Cerium-based Conversion Coatings," to be submitted to *Surf. Coat. Tech.*

10. W. Pinc, S. Maddela, W. Fahrenholtz, M. O'Keefe, "Corrosion Protection of Cerium-based Conversion Coatings with Subsurface Crevices," submitted to *ECS Trans*. on 25 May 2010.

11. T.J. O'Keefe, P. Yu, *Pourbaix Diagrams,* Encyclopedia of Materials: Science and Technology, Elsevier Science, 7774-7781 (2001).

12. M. Pourbaix, *Atlas of Electrochemical Equilibria in Aqueous Solutions*, 2nd Ed., Pergamon Press, (1974).

13. S. You, P. Jones, A. Padwal, P. Yu, M. O'Keefe, W. Fahrenholtz, T. O'Keefe, "Response of Nanocrystalline Cerium-Based Conversion Coatings on Al 2024-T3 to Chloride Environments," *Mat. Letters*, **61**, 3778-3782 (2007).

14. B.C. Bunker, G.C. Nelson, K.R. Zavadil, J.C. Barbour, F.D. Wall, J.P. Sullivan, C.F. Windisch Jr., M.H. Engelhardt, D.R. Baer, "Hydration of Passive Oxide Films on Aluminum," *J. Phys. Chem. B*, **106**, 4705-4713 (2002).

15. L.M. Serna, K.R. Zavadil, C.M. Johnson, F.D. Wall, J.C. Barbour, "A Critical Implanted Cl Concentration for Pit Initiation of Aluminum Thin Films," *J. Electrochem. Soc.*, **153**(8), B289-B295 (2006).

16. L.F. Lin, C.Y. Chao, D.D. Macdonald, "A Point Defect Model for Anodic Passive Films," *J. Electrochem. Soc.*, **128**(6), 1194-1198 (1981).

17. R.K. Hart, "A Study of Boehmite Formation on Aluminium Surfaces by Electron Diffraction," *Trans. Faraday Soc.*, **50**, 269-273 (1954).

18. R.K. Hart, "The Formation of Films on Aluminium Immersed in Water," *Trans. Faraday Soc.*, **53**, 1020-1027 (1957).

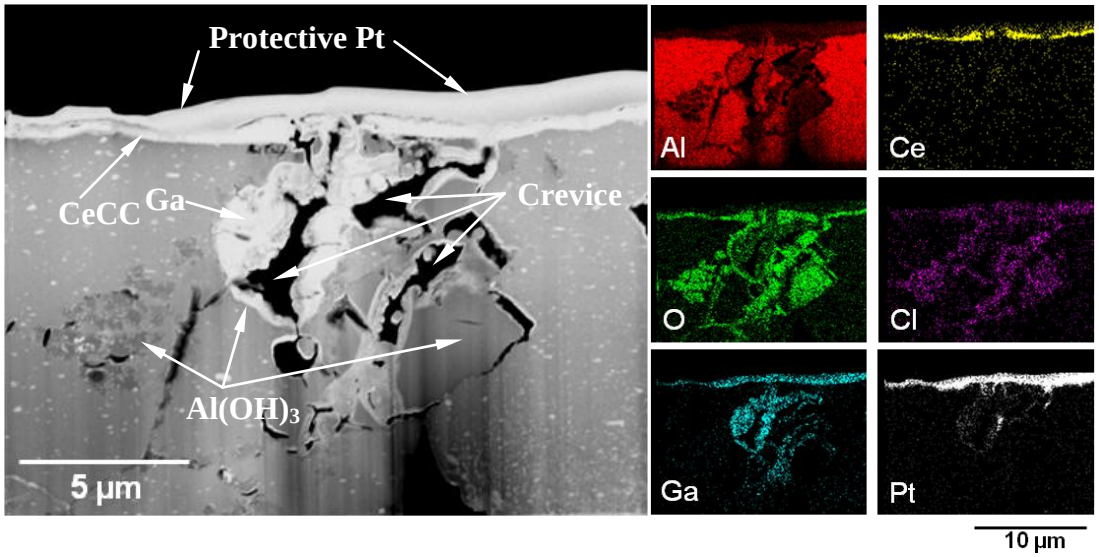

Figure 1. STEM/HAADF image of subsurface crevices on an as-deposited CeCC (no salt spray exposure) and corresponding EDS maps.

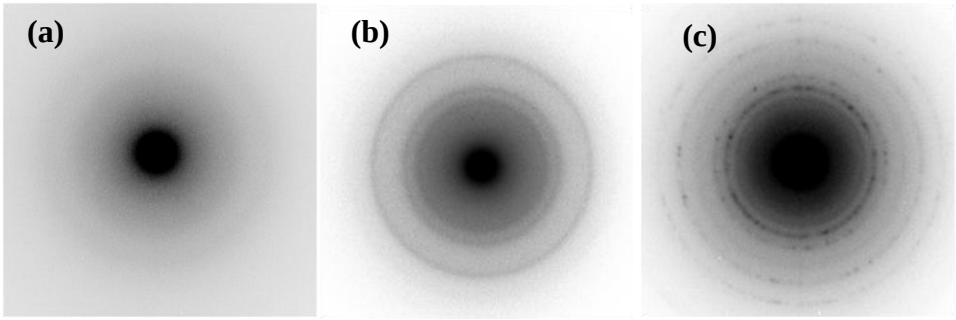

Figure 2. Diffraction patterns taken from phase formed on the surface of subsurface crevices for (a) as-deposited CeCC and (b-c), post-treated CeCC.

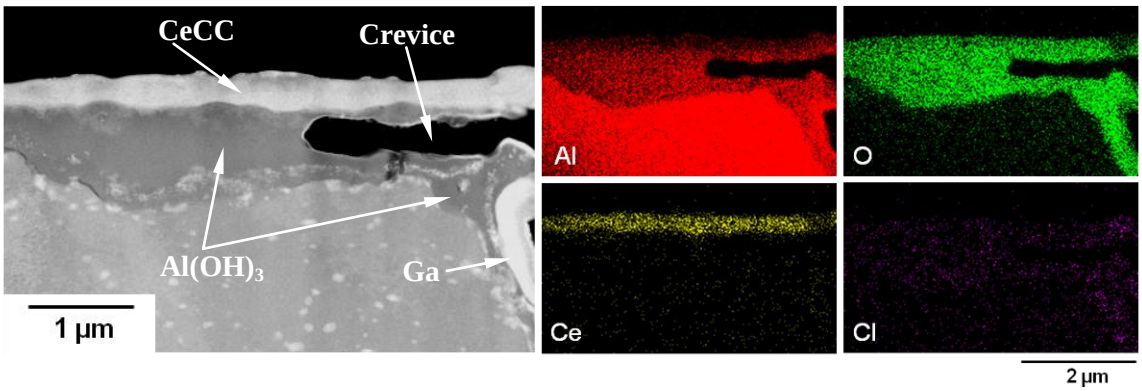

Figure 3. STEM/HAADF image of a subsurface crevice on a post-treated CeCC specimen (no salt spray exposure) and corresponding EDS maps.

SECTION

3. SUMMARY AND CONCLUSIONS

Phosphate post-treatment significantly improves the corrosion resistance of CeCCs on high strength aluminum alloy substrates. Post-treated CeCCs have been shown to withstand 14 days of ASTM B117 salt spray exposure without exhibited visible corrosion, whereas as-deposited CeCC show visible corrosion pits and tails after several days of exposure. The phase and morphology of post-treated CeCCs is dependent on kinetic factors such as time and temperature, but also on the phosphate source. Post-treatment in orthophosphate solutions for times of at least 2 min (at 85 °C) or temperatures of at least 70 °C (for 5 min) converted as-deposited cerium hydroxy/peroxy species to hydrated $CePO_4$ and minimized cracks in the coating, improving corrosion resistance. Electrochemical data was consistent with results from salt spray corrosion testing. Coatings in which hydrated $CePO_4$ had formed exhibited the least corrosion on the specimen surface after salt spray exposure and had more anodic pitting potentials, larger passivation regions, and higher impedance. The results indicated that the phase and morphology of CeCCs influence corrosion protection.

Analysis of directly deposited $CePO_4$ coatings revealed that the $CePO_4 \cdot H_2O$ phase alone does not guarantee protection despite having similar thicknesses (≈450 nm) and uniformly distributed cracks that were smaller than those observed in CeCCs. Specimens with directly deposited $CePO_4$ coatings had corrosion pits and tails distributed across the specimen surface after only 18 hours of salt spray exposure. As revealed by cross-sectional analysis, pits had formed at crack/substrate interfaces in specimens with directly deposited $CePO_4$ coatings, indicating that they functioned as inert barriers to corrosion by

only preventing corrosion on regions of the substrate that were not exposed by cracks in the coating. In contrast, post-treated CeCCs were able to inhibit the corrosion of similar areas where the substrate had been exposed by defects in the coating (i.e., cracks) and appeared to provide some electrochemical protection of the substrate.

The combination of dissolved chlorides and hydrogen peroxide in the coating solution aggressively etches the substrate and causes the formation of subsurface crevices. Cross-sectional analysis showed the presence of Al-O containing regions, believed to be $Al(OH)_3$, on crevice surfaces. In as-deposited CeCC specimens, this phase contained up to 8 at. % chlorine and was structurally amorphous. Examination after post-treatment revealed that the chlorine concentration had dropped to < 1.5 at. % and analysis by electron diffraction produced ring patterns indicating at least some of the $Al(OH)_3$ phase had crystallized as aluminum hydroxide (e.g., gibbsite) or hydrated aluminum oxides. Both reducing chlorine content and increasing crystallinity will increase the resistance of subsurface crevices to corrosion. The decreased concentration of chlorine will act to shift the pitting potential of subsurface crevices to more anodic potentials, and the crystallized aluminum hydroxide species may constitute a more effective barrier to corrosion.

Analysis of post-treated CeCCs revealed the formation of an interfacial reaction layer between the CeCC and substrate during salt spray exposure. The interfacial layer was comprised of Ce, Al, and O and had grown from a thickness of 10 – 20 nm before salt spray exposure to 60 – 100 nm after 7 days of exposure. A similar layer was not formed on specimens with as-deposited CeCCs or directly deposited $CePO_4$ coatings. After salt spray exposure, the d-spacings measured from electron diffraction ring patterns

of as-deposited CeCCs did not change significantly, indicating that no measurable structural changes occurred. However, electron diffraction in post-treated CeCCs revealed several d-spacings that were unique to post-treated CeCCs exposed to salt spray and did not match any of the d-spacings measured for as-deposited CeCCs either before or after salt spray exposure. The electron diffraction data suggests that a structural transition had occurred during salt spray exposure, potentially facilitating formation of the interfacial reaction layer. These results provide evidence that CeCCs are not static barrier coatings, but are able to inhibit corrosion by actively responding to the salt spray environment.

The series of papers included within this dissertation revealed that the corrosion resistance of CeCCs on high strength aluminum alloys depends on the phase and morphology of the coating. The reduction in cracks and the formation of $CePO_4 \cdot H_2O$ was dependent on the time, temperature, and phosphate source used for post-treatment and indicated that processes active during post-treatment were kinetically dependent. Post-treatment in aqueous orthophosphate solutions for at least five minutes at a temperature of at least 85 °C minimized cracks in the CeCC and promoted the formation of hydrated $CePO_4$, thereby improving the electrochemical properties and corrosion resistance of the coating.

Unlike $CePO_4 \cdot H_2O$ coatings that were deposited directly by precipitation from cerium citrate and phosphoric acid precursors, as-deposited and post-treated CeCCs prevented the formation of corrosion pits at crack/substrate interfaces during salt spray exposure, indicating that CeCCs provided some electrochemical protection to the substrate. Electron diffraction in as-deposited and post-treated CeCCs revealed that the

coatings changed structurally during salt spray exposure. Heterogeneous cerium species present immediately after deposition and/or post-treatment transitioned to $CeO_2 \cdot 2H_2O$ for as-deposited coatings and $CePO_4 \cdot H_2O$ for post-treated coatings. Furthermore, post-treated CeCC specimens exposed to the salt spray environment for 7 days developed an interfacial reaction layer between the CeCC and alloy substrate that was 60 – 100 nm thick and comprised of Ce, Al, and O, demonstrating that CeCCs were not static barrier coatings but exhibited an active response to the salt spray environment.

In addition to facilitating the formation of an interfacial layer that appeared vital to corrosion protection, post-treatment reduced chlorine concentration in an amorphous $Al(OH)_3$ phase formed within subsurface crevices during coating deposition and acted to crystallize the phase into gibbsite and other aluminum hydroxides and/or oxides. These changes increase the corrosion resistance of crevices and suggest that visible corrosion of post-treated CeCCs may occur via competing mechanisms, chloride ion attack at crack/substrate interfaces and at subsurface crevices.

4. SUGGESTIONS FOR FUTURE WORK

Understanding the formation of the interfacial reaction layer between post-treated CeCCs and the alloy substrate during salt spray exposure may be vital to establishing the corrosion protection mechanism of CeCCs. Several experiments could be conducted to determine the conditions under which the layer forms and whether it is feasible to artificially increase its thickness outside of salt spray exposure. Interesting questions include the following:

- Are chloride ions necessary to facilitate interfacial layer formation and growth?
- What is the structure and phase of the interface?
- Can a similar phase be reproduced by precipitation experiments and perhaps deposited onto a high strength aluminum alloy?

Precipitation strengthened, high strength aluminum alloys corrode by a pitting mechanism, but the failure origins of substrates with CeCCs was not established as part of this research. Since cerium was not detected in subsurface crevices, it was presumed that these sites may be most susceptible to corrosion and, therefore, be responsible for the eventual failure of the specimen in salt spray testing. However, the study on directly deposited $CePO_4$ coatings demonstrated that the alloy substrate is vulnerable to corrosion when exposed by defects, such as cracks in the coating or crevices that extend into the substrate. While this result suggests that post-treated CeCCs are able to provide some protection to these areas, it is unclear whether the formation of pits and tails occurs at regions containing crevices, areas where cracks exposed electrochemically active sites on the substrate, or when the interfacial layer reaches a critical thickness as a percentage of

the CeCC. Understanding more about how the coating fails may lead to additional insight into how it is able to protect.

Since reactions at the interface seem to have a significant impact on corrosion resistance, it may be worthwhile to conduct experiments that introduce different elements near the interface. This could be accomplished by modifying the first spray of a standard five spray deposition process by adding soluble salts of the desired metals to the coating solution. The remaining four sprays would consist of the standard Ce solution, after which the coating would be post-treated in a heated orthophosphate solution. Since a Ce, Al, and O containing phase(s) forms for the standard CeCC process, additional elements (e.g., multi-valent rare earths or transition metals) may promote formation of or alter the composition of this phase and influence corrosion protection.

CeCCs respond to the salt spray environment by changing structurally. What would happen if CeCC specimens were scribed panels after only several days of salt spray exposure? At this point, the active response of CeCCs is believed to have been triggered by salt spray exposure and specimens may exhibit a different response to the scribe. Preliminary results from scribing two sets of as-deposited and post-treated CeCCs (one set immediately after deposition and the other set after three days of salt spray exposure) revealed that the set exposed to the salt spray environment beforehand exhibited clean, dark scribes, whereas the as-coated set showed salting along the scribe and was only dark in some regions after three days of exposure. This experiment is worth repeating and examining the CeCCs and scribe in cross-section to determine the reasons for the increased protection exhibited by specimens that were exposed to salt spray before being scribed.

APPENDIX A.

PERFORMANCE OF MULTIFUNCTIONAL UV (MUV) CURABLE CORROSION COATING SYSTEMS TO AEROSPACE MILITARY TEST CRITERIA

Performance of Multifunctional UV (MUV) Curable Corrosion Coating Systems to Aerospace Military Test Criteria

A. Thomas, D. Heller, W. Gammill, W. Fahrenholtz, M. O'Keefe
Missouri University of Science and Technology

J. DeAntoni
Boeing Research and Technology

B. Curatolo
Light Curable Coatings

ABSTRACT

A coating system incorporating corrosion inhibiting compounds into an ultraviolet (UV) light curable polymeric matrix, referred to as a multifunctional UV (MUV) coating, has been developed. The performance of the coating system was evaluated on high strength aluminum alloys, which are commonly used on military aircraft. The MUV coatings were deposited on test panels with chromate or cerium-based conversion coatings. The coating systems were evaluated using military performance criteria for tests including neutral salt spray, wet and dry adhesion, fluid resistance, sulfur dioxide exposure, accelerated weathering, filiform corrosion, and flexibility. Commercially available chromate and non-chromate corrosion coating systems applied to high strength aluminum alloy panels were used as control specimens. Results indicate that the MUV coatings are capable of passing 2000 hour salt spray testing using a variety of oligomers on both chromate and cerium-based conversion coatings, with more consistent performance observed on chromate conversion coatings. The thickness and condition of

the cerium-based conversion coatings affected performance test results, with thinner conversion coatings typically performing better than thicker coatings. Adjustment of MUV composition to optimize performance will be discussed.

Keywords: conversion coating, ultraviolet

INTRODUCTION

High strength aluminum alloys such as Al 2024-T3 and Al 7075-T6 are commonly used for the construction of military and commercial aircraft. However, the intermetallic particles responsible for improving the strength of the alloys also make them vulnerable to localized galvanic corrosion. In halide containing solutions, the intermetallic particles become cathodic sites, which results in pitting corrosion.[1] A three part coating system is currently used for protection of aluminum alloy components for military applications. The coating system consists of a chromate conversion coating, a chromated primer, and a top coat. This system provides excellent corrosion protection, but contains hexavalent chromium in the conversion coating and primer. Hexavalent chromium is toxic and carcinogenic, and regulations have restricted the permissible exposure limit, resulting in increased lifecycle costs for performing scheduled paint removal and re-painting.[2] One potential replacement for the conventional chromated coating system is a two part coating system consisting of an environmentally benign cerium-based conversion coating (CeCC)[3] and MUV coating. In this system, the CeCC replaces the chromate conversion coating and the MUV coating provides the corrosion protection of the chromated primer with the appearance and weatherability of the top coat. A schematic comparing both coating systems is shown in Figure 1.

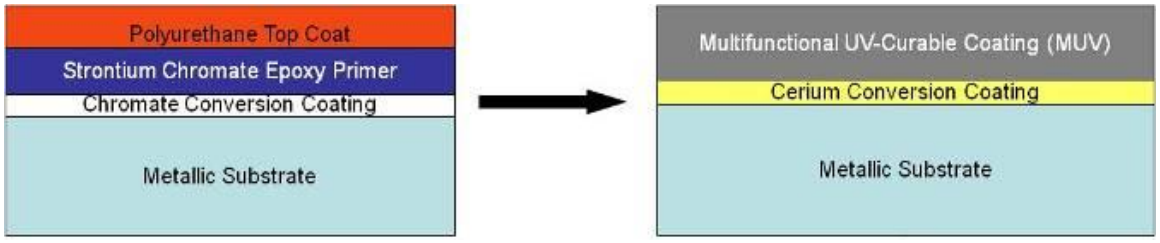

Figure 1: Comparison of a conventional three layer coating system to a two layer system employing a MUV.[4]

The CeCCs can be deposited by spontaneous processes that utilize the galvanic couples that exist (i.e. cathodic intermetallics and anodic matrix) to drive the deposition reaction[5,6] or they can be deposited using an electrolytic (i.e., current driven) process.[7] Coating solutions typically contain a cerium salt such as cerium chloride along with hydrogen peroxide. When the solution contacts the aluminum alloy substrate, electrons are released due to aluminum dissolution near the intermetallics, which reduces the H_2O_2 to hydroxide, increases the near surface pH, and leads to the precipitation of cerium species onto the substrate.[8] Because the cerium species begin to deposit when the solution contacts the alloy substrate, CeCCs can be deposited by using spray, immersion, or brush methods. The thickness, morphology, and corrosion resistance of CeCCs is controlled by the surface preparation of the alloy prior to deposition, coating solution chemistry, and post-treatment. For CeCC deposition on Al 2024-T3, the preferred surface preparation is alkaline cleaning followed by acid activation, which removes much of the native oxide layer and exposes intermetallic particles needed to drive precipitation for coating deposition.[9] As a standalone coating, CeCCs can protect Al 2024-T3 and Al 7075-T6 for up to two weeks in neutral salt spray testing.[6]

The MUV coating is free of volatile organic compounds (VOCs), eliminating their release during deposition of the coating. The MUV coating is a blend of monomers, oligomers, additives, and photoinitiators. The monomers and oligomers are used to tailor the physical properties of the coating such as hardness and fluid resistance. Oligomers are UV curable binders that form the structural matrix of the MUV coating. Monomers are cross-linkable organic species that dilute the oligomers and adjust the viscosity of the resulting paint between a typical upper limit of ~10,000 cps to a lower limit of ~100 cps, depending on the application requirements. Monomer content should be as low as possible to ensure effective curing of the coating.[10] The photoinitiators are used to absorb UV radiation and enable curing of the coating by initiating cross-linking polymerization. Additives are used to provide corrosion protection, improve adhesion, and provide the desired color. By tailoring the viscosity of the MUV formulation prior to deposition, coatings can be spray deposited or applied with a brush or roller, simulated on panels in the laboratory by application with a drawbar.

This work is a preliminary evaluation of the performance of panels with MUV coatings deposited on CeCCs and chromated conversion coatings (CrCC). In addition to neutral salt spray and filiform corrosion, adhesion, flexibility and weathering of the MUV coatings were also measured. Results after 2000 hours of salt spray testing are reported and compared to commercially available chromate and non-chromate systems. Results from this study will be used to further optimize the performance of MUV coatings on CrCCs and CeCCs.

EXPERIMENTAL PROCEDURE

Sheets of Al 2024-T3 and Al 7075-T6 were cut into 7.6 cm x 15.2 cm panels. To deposit CeCCs on the panels, the surfaces were prepared to remove contaminants and the native oxide, which exposed the intermetallic particles. Deionized (DI) water was used to rinse panels between each step of the surface preparation process to minimize cross contamination of solutions as well as clean the surface. For Al 2024-T3, panels were wiped with isopropyl alcohol to remove minor surface contamination. Then, panels were immersed in a 5 wt % alkaline cleaning solution (Turco 4215 NC-LT) for 5 minutes at 55°C for degreasing. Next, the panels were immersed in a 1.0 wt% sulfuric acid (H_2SO_4) solution for 10 minutes at 50°C to activate the surface. For Al 7075-T6, panels were wiped with isopropyl alcohol, rinsed with deionized water, and then immersed in the same alkaline cleaning solution (5 wt% Turco 4215 NC-LT) for 5 minutes at 55°C. The panels were then immersed in a room temperature solution of 2 wt% sodium hydroxide (NaOH) for 20 seconds to activate the surface.

Following surface activation, panels were placed at a 60° angle from horizontal and sprayed with the cerium-based coating solution for three to five seconds using a detail spray gun (Husky model 515-547) and allowed to drain for 35 seconds. For Al 2024-T3 panels, CeCCs were deposited using three spray/drain cycles, while only one spray/drain cycle was used for Al 7075-T6 panels. This spray cycle provides a uniform hydrated cerium oxide ($CeO_2 \cdot 2H_2O$) coating. Once the panels were coated, they were post-treated by immersion in a 2.5 wt% Na_3PO_4 solution for 5 minutes at 85°C. The post-treatment converts the as-deposited cerium hydroxide and peroxide species to

hydrated cerium phosphate ($CePO_4 \cdot H_2O$) which reduces cracking in the coating and improves salt spray corrosion performance when compared to as-deposited coatings. After CeCC deposition, panels were allowed to dry before MUV coating. The MUV coating is a proprietary blend of oligomers, monomers, photoinitiators, and additives. To promote flow during deposition, the mixture was heated slightly (~43°C). The panels were mounted horizontally for spraying. MUV was sprayed onto the panels using an overlapping pattern and then cured in one to two seconds using UV light (250-390 nm). After curing, the MUV was ~61 µm thick.

Commercially available chromate conversion coating, strontium chromate primer, and polyurethane topcoat were used as a chromated control system. In addition, a chromate-free control system was also used. The chromate-free control consisted of a trivalent chromium conversion coating, a commercial non-chromate primer, and a polyurethane topcoat. Once coated, panels are allowed to dry and/or age for up to fourteen days before further treatment.

Testing

Neutral salt spray. Corrosion performance was evaluated by exposing the panels to 5 wt% NaCl neutral salt spray in accordance with ASTM B 117 for up to 3000 hours. Each panel was scribed through the coating and into the underlying metal with an "X" pattern across the face using a NewHermes engraving machine before being placed into the salt spray chamber. The length of the scribes covered the majority of the test area and the ends were at least 1.25 cm from the edge. The edges and backs of the panels were covered with non-conductive tape to ensure that only the face of the panel was exposed to the salt spray. The panels were evaluated for performance every 500 hours and rated using a standardized alphanumeric scale, developed by Boeing, shown in Appendix 1.

Wet tape adhesion. Wet tape adhesion tests were performed by soaking panels in room temperature tap water for 24 hours. Two parallel lines were then cut into the panel ~5.1 cm long and ~1.9 cm apart. Then an "X" was scribed in-between the parallel lines. 3M #250 tape was then applied to the panels parallel to the first two cuts and pressed onto the surface by rolling a 1.8 kg, 60 durometer rubber roller four times back and forth across the surface. After the tape was applied to the surface it was immediately pulled

off at a 45° angle. The panels were then evaluated according to Method A of ASTM D 3359-97.

Flexibility. Flexibility was measured by two different testing methods. One test for flexibility was a low temperature test in which panels were exposed to temperatures of -51±6°C for 5 hours. After 5 hours, panels were bent over a 1.3 cm mandrel that was kept at the same temperature. Coatings were then examined for any visible cracks using the unaided eye. The other flexibility test was a GE room temperature reverse impact test. This test was performed in accordance with ASTM D 2794. The reverse impact test was performed by dropping weights at various heights to determine the failure point, which was cracking of the coating observed under 10x magnification.

Filiform corrosion. Filiform corrosion resistance was tested by scribing each panel through the coating and into the substrate with an "X" pattern across the face using a NewHermes engraving machine before being taped across the back and around the edges. Taped panels were placed vertically into a desiccator containing 12N hydrochloric acid for 1 hour. After removal from the desiccator, panels were immediately placed into a humidity cabinet held at 40±4°C and 80±5% relative humidity for 1000 hours. After 1000 hours in the humidity cabinet, the panels were examined as described in ASTM D 2803, which states filiform corrosion shall not extend farther than 0.635 cm from the scribe and most of the filaments should be less than 0.3175 cm in length.

Xenon arc weathering. Xenon arc weathering resistance was tested by exposing panels to a xenon arc weatherometer for 1000 hours. Xenon arc provides a wavelength and intensity of light similar to average solar radiation in the UV and visible spectra (200-700 nm). This test exposed the panels to cycles consisting of 102 minutes of light only followed by 18 minutes of light and water spray. Cycles were repeated for 500 hours before panels were examined to assess performance. At 500 hours the color change (ΔE) should be less than or equal to 1.0 and 60° gloss values should be less than or equal to 5.

Surface Roughness (Ra). MUV coated panels were soaked for two weeks in DI water and surface roughness values were measured daily. In addition, optical micrographs were taken daily of the panel surfaces. Values for Ra were measured using

a profilometer, which graphically determined the arithmetic average surface roughness according to ANSI Standard B46.1-1978. The profilometer had a vertical range of ±160 μm and a resolution of 5 nm. Blister size was measured from optical micrographs using image processing software (Image J, National Institutes of Health).

RESULTS

Figure 2 compares the salt spray corrosion performance of the MUV on CeCCs and CrCCs for aluminum alloys 2024-T3 and 7075-T6. The MUV/CrCC system performed very well (2,4,A rating) on three 7075-T6 panels, exhibiting scribes with almost no salting. MUV/CrCC on 2024-T3 also performed well, but did exhibit one small blister along the scribe with nearby salting, thus receiving a rating of 1,4,8,E. The MUV/CeCC system did not perform as well on either alloy receiving a rating of 2,5,8,14,H on all six of the tested panels. MUV/CeCC system exhibited several large blisters near the scribes, numerous smaller blisters in the fields, and salted scribes that tailed onto the fields. The blistering along with salting in the scribe caused these panels to fail the test. Figure 3 shows the salt spray performance of the chromate and non-chromate control on Al 7075-T6 and Al 2024-T3. After 2000 hours of salt spray testing the chromate and non-chromate control performed similarly, exhibiting no blisters and little salting in the scribe.

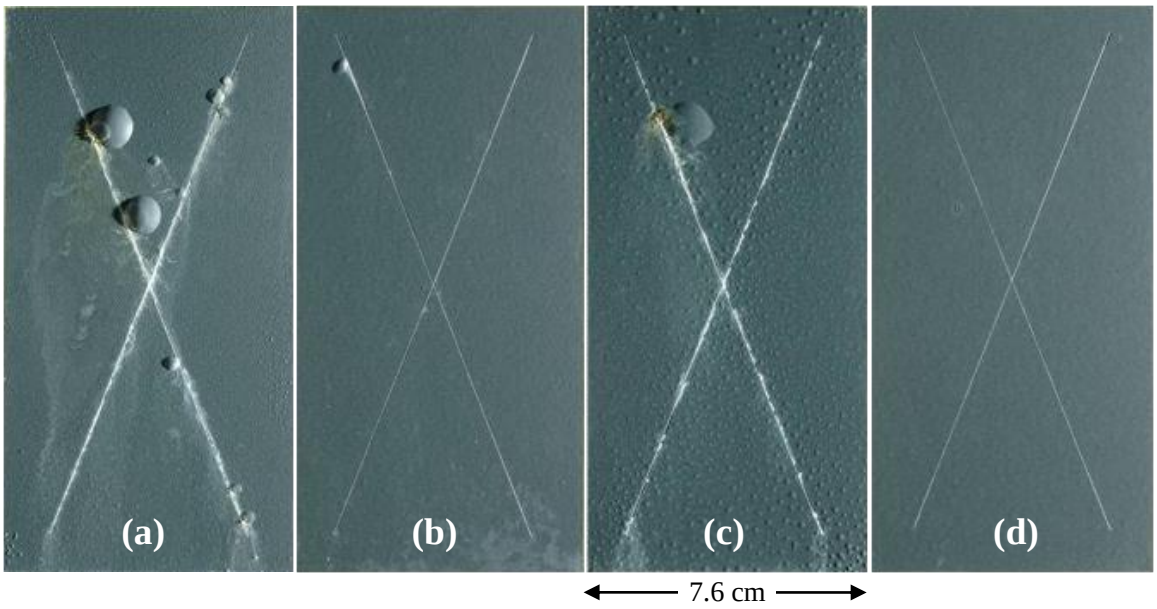

Figure 2: 2000 hour salt spray test results, (a) MUV/CeCC Al 2024-T3, (b) MUV/CrCC Al 2024-T3, (c) MUV/CeCC Al 7075-T6, and (d) MUV/CrCC Al 7075-T6.

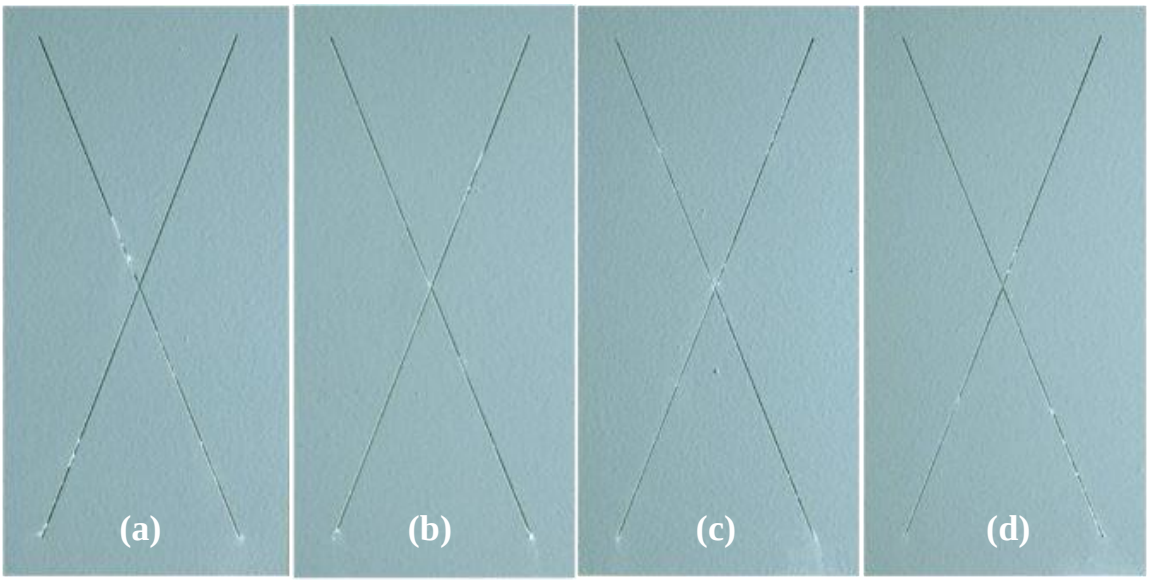

Figure 3: 2000 hour salt spray test results, (a) Chromate Control Al 2024-T3, (b) Non-chromate Control Al 2024-T3, (c) Chromate Control Al 7075-T6, and (d) Non-chromate Control Al 7075-T6.

As seen in Figure 2, blisters formed on the MUV during salt spray testing when it was deposited on CeCCs but were not evident when MUVs were deposited on CrCCs. It was found that blisters were also formed after the MUV/CeCC panels were immersed in DI water. Figure 4 shows optical images of MUV coatings on CeCCs taken after various

immersion times. Blisters were ~200 µm in diameter. The blisters formed within 48 hours, but did not increase in size over the course of two weeks. However, the number of blisters continued to increase over time. To observe the growth of the blisters over the course of two weeks, the surface roughness was measured. Figure 4d shows the change in the average Ra value for a MUV on a CeCC during two weeks of immersion. The average surface roughness remained between 5 and 7 µm after 12 days, which suggests that the blisters did not grow in size significantly during this time. In contrast, a few blisters continued to increase in size during salt spray testing, possibly due to the presence of NaCl in the spray, which could be transported through the MUV causing corrosion of the substrate beneath the coating leading to growth of some blisters. Blisters would grow if the corrosion products led to an increase in volume, which would require the blister to expand to accommodate the additional material. Exposure of MUV/CeCC panels to 85% humidity at 40°C for two weeks did not result in the formation of blisters, indicating that the system can be exposed to water vapor without an adverse effect. More work is being done to understand the mechanism by which the blisters form.

Figures 5a and 5b compare the results of the wet tape adhesion tests for MUV/CeCC and MUV/CrCC systems on Al 2024-T3. The MUV was adherent to the CrCC near the scribes and in the field. The MUV did not perform as well when deposited on CeCCs as the tape removed the MUV from several areas around the scribes. Subsequent testing has indicated that thinner CeCCs coatings have been found to lead to increased MUV adhesion. Figures 5c and 5d show the results of low temperature flexibility tests. The MUV deposited on CeCCs failed due to cracking and peeling when bent at low temperatures. When applied to CrCCs, the MUV passed low temperature flexibility tests with no visual cracking. Similarly, results of GE impact testing indicated that the MUV had a flexibility of ~10% elongation. Changes to the formulation of the MUV can improve the elongation and previous formulations have had up to a desired 20% elongation, indicating that different MUV formulations can meet the flexibility requirement. However, increasing elongation can be detrimental to other properties of the coating such as weathering and fluid resistance. Balancing flexibility and fluid resistance is one of the challenges that are currently being addressed to optimize performance of the MUV.

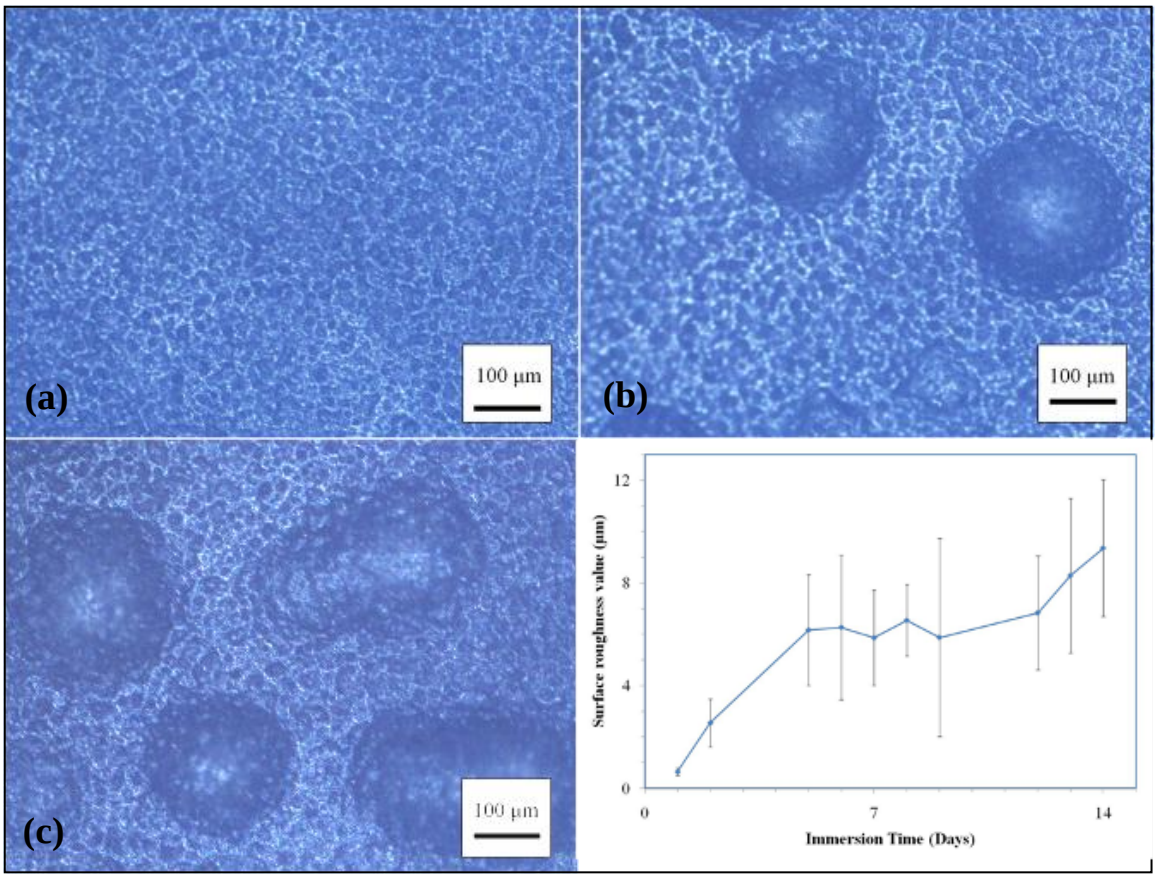

Figure 4: Optical images of the MUV surface showing on CeCC (a) the as-deposited coating, (b) blisters after 7 days of water immersion in DI water, (c) blisters after two weeks of immersion in DI water, and (d) average surface roughness vs. immersion time.

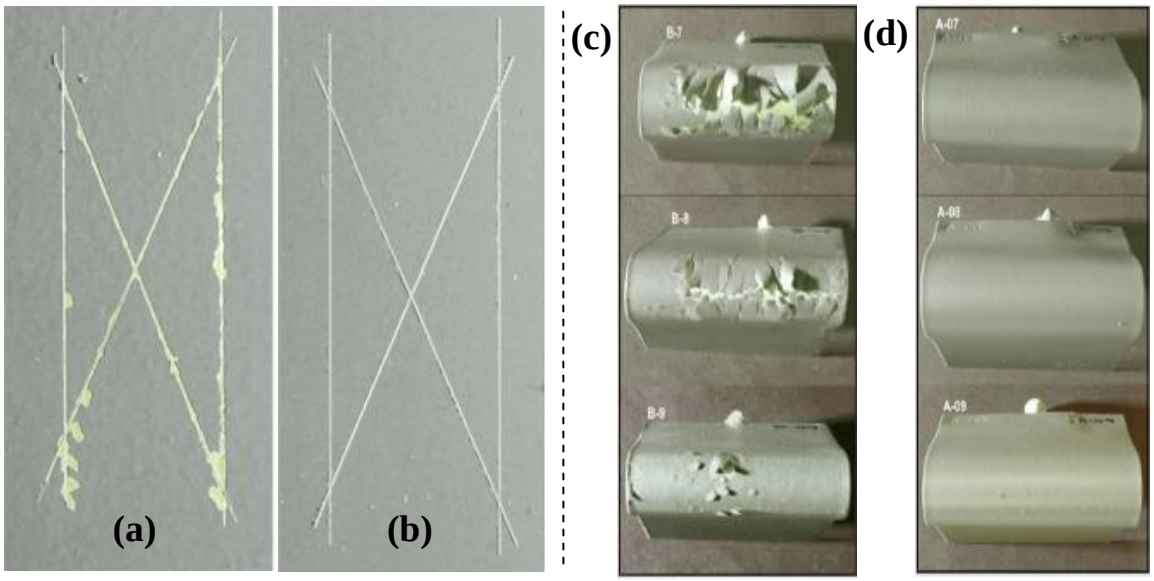

Figure 5: Wet tape adhesion test results (left) for (a) MUV on CeCC – Al 2024-T3, (b) MUV on CrCC – Al 2024-T3, and low temperature flexibility (right) of (c) MUV on CeCC and (d) MUV on CrCC.[4]

Figure 6 shows aluminum alloy 2024-T3 and 7075-T6 test panels with MUV/CeCC and MUV/CrCC after 1000 hours filiform corrosion testing. Very little corrosion occurred on panels with the MUV/CrCC system. The requirements for passing this test specify a maximum allowable length of 0.64 cm for the longest filament while the majority of the filaments must be less than 0.32 cm. The MUV on CrCC passed this test on both alloys. The MUV/CeCC on Al 2024-T3 failed the test because the longest measured filaments were ~1.3 cm, which is double the allowable length. In addition, a majority of the filaments were larger than 0.32 cm. However, the MUV/CeCC on Al 7075-T6 passed the filiform corrosion testing and performed similarly to the MUV/CrCC system. The fact that the MUV passed the filiform corrosion test on a CeCC demonstrates that the combination is capable of passing this test. Additional optimization is necessary for the MUV/CeCC to pass this test on Al 2024-T3.

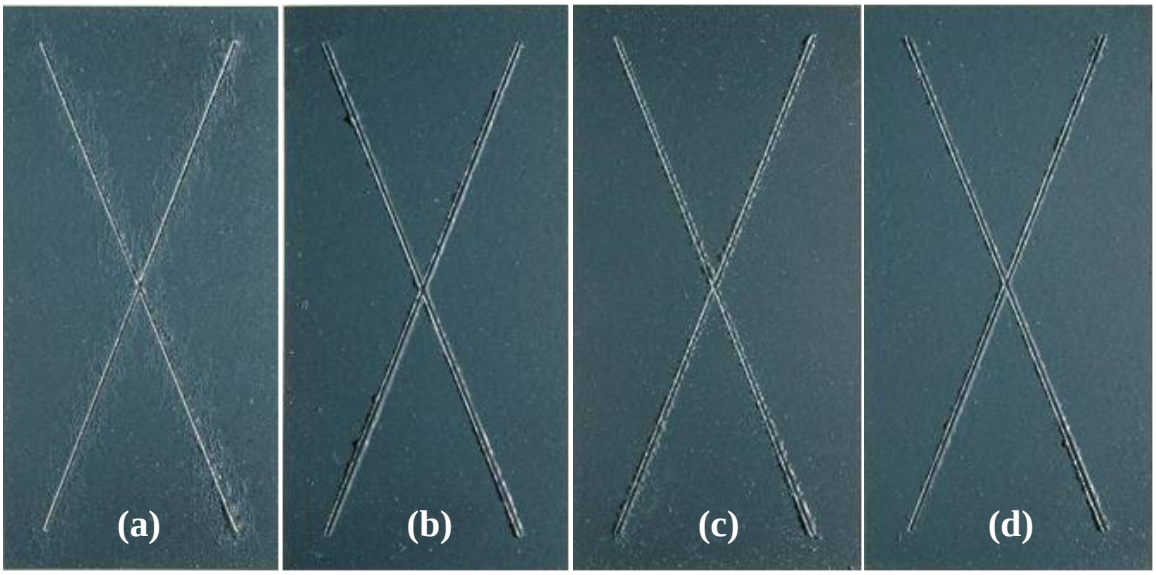

Figure 6: 1000 hours filiform corrosion test for (a) MUV on CeCC – Al 2024-T3, (b) MUV on CrCC – Al2024-T3, (c) MUV on CeCC - Al7075-T6, and (d) MUV on CrCC – Al7075-T6

After 500 hours of xenon arc accelerated weathering, none of the MUV systems passed the color change requirements. To meet the ΔE (i.e. color change) requirement, the MUV must have a ΔE less than or equal to 1.0 and the 60° specular gloss values must be less than 5. For all of the MUV coated panels, ΔE was around 3.4. Most of the delta E was attributed to the corrosion inhibitor, and was a result of a change in color and a darkening of the coating, rather than a lightening of the coating that would normally be

associated with polymer degradation due to weathering. Larger than normal delta E values have also been seen in other programs using this particular corrosion inhibitor.

Table 1 summarizes the test performance of all of the coating systems that were evaluated as part of this study. Commercially available chromate and non-chromate corrosion coating systems were used as controls for the study. Only the chromate system (CrCC/chromated primer/top coat) passed all of the tests.

MUV/CrCC coating systems on Al 2024-T3 and Al 7075-T6 met or exceeded the performance of the non-chromate controls for all tests except accelerated weathering. Based on this evaluation, the MUV appears to be a viable candidate for further analysis as a component in non-chromate coating systems that might incorporate alternative chromate-free conversion coatings. While the chromate-free MUV/CeCC systems did not perform as well as MUV/CrCC systems in this round of tests, additional progress towards modifying the CeCCs to work with the MUV coating has been made. As previously mentioned, subsequent testing has shown that the adhesion of MUV coating to CeCC can be improved by decreasing the thickness of the CeCC. The most promising result is that the MUV coating passes most of the testing when applied on CrCCs, indicating that optimization of the CeCC is likely to lead to acceptable performance of the complete chromate-free MUV/CeCC system as well.

Table 1: Summary of MUV performance in standard tests.

	Al 2024				Al 7075			
	MUV on CrCC	MUV on CeCC	Non-chrome control	Chrome Control	MUV on CrCC	MUV on CeCC	Non-chrome control	Chrome Control
2000 hours Salt Spray	Pass	Fail	Pass	Pass	Pass	Fail	Pass	Pass
1000 hours Filiform Corrosion	Pass	Fail	Pass	Pass	Pass	Pass	Fail	Pass
Wet Tape Adhesion	Pass	Fail	Fail	Pass	N/A	N/A	N/A	N/A
Room Temperature Flexibility	Fail	Fail	Fail	Pass	N/A	N/A	N/A	N/A
Low Temperature Flexibility	Pass	Fail	Fail	Pass	N/A	N/A	N/A	N/A
Xenon Arc Weathering	Fail	Fail	Pass	Pass	N/A	N/A	N/A	N/A

CONCLUSIONS

The corrosion resistance and low temperature flexibility results for the MUV corrosion coating system are encouraging for the replacement of chromated primer and topcoat systems currently used on military aircraft. When combined with a CrCC, the MUV performed as well or better than the chrome and chrome-free control in corrosion resistance. The MUV possesses many of the same properties as the top coat plus primer system without the long cure times or chromate additions. However, some points of improvement are needed before becoming a viable replacement of the current system, including flexibility and weathering. Continuing studies are being made to try to optimize the MUV performance. The MUV coating has been shown to pass 2000 hours salt spray on CrCC repeatedly and has, in some cases, been able to pass 2000 hours salt spray on CeCC, but in some cases blistering of MUV on CeCC has been observed. The blistering was related to water permeation but more studies are needed to understand the mechanism. MUV corrosion coatings have performed well during filiform testing on CrCC and CeCC. Overall, the MUV coating system has proven to be a promising alternative to the current chromate coating system.

ACKNOWLEDGMENTS

The authors would like to acknowledge the support and guidance of Bruce Sartwell of SERDP and Donna Ballard of AFRL/MLLB under SERDP Project WP-1519, Contract W912HQ-06-C-0030. The support of John Sinko at Wayne Pigment Corp. is gratefully acknowledged. Also, thanks are given to the contributions of Will Pinc, Simon Joshi, and Travis McKindra in the Materials Research Center at Missouri S&T.

REFERENCES

[1] W.J. Clark, J.D. Ramsey, R.L. McCreery, G.S. Frankel, "A Galvanic Corrosion Approach to Investigating Chromate Effects on Aluminum Alloy 2024-T3," *Journal of The Electrochemical Society*, **5**, B179-185 (2002).

[2] "Health Effects of Hexavalent Chromium," OSHA Fact Sheet, July 2006, OSHA, 20 May 2009, available from <http://www.osha.gov/OshDoc/data_General_Facts/hexavalent_chromium.pdf>.

[3] B.R.W. Hinton, D.R. Arnott, N.E. Ryan, "Cerium conversion coatings for the corrosion protection of aluminum," *Materials Forum*, **9** (3), 162-73 (1986).

[4] M.J. O'Keefe, W.G. Fahrenholtz, J. DeAntoni, B. Curatolo, "Development and Evaluation of Multifunctional UV (MUV) Curable Non-Chromate Corrosion Coating System," The Partners in Environmental Technology Technical Symposium and Workshop, December 2-4, 2008, Washington DC.

[5] P.S. Jones, P. Yu, W.R. Pinc, M.J. O'Keefe, W.G. Fahrenholtz, T.J. O'Keefe, "Spray deposition of cerium oxide-based conversion coatings on Al 2024-T3," *International Journal of Applied Ceramic Technology*, **5** (1), 63-73 (2008).

[6] B.F. Rivera, B.Y. Johnson, M.J. O'Keefe, W.G. Fahrenholtz, "Deposition and characterization of cerium oxide conversion coatings on aluminum alloy 7075-T6," *Surface and Coatings Technology*, **176** (3), 349-356 (2004).

[7] B.Y. Johnson, J. Edington, A. Williams, M.J. O'Keefe, "Microstructural characteristics of cerium oxide conversion coatings obtained by various aqueous deposition methods," *Materials Characterization*, **54** (1), 41-48 (2005).

[8] A.E. Hughes, F.H. Scholes, A.M. Glenn, D. Lau, T.H. Muster, S.G. Hardin, "Factors influencing the deposition of Ce-based conversion coatings, part I: The role of Al^{3+} ions," *Surface and Coatings Technology*, **203** (19) 2927-2936 (2009).

[9] W. Pinc, S. Geng, M. O'Keefe, W. Fahrenholtz, T. O'Keefe, "Effects of acid and alkaline based surface preparations on spray deposited cerium based conversion coatings on Al 2024-T3," *Applied Surface Science*, **255** (7) 4061-4065 (2009).

[10] V. Shukla, M. Bajpai, D. K. Singh, M. Singh, R. Shukla, "Review of basic chemistry of UV-curing technology," *Pigment & Resin Technology*, **33**, 272-279 (2004).

Appendix 1:

Alphanumeric scale for corrosion performance evaluation

Code	Corrosion Code Description
1	Scribe line beginning to darken or shiny scribe.
2	Scribe lines > 50% darkened.
3	Scribe line dark.
4	Several localized sites of white salt in scribe lines.
5	Many localized sites of white salt in scribe lines.
6	White salt filling scribe lines.
7	Dark corrosion sites in scribe lines.
8	Few blisters under primer along scribe line. (<12)
9	Many blisters under primer along scribe line.
10	Slight lift along scribe lines.
11	Coating curling up along scribe.
12	Pin point sites/pits of corrosion on organic coating surface (1/16” to 1/8” dia.).
13	One or more blisters on surface away from scribe.
14	Many blisters under primer away from scribe.
15	Starting to blister over surface

Code	Scribe Line Ratings - Corrosion Creepage Beyond Scribe
A.	No creepage
B.	0 to 1/64
C.	1/64 to 1/32
D.	1/32 to 1/16
E.	1/16 to 1/8
F.	1/8 to 3/16
G.	3/16 to 1/4
H.	1/4 to 3/8

APPENDIX B.

ELECTROCHEMICAL AND STRUCTURAL CHANGES IN CERIUM-BASED CONVERSION COATINGS DURING EXPOSURE TO SALT SPRAY

Electrochemical and Structural Changes in Cerium-Based Conversion Coatings During Exposure to Salt Spray

W. Pinc[a], D. Heller[a], W. Fahrenholtz[a], M. O'Keefe[a]

[a]Materials Research Center, Department of Materials Science Engineering, Missouri University of Science and Technology, Rolla MO 65401, USA

Abstract

Cerium-based conversion coatings on aluminum alloy 2024-T3 substrates were characterized after various exposure times in salt spray corrosion testing. Coatings post-treated in phosphate solutions exhibited no visible corrosion after seven days. Impedances doubled for these coatings after 12 hours of testing and a ~150 nm thick alumina layer developed after 24 hours of exposure, leading to the conclusion that post-treated coatings facilitated the formation of a protective alumina layer. As-deposited coatings exhibited significant corrosion after 24 hours of exposure and had impedances that were an order of magnitude lower than post-treated coatings. Subsurface voids present underneath coatings corroded into nodules of alumina on the surface of as-deposited coatings. In contrast, the voids corroded into small pits with little corrosion product present in post-treated coatings, which was attributed to a protective oxide present around the voids.

Introduction

For decades, chromate based conversion coatings have been utilized for the corrosion protection of high strength aluminum alloys used in aircraft (1,2). The toxicity of chromates, however, has led to increased regulation of their use and concomitant increases in the costs of application, removal, and disposal of chromate-containing materials. Therefore, the need for a suitable replacement has arisen (3). Cerium-based conversion coatings (CeCCs) are a promising alternative as studies have shown they are

environmentally friendly and have the ability to meet military requirements for salt spray corrosion resistance (4,5,6).

Since the initial research by Hinton (7), numerous studies have focused on various aspects of CeCCs such as the deposition mechanism (8,9,10) and impact of processing parameters (surface preparation (11,12), coating solution composition (13,14), post treatment, etc.) on corrosion resistance. Post-treatment of CeCCs in particular has been shown to affect the corrosion resistance. Non-post-treated coatings (i.e., as-deposited) typically exhibited significant corrosion after only a few days of salt spray testing. In contrast, post-treated coatings exhibited improved corrosion resistance and can inhibit corrosion for seven or more days of salt spray testing. (6,16) One common post-treatment process consisted of an immersion in a heated phosphate bath. Post-treatment was found to reduce the amount of cracking observed in the coatings and convert a majority of the cerium species to hydrated cerium phosphate, both of which increased the corrosion protection of post-treated coatings (6,15).

Another important feature of CeCCs that has recently been studied is the formation of subsurface voids (Figure 1), which are found in the substrate underneath a small fraction of the coating. These voids are formed during deposition of CeCCs from coating solution containing both Cl^- and H_2O_2, which act together to etch the aluminum alloy substrate. Typically, voids are found underneath areas of the coating exhibiting large cracks, which cover up to ~10 % of the coating surface. Both as-deposited and post-treated coatings contain subsurface voids. In both cases, a dark alumina phase has been observed around a large portion of the subsurface voids. It is interesting to note that the best performing CeCCs that can inhibit corrosion for seven days or more of salt spray testing have subsurface voids (16).

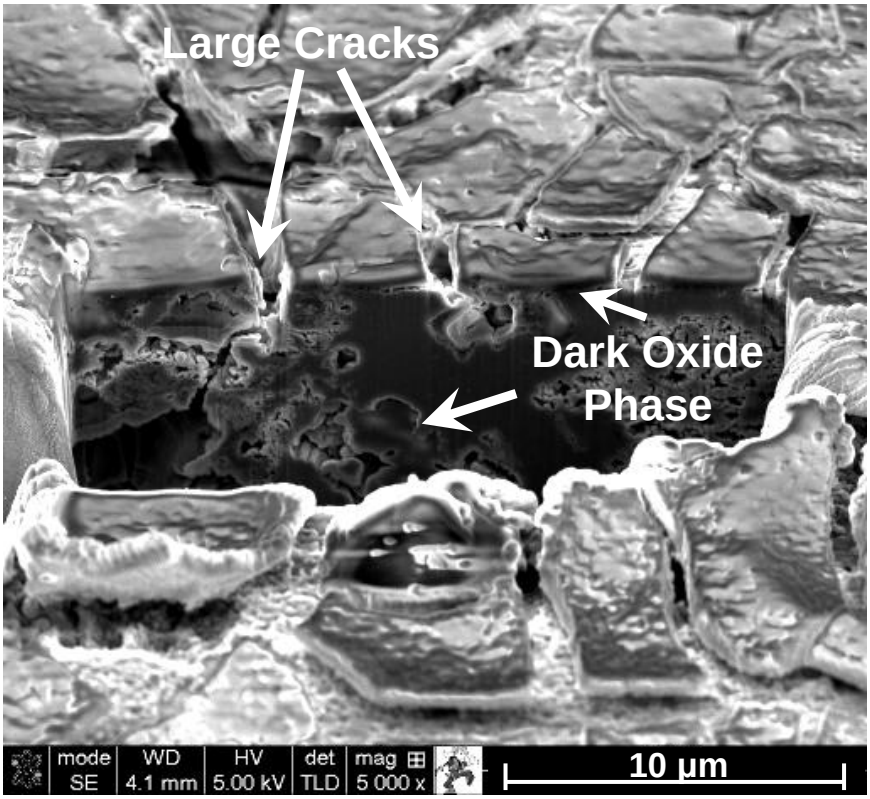

Figure 1: A cross section of a CeCC on 2024-T3 prepared by focused ion beam milling showing large cracks in the CeCC and subsurface voids present in the substrate beneath the coating.

One aspect of CeCCs that has not been adequately studied is the mechanism by which these coatings provide corrosion protection. Several studies have reported a decrease in the corrosion potential and a cathodic shift of the corrosion current for panels with CeCCs compared to bare aluminum alloy substrates (17,18). This indicates that coatings may prevent corrosion by inhibiting the oxygen reduction reaction at cathodic sites, which could be due to the coatings acting as a barrier to transport of either oxygen or electrons involved in corrosion reactions (17,18). While this cathodic inhibition likely plays a role in the corrosion protection mechanism of CeCCs, it fails to explain how the coatings are able to protect areas of the substrate such as the subsurface voids that are exposed directly to corrosive species nor does it explain why the cerium phosphate phase is needed for improved corrosion resistance. Thus, further studies into the corrosion protection mechanisms of CeCCs are needed.

The aim of this study is to investigate corrosion protection mechanisms of CeCCs. This study will focus on comparing changes observed in CeCCs with good corrosion resistance (post-treated) to those in poor performing coatings (as-deposited CeCCs) upon exposure to salt spray corrosion testing.

Experimental

Aluminum alloy 2024-T3 (nominal composition of Al 2024-T3 - Cu: 3.8-4.9 wt%, Mg: 2.1-1.8 wt%, Mn: 0.9-0.3 wt%, Fe: 0.5 wt%, Si: 0.5 at%, Zn: 0.3 wt%, Al: balance) sheets were cut into panels of 2.5 cm by 7.6 cm, which were used as substrates for coating deposition. Surface preparation of the panels consisted of wiping with isopropyl alcohol, followed by a 5 minute immersion in a 55ºC water solution of a commercial alkaline cleaning solution (55 g Turco-4215 NC LT + 1045 g deionized water). Panels were then activated using a 10 minute immersion in deionized water containing 1 wt% sulfuric acid that was heated to 50ºC.

Coatings were spray deposited using a detail spray gun (Husky, Model # 515-547). For deposition, panels were placed at an angle of ~ 60º to the horizontal. Panels were sprayed for 3-4 seconds followed by a 30 second delay for draining. The spray-drain cycle was repeated for a total of five cycles for each coating. The coating solution was composed of 0.162 M $CeCl_3 \bullet H_2O$, 1 M H_2O_2 and 2.4 g/L gelatin. Prior to the addition of H_2O_2 and gelatin, the solution pH was adjusted to 2.07 with HCl. After H_2O_2 and gelatin additions, the final pH of the coating solution was 2.3.

After deposition, coatings were either dried (i.e., as-deposited coatings) or post-treated. The as-deposited coatings (also referred to as unsealed coatings) were rinsed immediately after deposition, and dried overnight under ambient conditions. Post-treated coatings (also referred to as sealed coatings) were rinsed, then immersed for 5 minutes in a deionized water solution containing 2.5 wt% NaH_2PO_4 that was heated to 85°C. After post-treatment, panels were rinsed and dried overnight under ambient conditions.

Unsealed and sealed coatings were exposed to salt spray corrosion testing for times ranging from no exposure (0 hours) to 14 days. Tests were conducted according to the conditions specified in ASTM B117. After salt spray testing, electrochemical properties, surface morphologies, and compositions were characterized. Electrochemical impedance spectroscopy (EIS) was used to characterize the relative corrosion resistance of coatings before and after salt spray exposure. Three or more tests were run on two coatings for each exposure time and averaged. The electrolyte consisted of 0.35 wt% NaCl and 0.70 wt% $(NH_4)_2SO_4$. This modified prohesion solution was used due to previous success correlating salt spray testing results to coating impedance values obtained from electrochemical tests (13,19). Electrochemical testing was conducted using a Princeton Applied Research 273A potentiostat and a Solartron SI 1255 HF frequency response analyzer.

Coating thicknesses and composition depth profiles were characterized using Auger electron spectrometry (AES; Perkin-Elmer, Model 545). A sputter rate of 10 nm/min was estimated based on a Ta_2O_5 standard. Surface morphologies and compositions of the coatings were analyzed using scanning electron microscopy (SEM; Hitachi S570, Hitachi) and energy dispersive spectroscopy (EDS; Phoenix System, EDAX). Cross sections of CeCCs were prepared using focused ion beam (FIB; Helios NanoLab 600, FEI) machining, which used a gallium ion beam to selectively mill away material, revealing cross sectional structures of select areas. Cross sections were then imaged and analyzed using the SEM and EDS function of the FIB instrument.

Results and Discussion

As-deposited coatings performed poorly in salt spray corrosion testing, exhibiting light salt tailing after as little as one hour of exposure. With longer exposure times, the degree of salting present on the as-deposited coatings grew more severe to the point that after 24 hours the panels appeared corroded over the entire surface. In comparison, post-treated CeCCs exhibited improved corrosion protection. No visible corrosion was observed on

post-treated coatings through seven days of salt spray exposure. After 14 days of testing, post-treated CeCCs showed some visible salt tails.

Electrochemical changes occurring in CeCCs during salt spray exposure were characterized using EIS analysis. Nyquist plots of EIS data for post-treated coatings (Figure 2) showed that impedance values were ~40 kΩ-cm^2 prior to salt spray exposure (0 hours). Upon exposure, impedance values of the post-treated CeCC increased during the first 12 hours, and then stabilized at values of more than 100 kΩ-cm^2. Impedance values remained at about this level until ~14 days, when salt tailing was observed on the sealed coatings and the impedance decreased to ~70 kΩ-cm^2. Assuming that impedance is directly related to corrosion resistance, EIS testing showed that sealed CeCCs exhibited improved corrosion resistance after the first 12 hours of salt spray exposure.

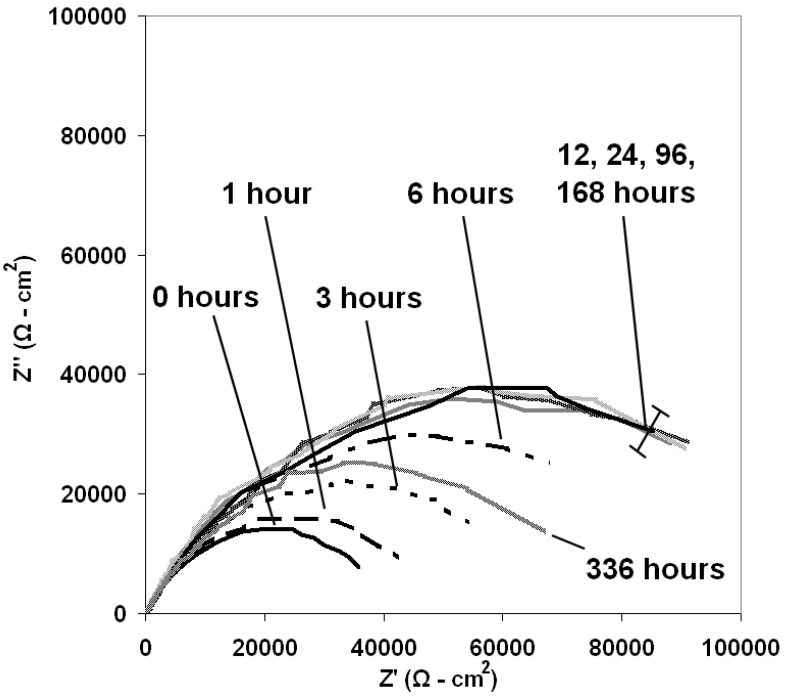

Figure 2: Nyquist plots of electrochemical impedance spectroscopy data for post-treated CeCCs after various salt spray exposure times.

Nyquist plots of EIS data for as-deposited coatings (Figure 3) did not exhibit similar trends to post-treated coatings. Measured impedances of as-deposited CeCCs were an order of magnitude less than the values observed for post-treated coatings. Prior to salt

spray exposure, as-deposited coatings had impedances of ~8 kΩ-cm^2. The impedance dropped after one hour of salt spray exposure to ~5 k Ω-cm^2, then increased back to its initial values for exposures ranging from three to 12 hours. Impedance values increased again to about 12 kΩ-cm^2 after about 24 hours, at which point panels exhibited heavy salting.

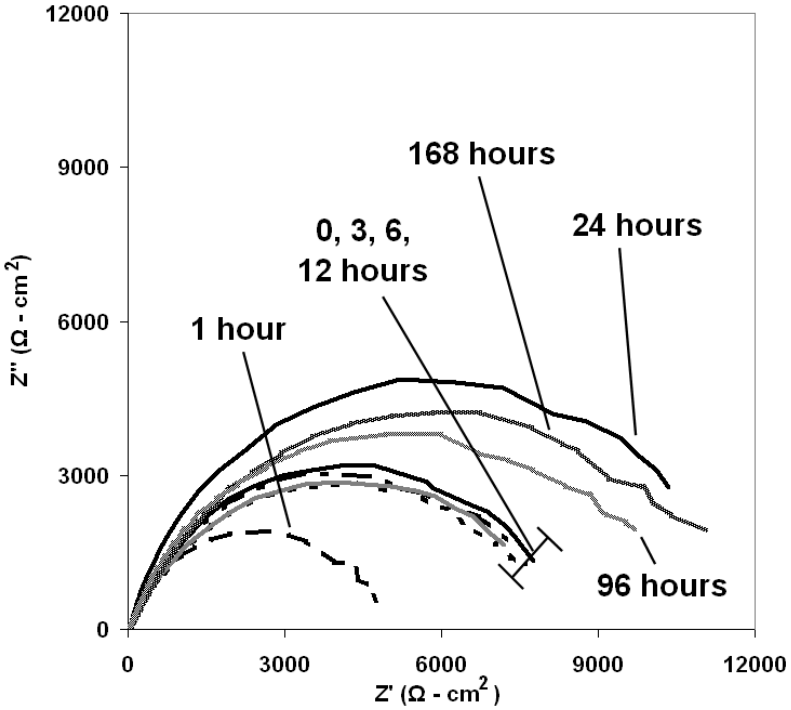

Figure 3: Nyquist plots of electrochemical impedance spectroscopy data for as-deposited CeCCs after various salt spray exposure times.

To understand how coatings changed during salt spray exposure, EIS data were fit to equivalent circuit models, which are illustrated in Figures 4a and b. The calculated parameter values for post-treated and as-deposited coatings are listed in Tables I and II, respectively. For post-treated coatings, the best fits were produced using models with two time constants, while data from as-deposited coatings could be fit to circuits with one time constant. These same equivalent circuits were used successfully in previous studies to calculate coating parameters in which the total resistance was made up of components from the solution (Rs), coating (Rp), and double layer (Rct) (13,15). In these studies, the measured capacitances were attributed to the capacitance of the coating (Qox) and double

layer (Qdl) (13,15). The errors between the fitted equivalent circuits and the data were under ten percent for all coatings in the present study.

Post-treated coatings exhibited no significant changes in capacitance, solution resistance, or coating resistance as salt spray exposure times increased. The charge-transfer resistance, however, increased from an initial value of 46 kΩ-cm^2 prior to salt spray exposure to 130 kΩ-cm^2 after 12 hours of exposure. Charge-transfer resistance remained between 120 – 130 kΩ-cm^2 through 168 hours of salt spray testing, then exhibited a decrease to 87 kΩ-cm^2 after 336 hours, at which time sealed coatings began to exhibit salt tailing. Thus, the increase in impedance of sealed coating with salt spray exposure was attributed to an increase in the charge-transfer resistance of the coatings. Charge-transfer resistance is related to the corrosion protection of exposed areas of the coating, such as cracks or other defects. Changes in the charge-transfer resistance can be due to break down or build up of corrosion protection in these areas and due to the formation of a passive layer. Therefore, based on the increases in charge-transfer resistance, EIS testing showed post-treated coatings formed a protective layer or otherwise passivated areas on the substrate that were exposed and not covered by the coating.

For as-deposited coatings, neither capacitance nor solution resistance exhibited significant changes during salt spray exposure. As with post-treated coatings, the charge-transfer resistance of as-deposited coatings exhibited change with increasing salt spray exposure time. Before salt spray exposure, the charge-transfer resistance of as-deposited CeCCs was ~9 kΩ-cm^2. After an initial drop to ~6 kΩ-cm^2 after the first hour of exposure, the resistance increased and remained between 8 – 9 kΩ-cm^2 through 12 hours of salt spray testing. For longer exposure times, as-deposited coatings exhibited an increase in impedance, which was due to an increase in the charge-transfer resistance to ~12 kΩ-cm^2, where remained through 168 hours of exposure. Thus, changes in impedance observed in as-deposited coatings were also the result of changes in the charge-transfer resistance, just as was observed for post-treated coatings. The impedance and the degree of change, however, were both significantly less for as-deposited coatings

with increases of ~ 3 – 6 kΩ-cm^2 for as-deposited coatings compared to increases of ~60 kΩ-cm^2 for post-treated coatings after 24 hours of salt spray testing.

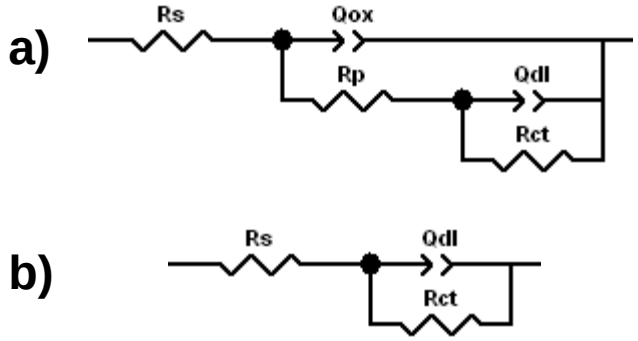

Figure 4: Models of the equivalent circuits used to fit EIS data from a) post-treated and b) as-deposited CeCCs

Table I: Parameter values for post-treated CeCCs, fitted from the equivalent circuit shown in Figure 4a: $R_s(Q_{ox}(R_p(Q_{dl}R_{ct})))$ (R_s – solution resistance, Q_{ox} – coating capacitance, R_p – polarization resistance, Q_{dl} – double layer capacitance, R_{ct} – charge transfer resistance)

Salt Spray Exposure Time	R_s (Ω-cm^2)	Q_{ox} (μΩ^{-1}sec^{n}cm^{-2})	R_p (Ω-cm^2)	Q_{dl} (μΩ^{-1}sec^{n}cm^{-2})	R_{ct} (kΩ-cm^2)
0 hours	16 ± 1	19 ± 4	190 ± 26	42 ± 10	46 ± 3
1 hour	14 ± 1	20 ± 6	356 ± 43	27 ± 5	51 ± 5
3 hours	17 ± 2	12 ± 2	355 ± 92	19 ± 11	74 ± 8
6 hours	16 ± 3	14 ± 3	317 ± 98	21 ± 7	99 ± 8
12 hours	8 ± 5	11 ± 2	246 ± 52	21 ± 3	126 ± 4
24 hours	12 ± 6	24 ± 3	308 ± 67	28 ± 1	130 ± 5
48 hours	10 ± 1	23 ± 8	316 ± 24	33 ± 5	125 ± 12
168 hours	14 ± 5	17 ± 4	339 ± 36	30 ± 10	125 ± 8
336 hours	7 ± 3	22 ± 6	290 ± 30	21 ± 4	87 ± 8

Table II: Parameter values for as-deposited coatings, fitted from the equivalent circuit shown in Figure 4b: $R_s(Q_{dl}R_{ct})$ (R_s – solution resistance, Q_{dl} – double layer capacitance, R_{ct} – charge transfer resistance)

Salt Spray Exposure Time	R_s (Ω-cm^2)	Q_{dl} ($\mu\Omega^{-1}$sec^{n}cm^{-2})	R_{ct} (kΩ-cm^2)
0 hours	15 ± 8	29 ± 6	9 ± 1
1 hour	20 ± 3	38 ± 6	6 ± 1
3 hours	21 ± 2	59 ± 15	8 ± 1
6 hours	23 ± 2	50 ± 3	8 ± 2
12 hours	18 ± 1	33 ± 19	9 ± 1
24 hours	20 ± 2	76 ± 8	12 ± 1
48 hours	19 ± 2	75 ± 6	12 ± 2
168 hours	22 ± 5	83 ± 18	13 ± 2

Changes in surface compositions of CeCCs during salt spray exposure were analyzed using AES depth profiling. Prior to corrosion testing, sealed CeCCs (Figure 5a) were ~450 nm thick, based on the depth at which cerium concentrations fell below those of aluminum. In addition, AES detected ~40 at% oxygen, but minimal aluminum (<5 at%) at the surface of the coatings before salt spray exposure. After six hours of exposure (Figure 5b), aluminum and oxygen concentrations at the surface increased to 20 at% and 50 at% respectively. After 24 hours of exposure (Figure 5c), an aluminum-rich layer ~150 nm thick, based on the depth at which the aluminum concentrations fell below that of cerium, was detected on the surface. The thickness of the aluminum-rich layer remained in the range of 100 to 150 nm through 14 days of salt spray exposure for post-treated coatings.

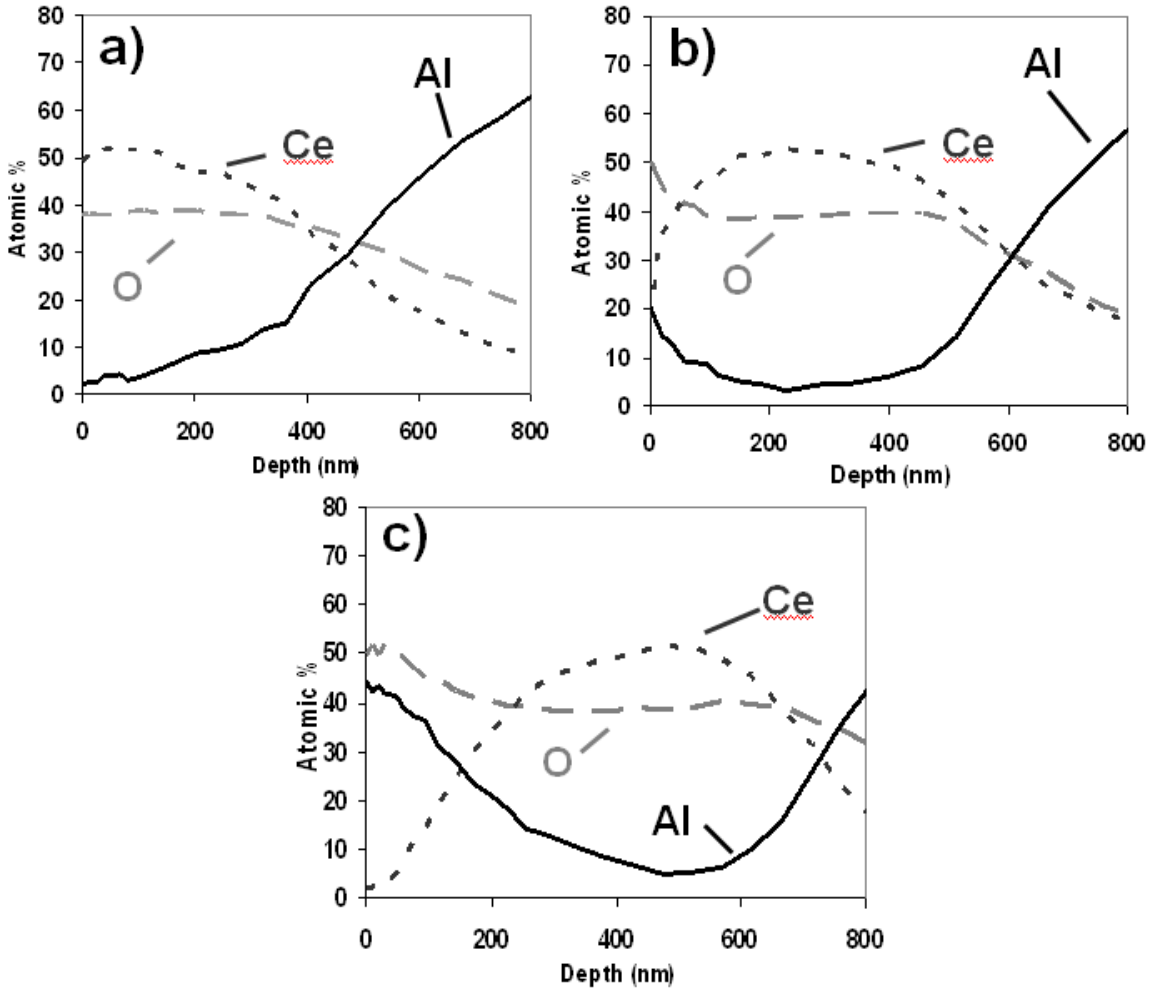

Figure 5: AES depth profiles for post-treated CeCCs a) before salt spray exposure and after b) 6 hours and c) 24 hours of exposure.

Prior to salt spray exposure, as-deposited CeCCs exhibited an AES depth profile (Figure 6a) similar to that of the sealed coatings. The coating thickness was ~450 nm with aluminum and oxygen concentrations at the surface of the coating of ~5 at% and 40 at%, respectively. After six hours of salt spray exposure (Figure 6b), an aluminum-rich layer ~150 nm thick was present on the as-deposited coatings, which had surface concentrations of aluminum and oxygen of 40 at% and 50 at%, respectively. The thickness and composition of the alumina layer remained at ~150 nm after 24 hours of testing (Figure 6c) and through 14 days of exposure.

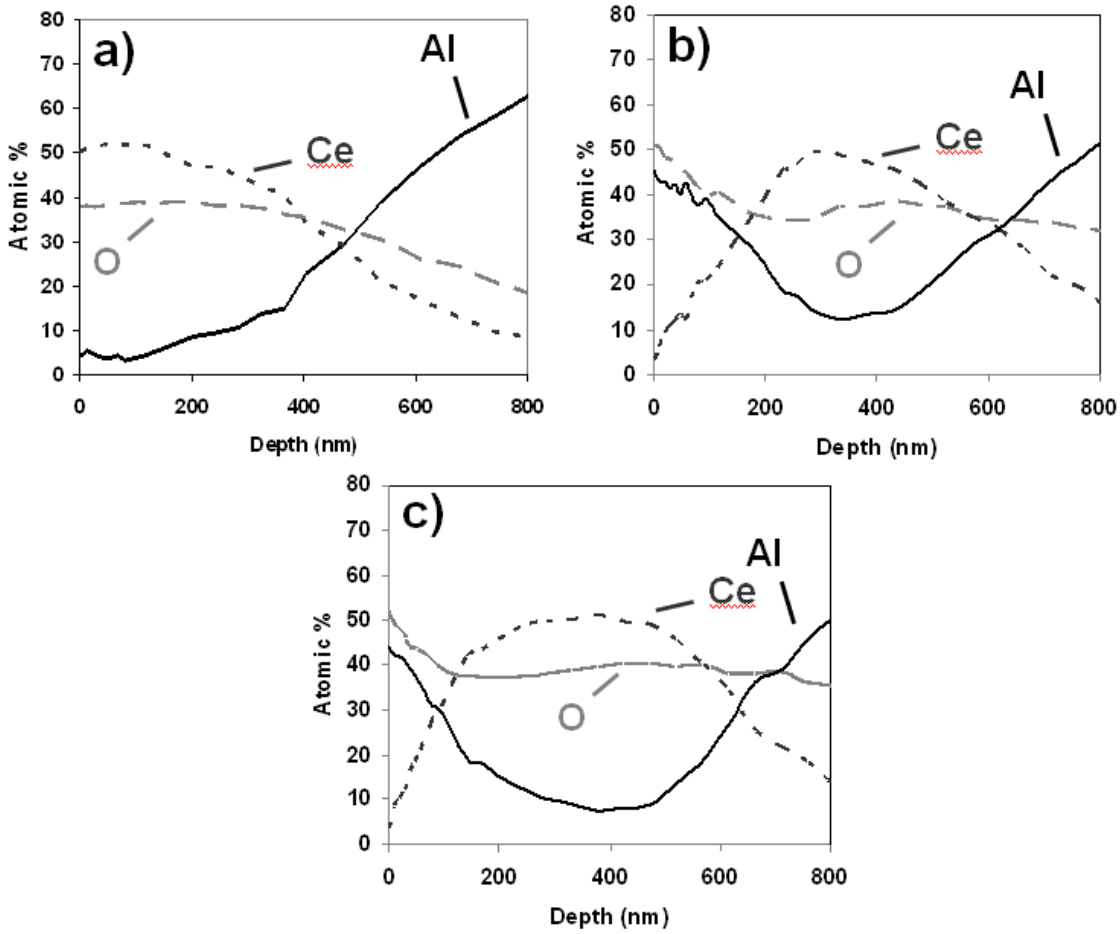

Figure 6: AES depth profiles of as-deposited CeCCs a) before salt spray exposure and after b) 6 hours and c) 24 hours of exposure.

During the first 24 hours of salt spray exposure, post-treated CeCCs exhibited significant increases in impedance and developed an aluminum-rich layer ~150 nm thick on the surface while having no visible corrosion. Given the correlation between the increase in impedance and the development of the aluminum-rich layer, it is hypothesized that post-treated CeCCs facilitated the formation of a protective alumina layer during salt spray exposure. The source of aluminum, phase of the layer, and areas covered by the layer have not been investigated extensively, but remain the subject of continuing research on the corrosion protection mechanisms of CeCCs.

In contrast to post-treated coatings, as-deposited CeCCs did not exhibit the same increases in impedance during salt spray exposure. Instead, the impedance remained

relatively constant (after an initial drop) during the first 24 hours of salt spray exposure. The aluminum-rich layer on the surface of as-deposited coatings was thicker after the same salt spray exposure times as compared to the aluminum-rich layer on post-treated coatings. Unlike the aluminum-rich layer that formed on sealed CeCCs, the aluminum-rich layer on unsealed coatings did not appear to be protective, since coating impedance did not increase with the presence of the layer. Additionally, significant salting was observed on as-deposited coatings after 24 hours of salt spray exposure. Thus, the aluminum-rich layer that formed on as-deposited CeCCs during salt spray exposure did not exhibit protective properties, appearing to be more of a corrosion product.

In addition to studying the electrochemical and surface chemical changes that occurred during salt spray exposure, structural changes were also characterized. Specifically, subsurface voids were found in both sealed and unsealed coatings. Subsurface voids were found in areas of CeCCs that exhibited large cracks on the surfaces. For post-treated CeCCs, large cracks were present over ~10% of the area of the coated surfaces and sub-surface voids were found in most of these areas. After six hours of salt spray exposure, large cracked areas of post-treated CeCCs exhibited small pits (Figure 7). With longer exposure times, pits were still observed, but neither the number nor the size appeared to change.

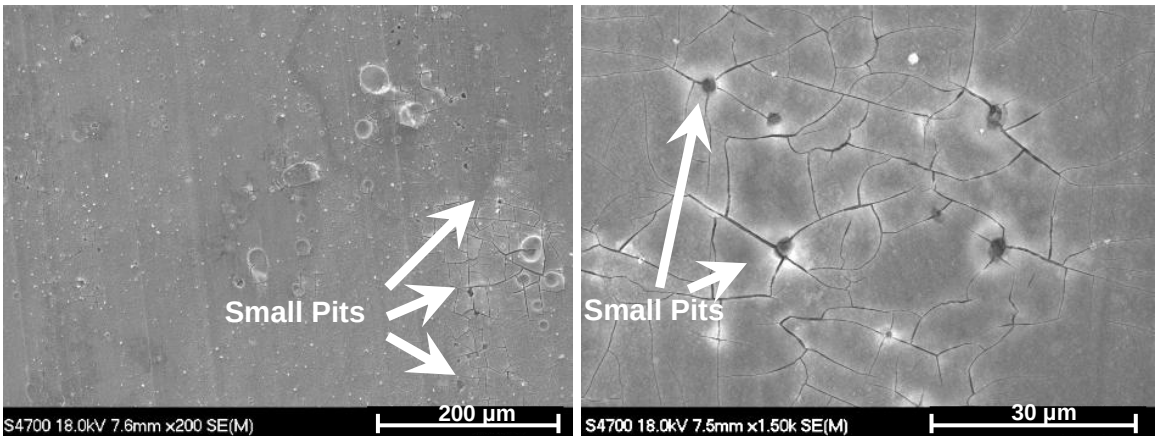

Figure 7: SEM images of a post-treated CeCC after six hours of salt spray exposure in which areas of the coating (~10% of the total area) exhibiting large cracked were found to have developed small pits.

FIB cross sectioning was done on a corrosion pit found in an area with large cracks on a post-treated CeCC after seven days salt spray exposure (Figure 8). The cross section of the pit revealed the presence of subsurface voids underneath the pit. In addition, a dark aluminum-rich phase was observed surrounding most of the perimeter of voids. After seven days of salt spray testing, the dark aluminum-rich phase in the void remained intact, with few, if any, defects such as pores or cracks. Given the lack of corrosion product either in the voids or on the surface of the panels, post-treated CeCCs appear to be able to protect the alloys from corrosion even inside subsurface voids. Within the voids, the protection may be due to the oxide surrounding these features, which could be resistant to the corrosive conditions that develop in salt spray testing.

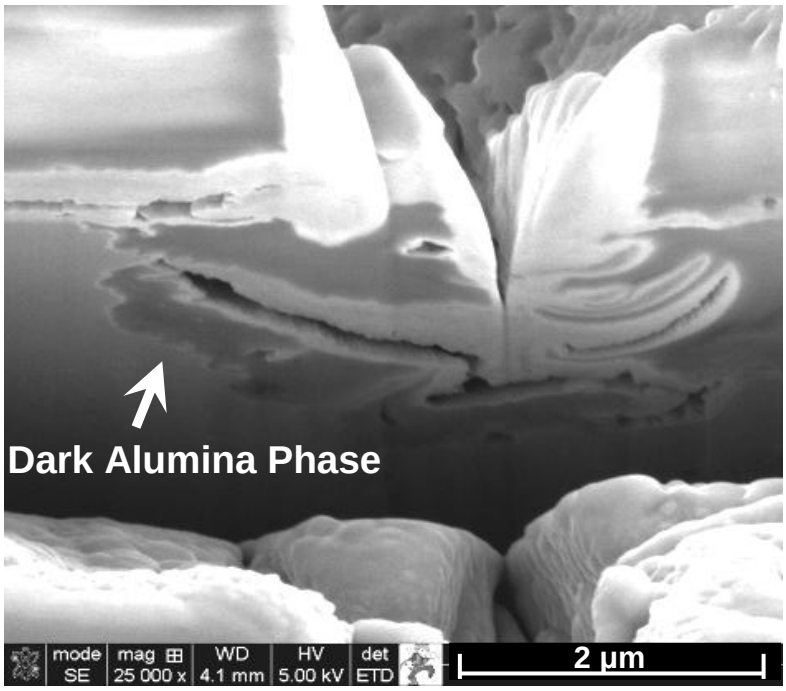

Figure 8: FIB cross section of a pit found in a post-treated CeCC after seven days of salt spray testing.

As-deposited coatings had large cracks present in over half of the area of the coated surface, however sub-surface voids were found in only a small fraction of the areas with large cracks. Large cracked areas of as-deposited coatings did not develop pits as was observed for post-treated CeCCs. Rather, these areas developed nodules that were rich in aluminum and oxygen after 6 hours of salt spray exposure (Figure 9a). The alumina

nodules became more prevalent with time until ~24 hours of exposure at which time the large cracked areas were completely covered by the aluminum-rich material (Figure 9b). Combined with the observation of salt tails and analysis of the EIS data, the aluminum-rich phase on these coatings was a corrosion product that deposited on isolated areas of the coating surfaces, not a protective layer that formed in the post-treated CeCCs.

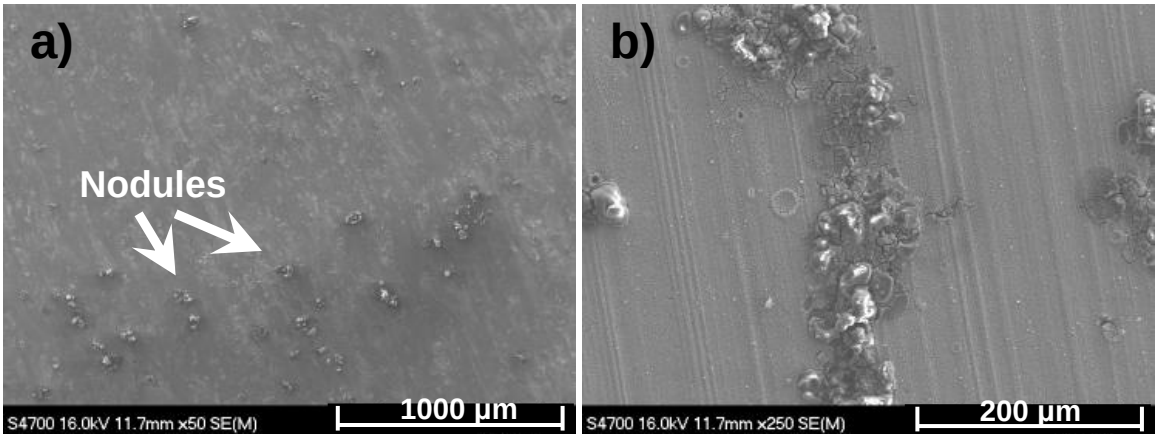

Figure 9: Surface morphology of as-deposited CeCCs after a) six hours and b) 24 hours of salt spray exposure.

The cross sectional structure, prepared by FIB milling, of an aluminum-rich nodule found on an as-deposited CeCC after 6 hours of salt spray exposure (Figure 10) revealed subsurface voids present underneath these features, just as they were found underneath pits in the post-treated coatings. The dark oxide phase around these voids, however, exhibited a large degree of porosity. This morphology indicated that the oxide found around the perimeter of the voids in as-deposited coatings did not have the protective properties of the dense, coherent oxide found around the voids of post-treated coatings.

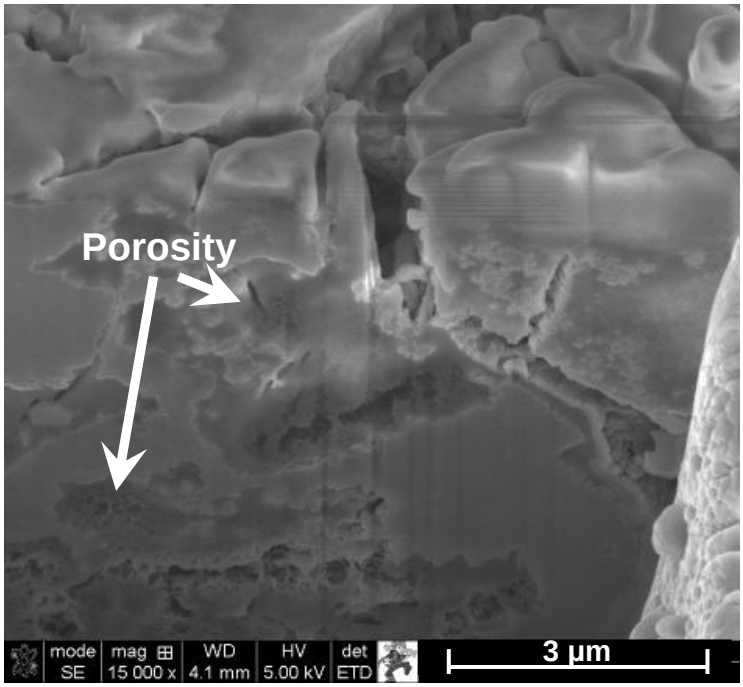

Figure 10: FIB cross section of an alumina nodule found in an unsealed CeCC after 6 hours of salt spray testing.

The FIB/SEM analysis revealed that the corrosion protection of CeCCs depended on the coating processing conditions. Specifically, post-treatment affected the morphology of aluminum-rich oxide phases that formed inside subsurface voids and on the surfaces of CeCCs. The surfaces of as-deposited CeCCs exhibited a large degree of corrosion product (aluminum-rich nodules) in the first 24 hours of salt spray exposure, while the surfaces of post-treated coatings developed small pits with no visible corrosion product. Based on these observations, post-treated coatings were able to protect the alloys to a greater degree than as-deposited coatings. The CeCCs protected the alloys despite the presence of uncoated subsurface voids that formed during coating deposition. While further studies are needed to understand this behavior, SEM imaging of cross sectional structures showed that the oxide present around the voids in post-treated coatings was dense and coherent, while the oxide present in the voids of as-deposited coatings exhibited a significant amount of porosity after salt spray exposure. This result suggested that post-treatment may alter the oxide present around subsurface voids to a phase and/or structure that can better protect the surrounding substrate compared to the oxide present in the voids of an unsealed coating.

Summary

Electrochemical and structural changes were characterized for CeCCs as a function of salt spray exposure time. Sealed CeCCs exhibited no visible corrosion through seven days of salt spray exposure. During the first 12 hours of salt spray testing, the impedance of the coatings increased to more than twice its initial value. This increase was accompanied by the formation of an aluminum-rich layer that was ~150 nm thick, indicating sealed coatings may facilitate the development of a protective alumina layer in the early stages of salt spray exposure. In contrast, as-deposited CeCCs corroded heavily in the first 24 hours of salt spray testing and exhibited impedances an order of magnitude less than post-treated CeCCs. After a drop in impedance during the first hour of salt spray exposure, the impedance remained near its initial value until after ~24 hours. During this time, significant corrosion was observed for panels with as-deposited CeCCs. An aluminum-rich layer ~200 nm thick was detected on as-deposited coatings after just 6 hours of salt spray exposure. Unlike post-treated coatings, however, the formation of this layer occurred with visible corrosion on the panels. Based on these results and SEM observations, it was concluded that the aluminum-rich layer that formed on as-deposited CeCCs was not protective, but was a corrosion product.

Corrosion protection of aluminum alloys with subsurface voids depended on whether the CeCCs were post-treated or not. Areas with voids in post-treated coatings developed small pits in the first 24 hours of exposure, but did not show any signs of the formation of corrosion products on the panel surfaces. The protection of the voids for post-treated coatings appeared to be related to the presence of an aluminum-rich oxide that formed on the perimeters of these features. The oxide was dense and coherent and it remained intact during salt spray exposure. For as-deposited coatings, aluminum-rich oxide nodules formed on the surface and increased in size with longer salt spray exposure times. The aluminum-rich oxide around the perimeters of subsurface voids in as-deposited coatings was porous after salt spray exposure, indicating that the layer may not be protective. Collectively, the formation of a protective alumina layer on the panel surface and the

presence of a dense oxide around the perimeters of subsurface voids appear to be responsible for the enhanced corrosion protection of post-treated CeCCs compared to as-deposited coatings.

Acknowledgements

This work was funded through the Strategic Environmental Research and Development Program (SERDP) under contract W912HQ-08-C-0008. The authors would like to acknowledge the technical guidance and support of Bruce Sartwell at SERDP. We also appreciate the technical assistance of Jeff Wight (AES) and Ming Zhang (FIB) at Missouri University of Science and Technology. Discussions and collaborations with Eric Morris and Rich Albers of Deft are also acknowledged.

References

1. A.E. Hughes, R.J. Taylor, B.R.W. Hinton, *Surf. Interface Anal.*, **25**(4), 223 (1997).
2. D. Baudrand, *Plat. Surf. Finish..*, **92**(1), 30 (2005).
3. M. Costa and C.B. Klein, *Crit. Rev. Toxicol.*, **36**(2), 155 (2006).
4. S. You, P. Jones, A. Padwal, P. Yu, M. O'Keefe, W. Fahrenholtz, T. O'Keefe, *Mater. Lett.*, **61**, 3778 (2007).
5. M. Bethencourt, F.J. Botana, M.J. Cano, M. Marcos, *Appl. Surf. Sci.*, **189**, 162 (2002).
6. H. Zhang and Y. Zou, *App. Surf. Sci.*, **254**(16), 4930 (2008).
7. B.R.W. Hinton, D.R. Arnott, N.E. Ryan, *Mater. Forum*, **9**(3), 162 (1986).
8. A.E. Hughes, J.D. Gorman, P.R. Miller, B.A. Sexton, P.J.K. Paterson, R.J. Taylor, *Surf. Interface Anal.*, **36**, 290 (2004).
9. F.H. Scholes, C. Soste, A.E. Hughes, S.G. Hardin, P.R. Curtis, *App. Surf. Sci.*, **253**, 1770 (2006).
10. S.A. Hayes, P. Yu, T.J. O'Keefe, M.J. O'Keefe, J.O. Stoffer, *J. Electrochem. Soc.*, **149**(12), C623 (2002).

11. W. Pinc, S. Geng, M. O'Keefe, W. Fahrenholtz, T. O'Keefe, *Appl. Surf. Sci.*, **255**(7), 4061 (2009).

12. A. de Frutos, M.A. Arenas, Y. Liu, P. Skeldon, G.E. Thompson, J. De Damborenea, A. Conde, *Surf. Coat. Tech.*, **202**(16), 3797 (2008).

13. W. Pinc, P. Yu, M. O'Keefe, W. Fahrenholtz, *Surf. Coat. Tech.*, **203**, 3533 (2009).

14. S. Geng, P. Yu, M.J. O'Keefe, W.G. Fahrenholtz, T.J. O'Keefe, Accepted for publication in *J. App. Electrochem.*, (2009).

15. D.K. Heller, W.G. Fahrenholtz, M.J. O'Keefe, *J. Electrochem. Soc.*, **156**(11), C400 (2009).

16. B.L. Treu, S. Joshi, W.G. Fahrenholtz, M.J. O'Keefe, Accepted for publication in *T. Electrochem. Soc.*, **19**, (2009).

17. B.R.W. Hinton, D.R. Arnott, N.E. Ryan, *Mater. Forum.*, **9**(3), 162 (1986).

18. C. Wang, F. Jiang, F. Wang, *Corrosion*, **60**(3), 237 (2004).

19. W. Pinc, S. Joshi, M. O'Keefe, W. Fahrenholtz, Accepted for publication in *The Proceedings of the 2009 DoD Corrosion Conference*.

APPENDIX C.

UNPUBLISHED DATA

Electrolyte Selection

Electrolyte solutions containing only 1.6 or 3.5 wt. % NaCl were determined to be too aggressive for attaining the most detail during polarization scans of CeCCs. Using a prohesion solution (0.05 wt. % NaCl + 0.35 wt. % $(NH_4)_2SO_4$) with the flat cell resulted in unacceptable noise in the collected data. Formulating a modified prohesion solution by changing the relative concentrations of sodium chloride and ammonium sulfate in the electrolyte produced relatively clean curves with a well defined anodic plateau. When the same specimens were tested using more aggressive electrolytes (i.e., 1.6 wt. % NaCl), a passivation region is not observed and the open circuit potential is approximately the breakdown potential of the specimen as shown in Figure C1.

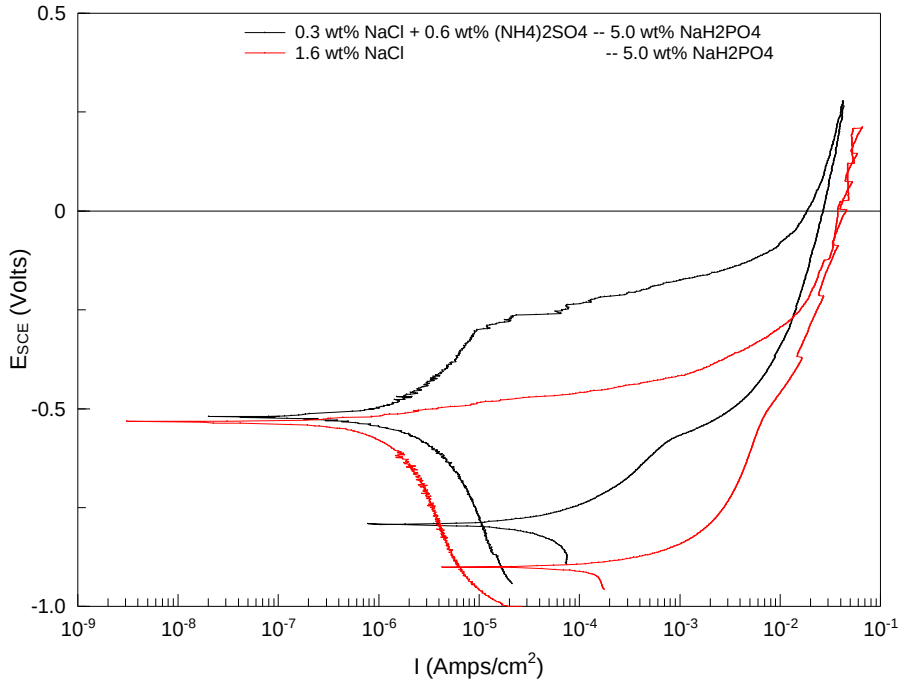

Figure C1. Cyclic potentiodynamic curves obtained with solutions of 1.6 wt% NaCl (red) and 0.3 wt% NaCl + 0.6 wt% $(NH_4)_2SO_4$ (black).

Effect of Phosphate Concentration

As-deposited CeCCs were post-treated in solutions of 2.5, 5.0, and 10 wt. % Na_3PO_4 and NaH_2PO_4. The surface cleaning and activation process was the same for all panels and consisted of an acetone rinse, 5 minute Turco clean, and a 10 minute sulfuric

acid etch. The post-treatment solution was maintained at 85 °C with a pH of 4.4 to 4.5 (adjusted with H_3PO_4) and panels were immersed for five minutes.

After salt spray testing, each of the specimens exhibited a similar quantity of corrosion on the panel surface, indicating that the different phosphate concentrations did not have a large impact on the corrosion performance. The surface morphology of panels post-treated in solutions containing higher orthophosphate concentrations (i.e., 5.0 and 10.0 wt. %) contained more regions of large cracks than the 2.5 wt. % solution. Despite containing more cracks, these specimens were still able to provide equivalent corrosion protection as a sample containing fewer, or smaller, cracks. This suggests that coating performance does not directly relate to the number of cracks in the CeCC.

EDS data averaged over three areas is shown below in Table C1. Increasing the phosphate concentration in the sealing solution only increased the amount of phosphorus detected in the coating by one to two atomic percent, revealing that increasing the phosphate concentration of the solution does not result in a large increase in the phosphorous incorporated into the CeCC. Grazing incidence XRD patterns indicated that the higher phosphate concentrations did not affect the crystalline phase of the CeCC, with all concentrations producing materials matching closely with hydrated $CePO_4$.

Table C1. Collected EDS data for NaH_2PO_4 at 2.5, 5.0, and 10.0 wt% (compositions listed in atomic %).

NaH_2PO_4	2.5 wt %	5 wt %	10 wt %
Sodium	7.6	8.2	9.5
Cerium	1.9	2.1	2.0
Aluminum	17.8	11.3	12.3
Phosphorus	15.6	17.3	16.7
Oxygen	57.2	61.1	59.6
P/Ce	8.0	8.2	8.2

Normalized phosphorus concentration

CeCCs were post-treated in solutions produced from different phosphate sources. The solution compositions were adjusted so each solution had a phosphorus concentration of 0.22 M. The tested phosphates included $NH_4H_2PO_4$, NaH_2PO_4, Na_3PO_4, $K_4P_2O_7$, and $Na_2H_2P_2O_7$. After reaching 85 °C, the solution pH was adjusted to 4.5 with

phosphoric acid. Optical images of the panels after two weeks of salt spray exposure are shown in Figure C2. Panels sealed in solutions made from pyrophosphate compounds showed increased salting compared to panels sealed with solutions of orthophosphate compounds, consistent with previous studies.

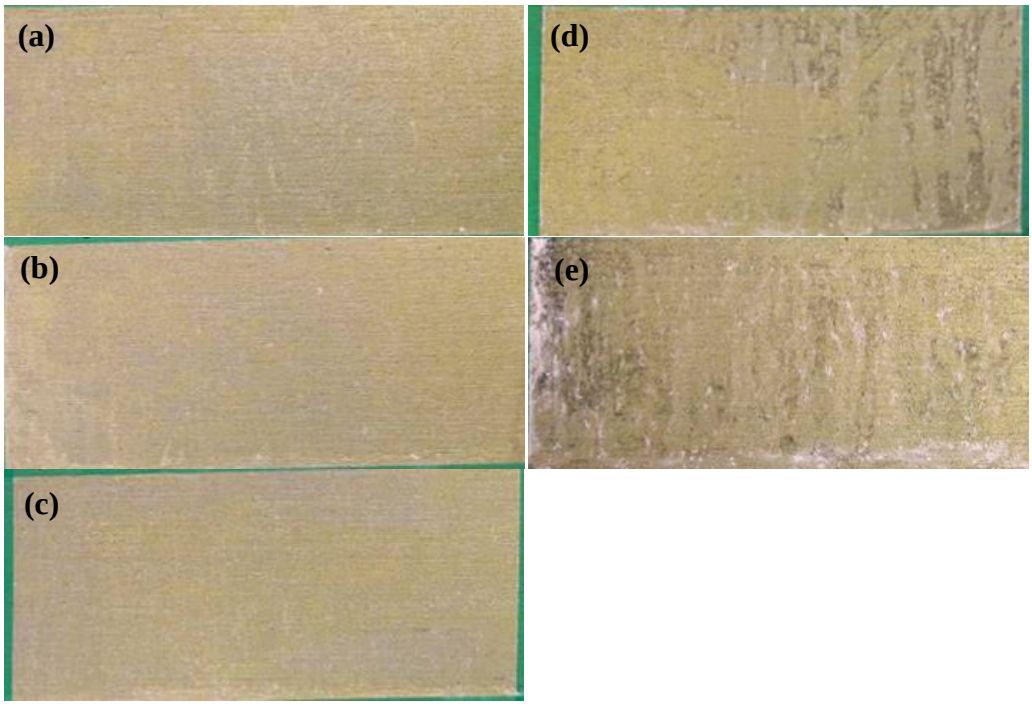

Figure C2. Panels sealed in solutions containing normalized phosphorus concentration after 14 days of salt spray testing, (a) $NH_4H_2PO_4$, (b) Na_3PO_4, (c) NaH_2PO_4, (d) $K_4P_2O_7$, and (e) $Na_2H_2P_2O_7$.

Electrochemical impedance spectroscopy (EIS) and potentiodynamic scans performed one month after coating deposition were in good agreement with results from salt spray testing (Figure C3). Prior studies demonstrated a correlation between salt spray performance and the phosphate source used to prepare the post-treatment solution. Previously, 2.5 wt% solutions of various phosphates were compared; the present analysis accounts for effects that may have been caused by varied phosphorus concentration by normalizing the concentration of all post-treatment solutions to 0.22 M phosphorus. The results show that individual phosphates have a distinct affect on the resistance of the CeCC. The EIS data correlates to salt spray results, indicating that higher coating resistance corresponds to improved corrosion resistance. Panels with a coating resistance

near or surpassing 50,000 Ω cm^2 (e.g., Na_3PO_4, $NH_4H_2PO_4$, NaH_2PO_4) performed similarly in salt spray testing. The lowest coating resistance of ≈14,500 Ω cm^2 was recorded for $Na_2H_2P_2O_7$ which exhibited the worst corrosion resistance. Panels post-treated in the $K_4P_2O_7$ solution show impedance near 39,000 Ω cm^2 on average with corrosion performance lying between the orthophosphate sources and $Na_2H_2P_2O_7$.

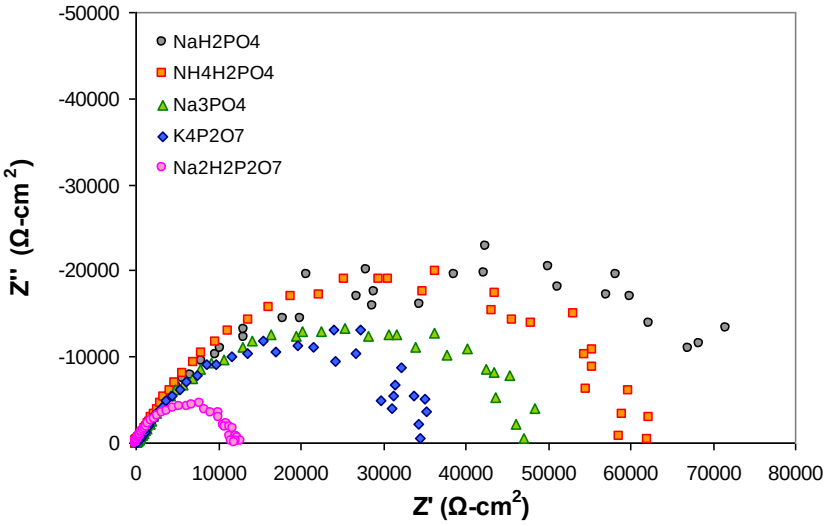

Figure C3. EIS data collected for panels sealed in normalized phosphate solutions.

Each of the potentiodynamic scans were similar, Figure C4. The CeCC post-treated in the $Na_2H_2P_2O_7$ solution had less anodic pitting potential and a higher corrosion current density that any of the other conditions. CeCCs post-treated with the orthophosphate sources performed the best, exhibiting more anodic pitting potential and lower corrosion current densities. The 'saw tooth' pattern evident in the anodic sweep suggests the formation of metastable pits, a response not observed for specimens post-treated in $Na_2H_2P_2O_7$, indicating less resistance to pitting corrosion. Despite exhibiting a polarization response similar to the orthophosphate sources, CeCCs post-treated with $K_4P_2O_7$ have approximately half the total resistance, resulting in decreased corrosion resistance.

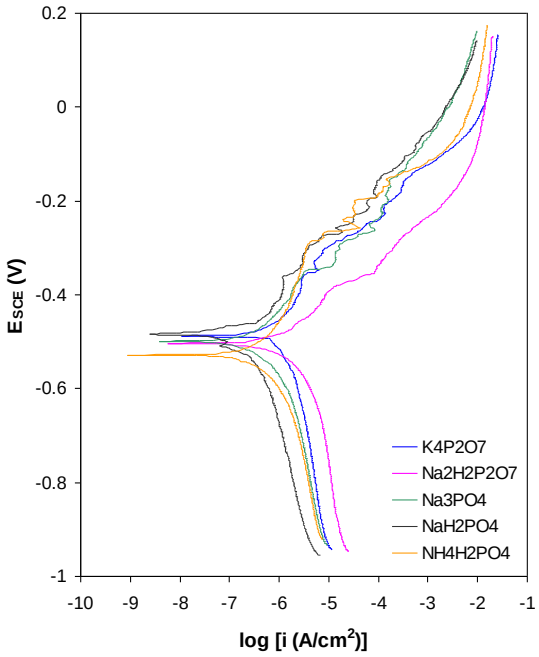

Figure C4. Polarization curves for panels sealed with solutions produced from various phosphate sources but maintaining a 0.22 M phosphorus concentration

Tributyl Phosphate

As-deposited CeCCs were post-treated in aqueous solutions containing tributyl phosphate. SEM analysis revealed that the post-treatment affected the adherence of the coating, causing areas up to 75 µm in diameter to flake off. Despite these defects, CeCCs post-treated with 3 – 5 ml of TBP per 150 ml deionized water performed better than unsealed specimens. EDS analysis revealed that the phosphorous concentration in the CeCC was approximately 10 at. %, over half that measured for CeCCs post-treated in solutions up to 10 wt. % orthophosphate.

Fluoride-based surface activation

Panels were immersed in solutions containing 0.5 wt. % HF, 0.5 wt. % HBF_4, 0.25 wt. % HCl + 0.25 wt. % HF for 20 seconds, coated with 5 sprays, and sealed in 2.5 wt% NaH_2PO_4. The images of the panels after two weeks of salt spray testing are shown in Figure C5. Etching with 0.5 wt. % HBF_4 provided the best corrosion performance and was equivalent to the standard H_2SO_4 surface activation. To examine the effect of etching time, 3" x 6" panels immersed for 20 sec, 1 min, and 2 min immersions in 0.5 wt.

% HBF_4, coated, and post-treated. After one week of salt fog testing, panels subjected to shorter etching times showed fewer corrosion pits and salt tails.

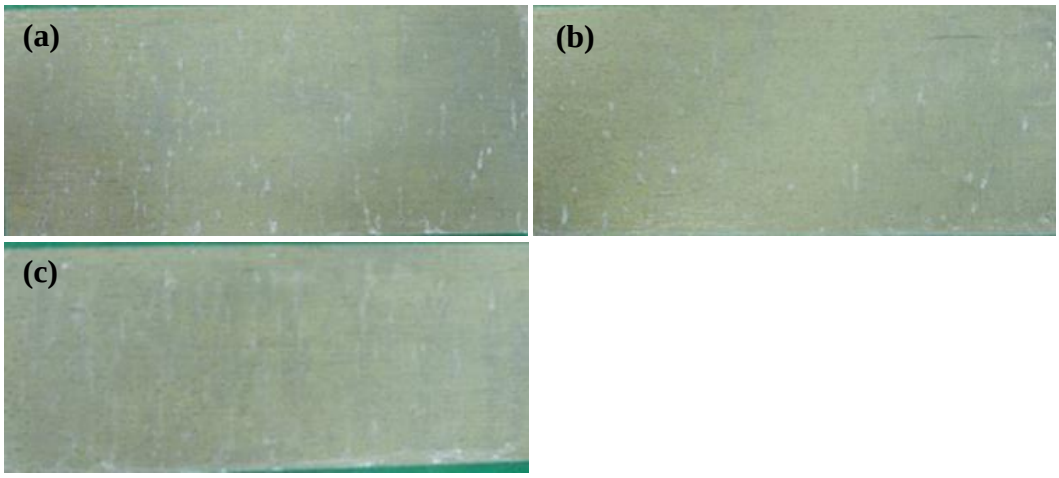

Figure C5. Fluoride surface preparation after two weeks of salt fog testing, (a) 20 sec 0.25 wt% HCl + 0.25 wt% HF, (b) 20s 0.5 wt% HBF4, (c) 20s 0.5 wt% HF.

Dynamic open circuit potential

The open circuit potential was recorded during post-treatment in three different phosphate solutions: 2.5 wt. % Na_3PO_4, 2.5 wt. % $K_4P_2O_7$, and 2.5 wt. % NaH_2PO_4 and the data reported in Figure C6. Differences were observed in three different regions of the plot, the initial peak, the subsequent trough, and the final slope. Phosphate seals denoted by the red (2.5 wt. % Na_3PO_4) and green (2.5 wt. % NaH_2PO_4) curves are known to do well in salt spray testing whereas the blue curve (2.5 wt. % $K_4P_2O_7$) exhibits intermediate performance. Upon placing the specimen in the sealing solution, the open circuit potential rapidly decreased by ≈600 mV until reaching a minimum of -0.8 to -0.9 V(SCE), then began increasing slowly or stabilizing near -0.7 to -0.8 V(SCE).

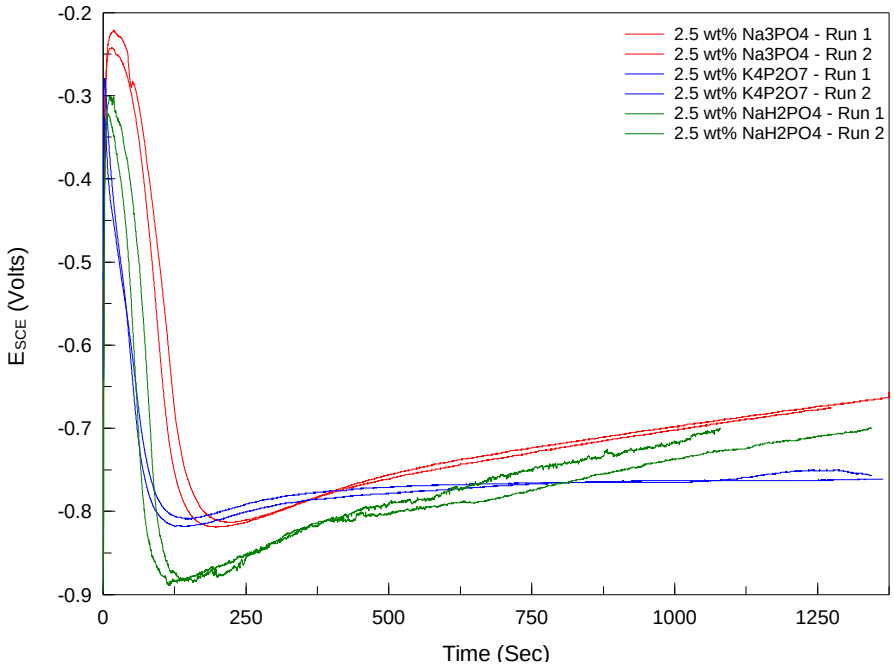

Figure C6. Dynamic open circuit potential recorded during sealing in phosphate solutions containing 2.5 wt. % Na_3PO_4, 2.5 wt. % K_4P2O_7, or 2.5 wt. % NaH_2PO_4.

Titration of Post-treatment Solutions

Titrations of 2.5 wt% solutions of $Na_2H_2P_2O_7$, NaH_2PO_4, and Na_3PO_4 were performed at room temperature and 85 °C (Figure C7). In each case the solution was adjusted to a pH of 4.4 with H_3PO_4, and then reduced to 1.5 with 9 M HCl. At this point, 7.5 M NaOH was used to titrate the solution past pH ~ 12; varying volumes of the NaOH solution were added depending on the pH sensitivity (i.e., larger additions at low sensitivity and smaller additions at high sensitivity) as the titration proceeded to ensure that the resulting curve would be continuous. While all of the curves are similar, the data indicate that there were small differences between the phosphate sources in the rate of transition between pK_a's, the pH range over which the transition occurs, and the requisite NaOH to produce a given pH. At 85 °C, the curves are shifted to the right, indicating that more NaOH is required to attain the same pH observed at room temperature and the slope of the curve in the transition region has been suppressed. The important observation is that the pH where best corrosion performance is achieved (for all phosphate sources) laid in the middle of the transition region of the titration curves.

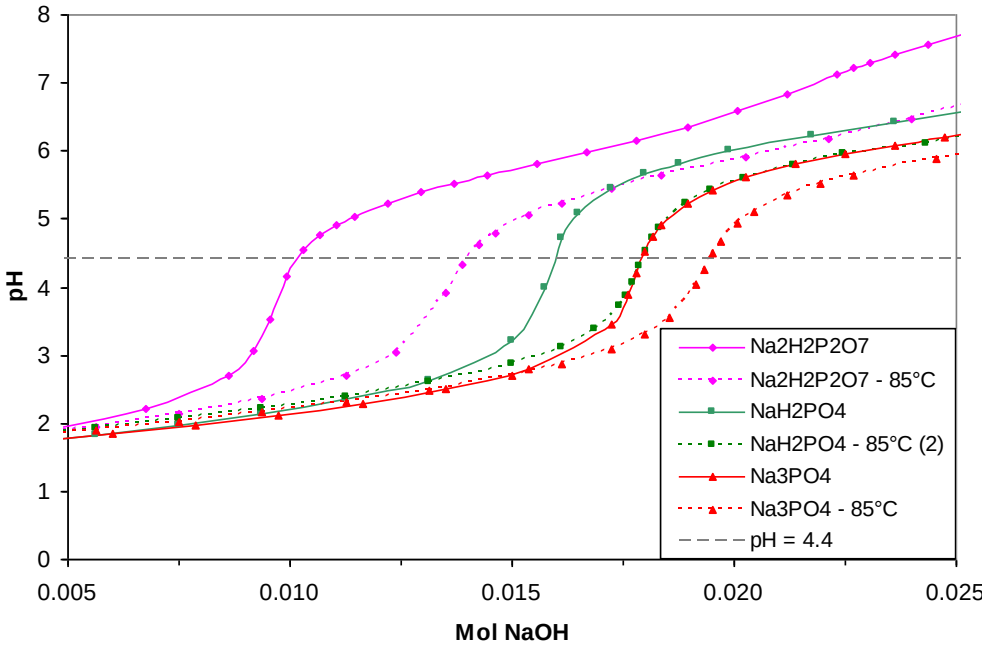

Figure C7. Titration curves for 2.5 wt% solutions of $NaH_2P_2O_7$, NaH_2PO_4, and Na_3PO_4 at room temperature and 85 °C.

The initial pH of the phosphate solutions was weakly dependent on temperature (Table C2). Heating the solutions shifted the pH to more neutral values (i.e., acidic pH values increased and basic pH values decreased). The pH change affected the concentration of H_3PO_4 added to the sealing solution, but was determined to have no effect on corrosion performance. Dihydrogen phosphate species are preferred because their natural pH is near the value where typical post-treatments are performed, 4.0 – 4.5.

Table C2. Initial solution pH of phosphate solutions at room temperature and 85 °C.

Phosphate Source	**Initial pH**	
	25 °C	**85 °C**
$NaH_2PO_4 \cdot H_2O$	4.4	4.6
$Na_3PO_4 \cdot 12H_2O$	12.4	11.2
$K_4P_2O_7$	10.5	10.7
$Na_2H_2P_2O_7$	4.3	4.5
$Na_5P_3O_{10}$	9.1	9.5

As a follow up to the above, coated panels were sealed in five different phosphate solutions at a pH near 3.5 and 4.0. After 3 days of salt fog testing, definitive differences were observed in the performance of 2.5 wt% $K_4P_2O_7$ which showed significant deterioration from pH 4.0 to 3.5 and $Na_5P_3O_{10}$ which exhibited vastly improved performance when sealed at a pH of either 3.5 or 4.0 as opposed to the standard treatment near 4.5. The initial explanation is an extension of the above observations in that different species had shifted titration curves and by changing the sealing pH, the slope of the curve at that pH will also change. Further analysis will assist in determining if this correlation is accurate.

Water Post-treatment

As-deposited CeCC were post-treated for 5 min in 85 °C water. The surface morphology exhibited less cracking than an unsealed panel but retains craters thought to be created by gas evolution. Bubble formation during water post treatment is more vigorous than phosphate containing treatments. This evolution is thought to be caused by the decomposition of peroxy and hydroxy species when exposed to the elevated temperature of the sealing solution. Salt spray testing of the water treated sample shows improved corrosion performance compared to an untreated panel; after testing, the panel has significantly fewer pits when compared to the unsealed condition (Figure C8).

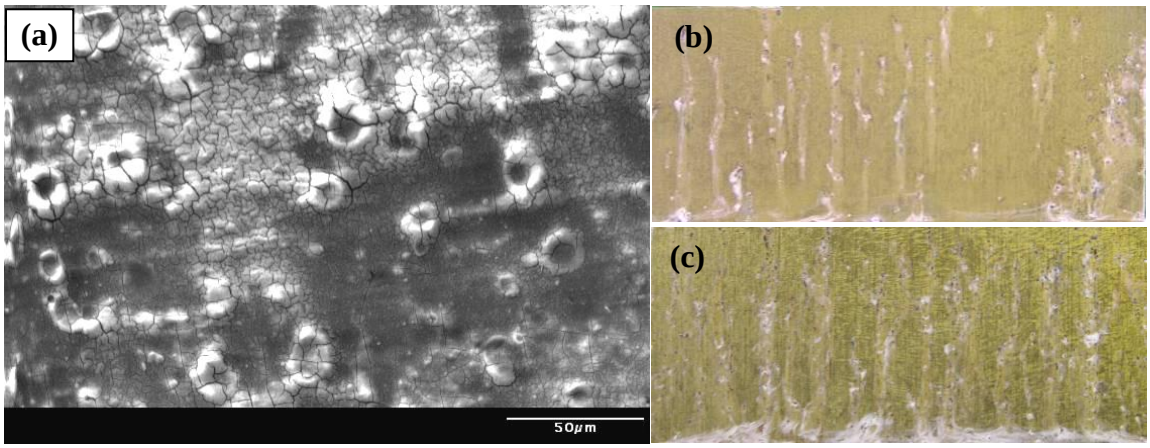

Figure C8. SEM micrograph and included optical images of unsealed and water sealed CeCC, (a) as-coated water sealed, (b) water sealed after 14 days of salt spray, and (c) unsealed after 14 days salt spray.

Post-treatment Time and Temperature – XPS

Analysis by XPS of CeCCs post-treated in 85 °C orthophosphate solutions for 10 sec, 30 sec, 2 min, and 10 min revealed nearly complete reduction of Ce^{4+} to Ce^{3+} at the specimen surface after 30 sec of immersion (Figure C9). As reported in Section 3, specimens post-treated for 2 or 10 minutes showed less corrosion after two weeks of salt spray exposure than specimens post-treated for times ≤ 30 sec. Longer post-treatment times probably promote the reduction of Ce^{4+} species deeper within the CeCC and result in the formation of $CePO_4$ species throughout the entire coating after 5 or 10 min immersions. While phosphorous was detected throughout the entire CeCC thickness after a 5 min post-treatment, TEM analysis indicates that the coating phase is not uniform and suggests the presence of either unstable cerium hydrogen phosphate species or even unreacted cerium hydroxy/peroxy or hydroxide species. Similar data were obtained with respect to post-treatment temperatures (i.e., 55, 70, and 85 °C). Data from XPS analyses confirmed nearly complete reduction of Ce^{4+} to Ce^{3+} at the CeCC surface for temperatures of at least ≈70 °C. The time and temperature studies suggest that the process active during post-treatment are strongly dependent on kinetic factors.

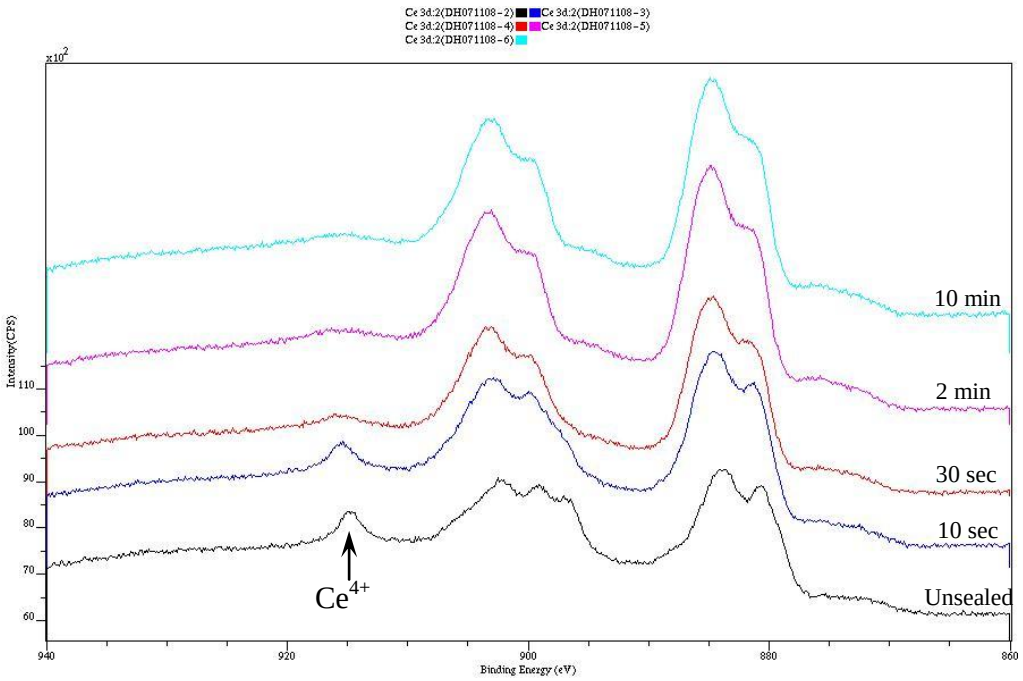

Figure C9. Ce 3d spectrum for panels sealed in $NH_4H_2PO_4$ as a function of time

CeCC deposition based on cerium nitrate

Preliminary experiments were performed to assess the experimental parameters needed to form a CeCC using nitrate precursors (i.e., $Ce(NO_3)_3$). Process variables may include H_2O_2 concentration, solution pH, temperature, chloride addition, nitrate concentration, and surface activation. Several published articles refer to $Ce(NO_3)_3$ coatings solutions containing ≈3 g/L $Ce(NO_3)_3$ and one instance of a concentrated solution of 43 g/l. It is also common to heat nitrate based coating solutions prior to immersion. Surface activations varied widely, covering several acids and acid solutions. Missouri S&T's standard coating solution contains ≈49 g/L of cerium salt. Initial experiments were conducted using this concentration while adding 2.5, 7.5, or 15 ml of H_2O_2 to coating solutions containing 5 g of $Ce(NO_3)_3 \cdot 6H_2O$, 110 g H_2O, and 0.4 g of gelatin (Rousselot, RDH). This variation of H_2O_2 content was examined with coating solution pH values of 2 and 4, adjusted by adding HNO_3 to produce a chloride free solution.

Surface activation was performed by immersing the panels in Turco 4215 NCLT for 5 min at 55 °C followed by an immersion in a solution of 0.5 wt% HBF_4 for 30 sec. After 10 spray cycles, no coating deposition was observed. Using the remaining coating solution, surface activated 1.5 x 1.5 inch coupons were placed upright in the respective coatings solutions and allowed to sit overnight (≈18 hours). Optical images of the resulting panels are shown in Figure C10. The dark orange lines extending horizontally across the panel correspond to the depth of the coating solutions (only the bottom section was exposed to the solution). Coating deposition was observed for panels shown in Figure C10b and C10c (pH = 2, 7.5 and 15 ml H_2O_2 respectively). By inspection, the panel coated with the solution at pH = 2 with 15 ml H_2O_2 was the thickest (darkest) and exhibited a uniform appearance across the immersed surface. The panel exposed to the solution at pH 2 with 7.5 H_2O_2 also exhibited a uniform coating but it was thinner (lighter). Other conditions produced either a very thin, or no, coating.

The stability of the coating solutions was different upon adding H_2O_2 and after the immersion deposition. No precipitation was observed after H_2O_2 addition or after immersion testing for the pH 2, 2.5 ml H_2O_2 condition (the solution remained clear). At a

pH of 2, no precipitation was observed immediately after adding H_2O_2; however, precipitation was observed in the solution the following morning. In contrast, coating solutions at a pH of 4 all began precipitation within 15 – 120 sec after adding H_2O_2. Formation of a coating using a nitrate based (chloride free) solution is possible, but the deposition rate is slower than the chloride-based solution currently used.

As a continued study from previous results, nitrate based deposition of CeCCs was attempted using different surface activations as shown in Table C3. A pH of 2.0 (adjusted with HNO_3) and a H_2O_2 content of 15 ml (per 125 ml solution) was selected based on the results of initial experiments. In an attempt to accelerate coating deposition, gelatin was not incorporated into the solution since it is thought that one of the roles of gelatin is to slow down the coating process. In each case, samples were treated with the standard solvent wipe and alkaline clean prior to surface activation. One sample, immersion coated after an HBF_4 activation, was placed in a sealing solution consisting of 2.5 wt% $NH_4H_2PO_4$ for 5 minutes and analyzed in addition to the other samples.

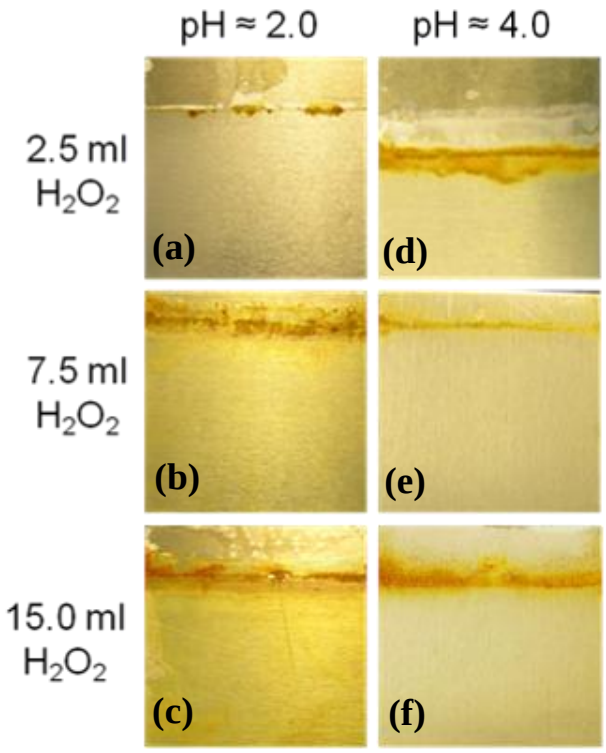

Figure C10. Optical images after immersion in $Ce(NO_3)_3$ based solution overnight.

Table C3. Experimental parameters of nitrate based CeCC coating deposition

Round	H_2O (g)	$Ce(NO_3)_3$ (g)	H_2O_2 (ml)	RDH (g)	pH	Surface Activation	Coating Formation
1st	110	5.0	15.0 7.5 2.5	0.4	2.0 4.0	30 sec HBF_4	Little to no coating formation after 18 hr immersion, 7.5 and 15 ml H2O2 at pH = 2 produced coatings.
2nd	110	5.0	15.0	0.0	2.0	10 min H_2SO_4 30 sec HBF_4 30 sec NaOH 15 min HNO_3 15 min H_3PO_4	Coating evident after 30 - 45 min immersion, removed from coating solution after 1.0 - 1.5 hrs. Spray deposition yielded a very thin coating after 10 sprays, and a thicker, more uniform coatings after 20 sprays (only HBF_4 activated was spray deposited).

After one day of exposure, the surface of each specimen exhibited extensive pitting and large salt tails. SEM micrographs of the surface for each of the conditions are shown in Figure C11. The surface morphologies of the coatings deposited with an immersion process exhibited uniform cracking, and did not suggest the presence of the 'large' and 'small' cracked areas commonly observed from CeCCs deposited from chloride based solutions via a spontaneous spray process. The samples with CeCCs deposited from an immersion bath exhibited uniform cracking that was smaller than that observed in 'large' cracked areas and perhaps on the same order as cracks observed from typically 'small' cracked areas in CeCCs deposited under standard conditions (i.e., acid activation, spray deposition, 10 g $CeCl_3$, 220 g H_2O, 0.6 g gelatin, and 20 ml H_2O_2). In contrast, CeCCs deposited using the spray technique resulted in a coating with much finer cracking than is commonly observed. The coating that was placed in the sealing solution (after immersion deposition) exhibited fewer and finer cracks compared to an unsealed sample, Figure C11e and Figure C11a respectively.

The composition for producing a conversion coating used with chromate and chrome free primers, described in Eric Morris' patent (application number: 11/002,741), was 16.0g $Ce(NO_3)_3$, 7.33g $CeCl_3$, 2.67g H_2O_2, and 140.67g H_2O. Conversion coatings were prepared using wipe application and immersion methods. Panels were cleaned by immersion 5 min immersion in Turco (55 °C), followed by 1.0wt % H_2SO_4 (10 min, 50 °C) or 0.5 wt% HBF_4 (20 sec) using both sealed and unsealed permutations. In each case, a coating was formed. Wipe application methods produced coatings that appeared thin and highly uniform after continuous wiping for ~ 30-60 sec. Immersion coatings

were formed by placing the panel in a beaker containing the weakly agitated coating solution for 5 minutes. These coatings were visually less uniform but did cover the entirety of the panel surface. Conversion coatings were wipe applied to two additional panels, one cleaned with H_2SO_4 and the other with HBF_4. These coatings were then post-treated in a 2.5 wt% solution of NaH_2PO_4 at 85°C for 5 min. All panels were tested in salt spray and exhibited corrosion across the entire panel surface after 3 days of exposure.

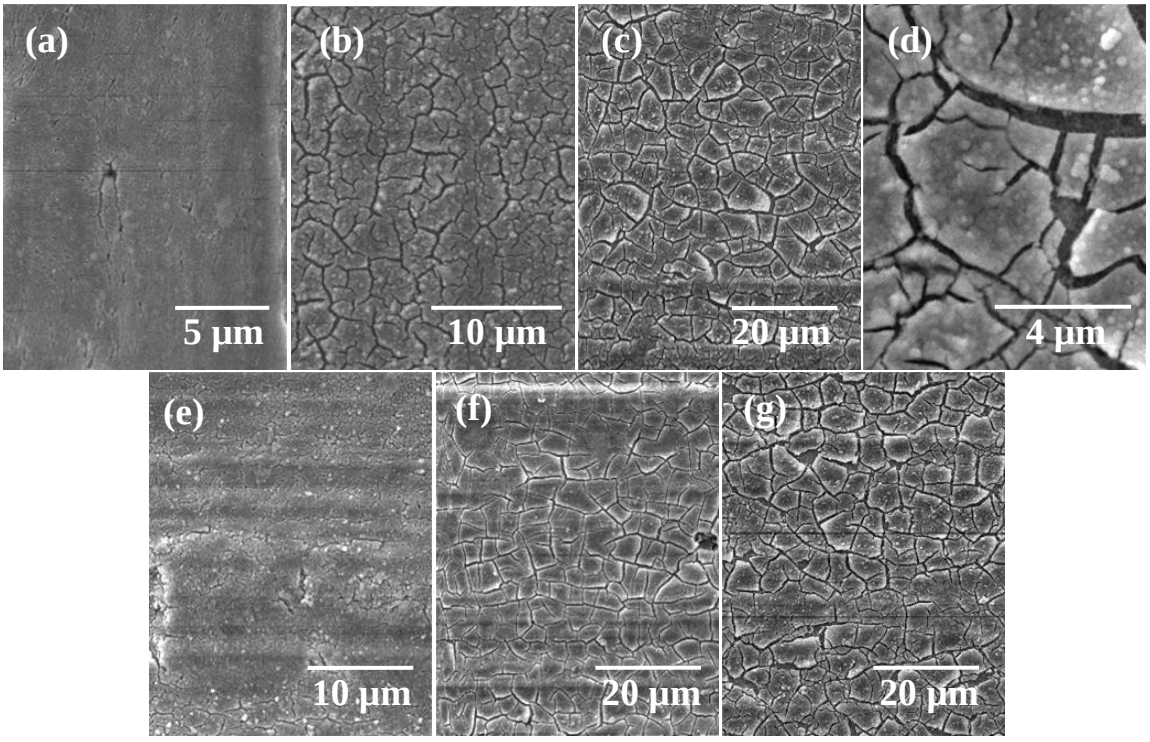

Figure C11. Nitrate-based, chloride free, CeCCs (a) nitrate spray deposition w/ HBF_4 activation, (b) H_2SO_4 – immersion, (c) H_3PO_4 – immersion, (d) HBF – immersion, (e) HBF_4, spray dep., sealed, (f) NaOH immersion, (g) HNO_3 immersion

Different cleaning processes were attempted: 1) 0.5 wt% HBF_4 – 25 seconds 2) three and seven minute immersion in 1.0 wt% H_2SO_4, and 3) five minute immersion in a 'basic pre-treatment cleaner' as described in the patent (0.1g NaOH, 0.05g $PrCl_3$, 0.1g $CeCl_3$, and 149.75g H_2O). In most cases very light coatings were produced and exhibited extensive corrosion after < 24 hours of salt spray exposure.

Corrosion Mapping of Al 2024 (with exposure to NaCl + H_2O_2 solution)

Coupons of Al 2024-T3 were polished, activated by immersion in heated H_2SO_4 (1 wt %), and exposed to an aqueous solution containing 110 ml H_2O, 0.23 g NaCl, and 0.6 ml H_2O_2. The sample was imaged in the as-polished state, after surface activation, and again after each exposure to the NaCl/H_2O_2 solution. Observations of the sample after each of the exposures are summarized in Table C4, optical images are shown in Figure C12. By inspecting the image, no indication of the location of pits is evident until exposure three or four, at which point larger darker regions are observed which begin to salt, well after the onset of corrosion.

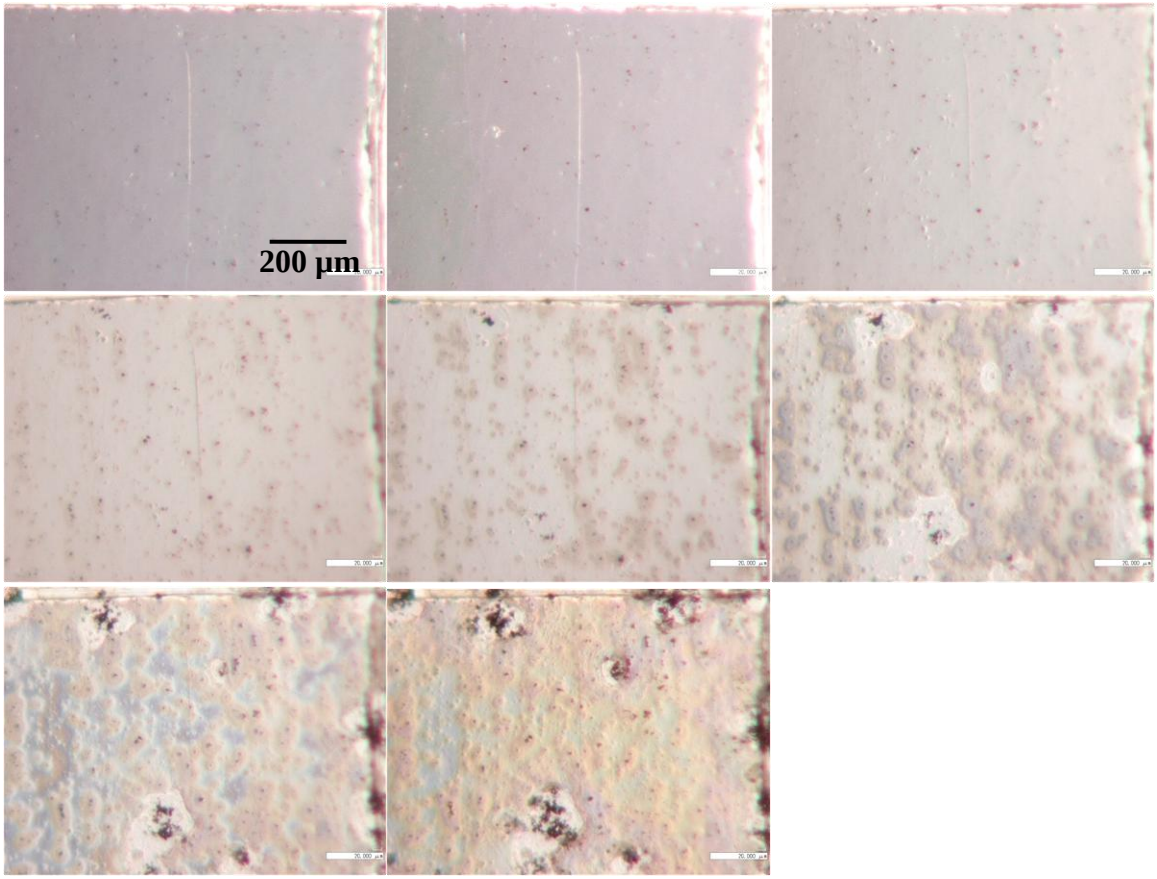

Figure C12. Corrosion mapping experiment

Table C4. Observations of Al 2024 coupon after incremental exposures to $NaCl/H_2O_2$ solution.

Exposure #	Approx. Time (sec)	Observations
1	1 - 2	Slight discoloration around some intermetallics
2	2 - 3	Increasingly pronounced discoloration around more of the intermetallics
3	5	First indication of areas likely to become pits
4	15	Pit formation, intial salting, buildup of material around intermetallics
5	40	Pit growth, more salting, noticeable buildup of material around intermetallics
6	85	Additional growth, salting, and formation of new pits

The Effect of pH on Post-treatment

Five different phosphates were selected to post-treat CeCCs over a pH range from 3.0 to 5.0. Solutions of 2.5 wt% $Na_2H_2P_2O_7$, NaH_2PO_4, Na_3PO_4, $Na_5P_3O_{10}$, and $K_4P_2O_7$ were prepared; solution pH was adjusted with phosphoric acid and/or a common cation hydroxide. In four out of five cases, the best corrosion resistance was observed when sealed at a pH just below that at which the maximum pH transition occurs. It is believed that hydroxide ions are introduced into the solution during the sealing process, thereby raising the solution pH. At the pH of maximum sensitivity in the titration curve, addition of a given amount of hydroxide ions will produce the largest achievable pH change under the experimental conditions. Overall, these results indicate that sealing at a pH of 3.5 – 4.0 may produce the best corrosion performance for the majority of phosphate sources. Subsequent analysis reported in TEM studies of as-deposited and post-treated CeCCs indicate structural heterogeneity that may be promoted by the reaction with different phosphate species. The transition region in the titration curve is that between $H_2PO_4^-$ and HPO_4^{2-}. It is believed that each of these species may complex with unstable cerium species to form cerium hydrogen phosphate species during post-treatment, which may then transition into the favored $CePO_4 \cdot H_2O$ rhabdophane phase.

High pH Post-treatment

CeCCs were prepared via the standard spray deposition process and post-treated in 85 °C solution of NaH_2PO_4 at pHs of 4, 7, and 10. The selected pH values were based on the corrosion rate of aluminum as a function of pH. At lower or higher pH, the corrosion rate increases, but is at a minimum near more neutral values. After 4 days of salt spray exposure, the corrosion resistance of the coatings was observed to decrease as

the pH of the post-treatment solution was increased. CeCCs post-treated at pH values of 7 and 10 did not transform the as-deposited coating to hydrated $CePO_4$. SEM analysis revealed the presence of defects as shown in Figure C13.

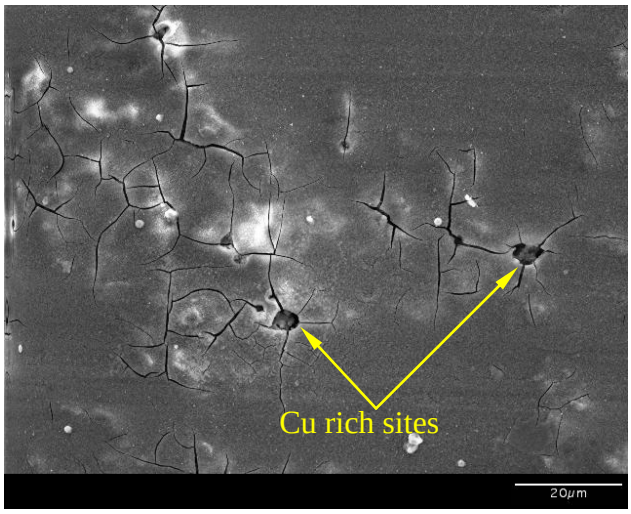

Figure C13. Post-treatment in solution of 2.5 wt% NaH_2PO_4 adjusted to pH of 10 with NaOH (5 min at 85 °C).

As the pH of the post-treatment solution was increased to 7 and 10, the density of defects observed in the coating increased. EDS analysis was performed on these defects and it was determined that they consistently occurred on copper rich sites as labeled in Figure C13, and seem to consistently appear in areas of large cracks. The larger quantity of defects observed in the CeCCs after post-treatment at higher pH values correlates well to salt spray corrosion tests since those coatings exhibited more corrosion after salt spray exposure than CeCCs post-treated at a pH of 4.5.

AES and XPS of Phosphate Treated, Uncoated, Al 2024-T3 Panels

Al 2024-T3 panels were post-treated in 2.5 wt% NaH_2PO_4 after each step of the standard cleaning process (isopropyl wipe, 5 min Turco immersion, and 10 min H_2SO_4 immersion). The samples were characterized using AES depth profiling (Figure C14). The AES data did not reveal the presence of a phosphorus rich film on the surface of the panel and demonstrated that the oxide layer present after acid treatment is nominally unchanged by the post-treatment (with respect to Will's surface activation paper). The

results indicate a maximum phosphorus content near the surface of less than or equal to one atomic percent. Duplicate panels were tested in salt spray exposure. Panels immersed in the phosphate solution after isopropyl and isopropyl/Turco cleans performed similarly, with the acid treated panel showing extensive pitting after < 24 hrs of exposure. None of the conditions exhibited improved corrosion resistance compared to a bare (uncoated) substrate.

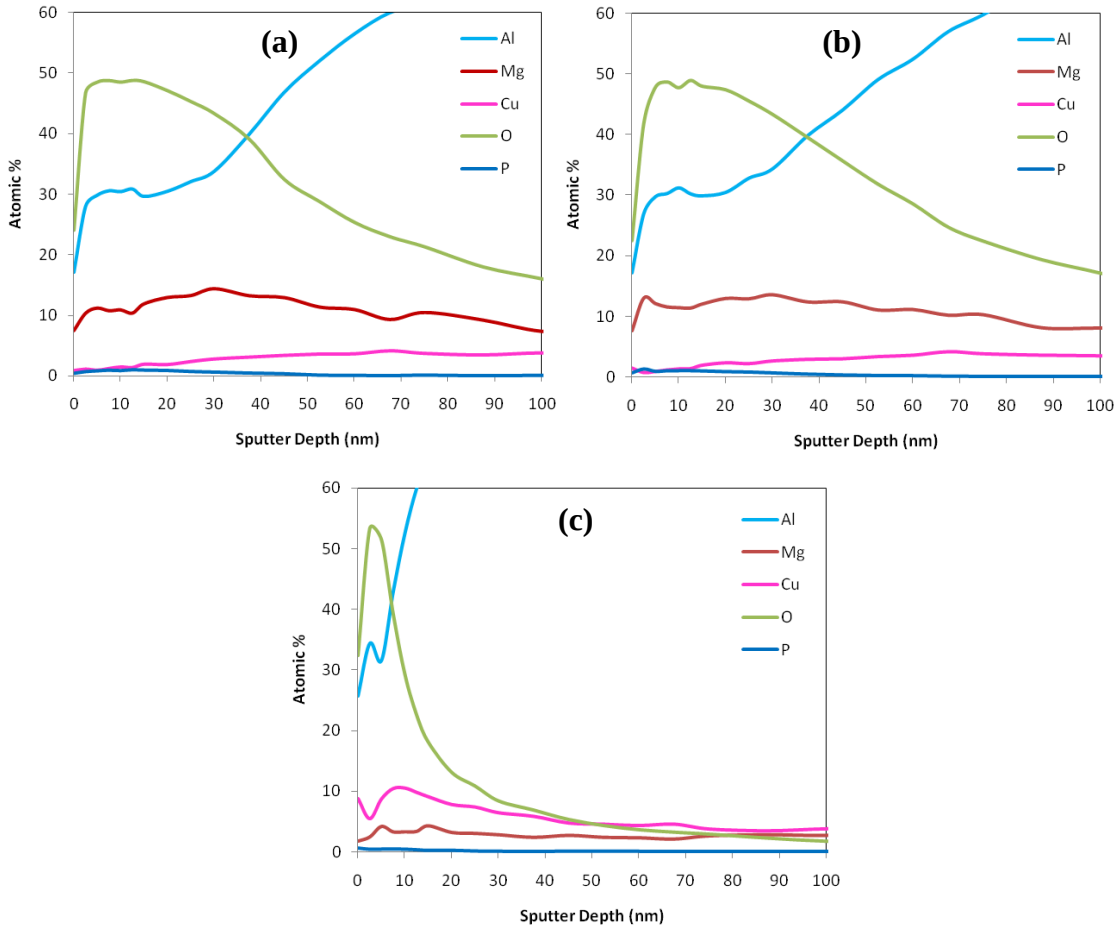

Figure C14. AES data from samples immersed in 2.5 wt% NaH_2PO_4 solution (5 min, 85 °C) after each step of the standard surface activation process, (a) isopropyl clean only, (b) isopropyl and alkaline clean (Turco), and (c) isopropyl, alkaline, and H_2SO_4 immersion.

Directly Deposited $CePO_4$ Coatings

Directly deposited $CePO_4$ coatings applied using the experimental conditions described in Section 6. Auger depth profiles were collected from two different areas of each specimen deposited with four coatings cycles and suggest an average thickness of

≈250 nm as determine by the sputter depth when the Ce concentration fell below the Al concentration. The morphology of the coatings was dominated by particulates and small agglomerates and contained uniformly distributed cracks that were finer than cracks associated with 'small' cracked regions of the standard CeCC. Analysis of the panel surface after sputtering off the coating (during AES analysis) did not reveal the presence of subsurface crevices. XRD analysis was performed on as-received samples with four coating cycles, and specimens with four coatings cycles that were post-treated for 5 min at 85 °C in $NH_4H_2PO_4$. There was no difference in the resulting patterns or corrosion performance. XPS analysis also confirmed the presence of $CePO_4$, with Ce^{3+} as the dominate oxidation state, and was consistent with the spectra observed from standard, post-treated CeCCs.

Directly deposited $CePO_4$ coatings were applied to Al 2024-T3 substrates using five different conditions:

- **[A]** standard four coat process from Round 1 (used as a control),
- **[B]** two four coat cycles separated by an immersion in DI water,
- **[C]** four coat cycle with 3X concentration of the standard process (designed to yield 100 g/L of monazite instead of 33 g/L),
- **[D]** four coat process followed by an overnight dry, then 2 coats, another overnight dry, and a final two coats,
- **[E]** four coat process followed by an overnight dry, then 2 additional coats.

The panels were exposed to neutral salt spray for 18 hours. Each of the panels exhibited corrosion pits and tails as shown in Figure C15. Conditions [B] and [D] showed the least amount of corrosion after 18 hours of salt spray exposure, and conditions [C] and [E] performed the worst. Initial observations suggest that increased number of coats may help to improve corrosion resistance as eight total coats were used for conditions [B] and [D], compared to four or six for the remaining panels. Auger depth profiling suggested that the coatings were ≈200 nm thick, but ≈600 nm thick for condition [B]. Conditions in which the substrate was allowed to dry seemed to shut down additional coating growth, whereas thicker coatings could be deposited by increasing the number of coating cycles while maintaining a non-breaking water film.

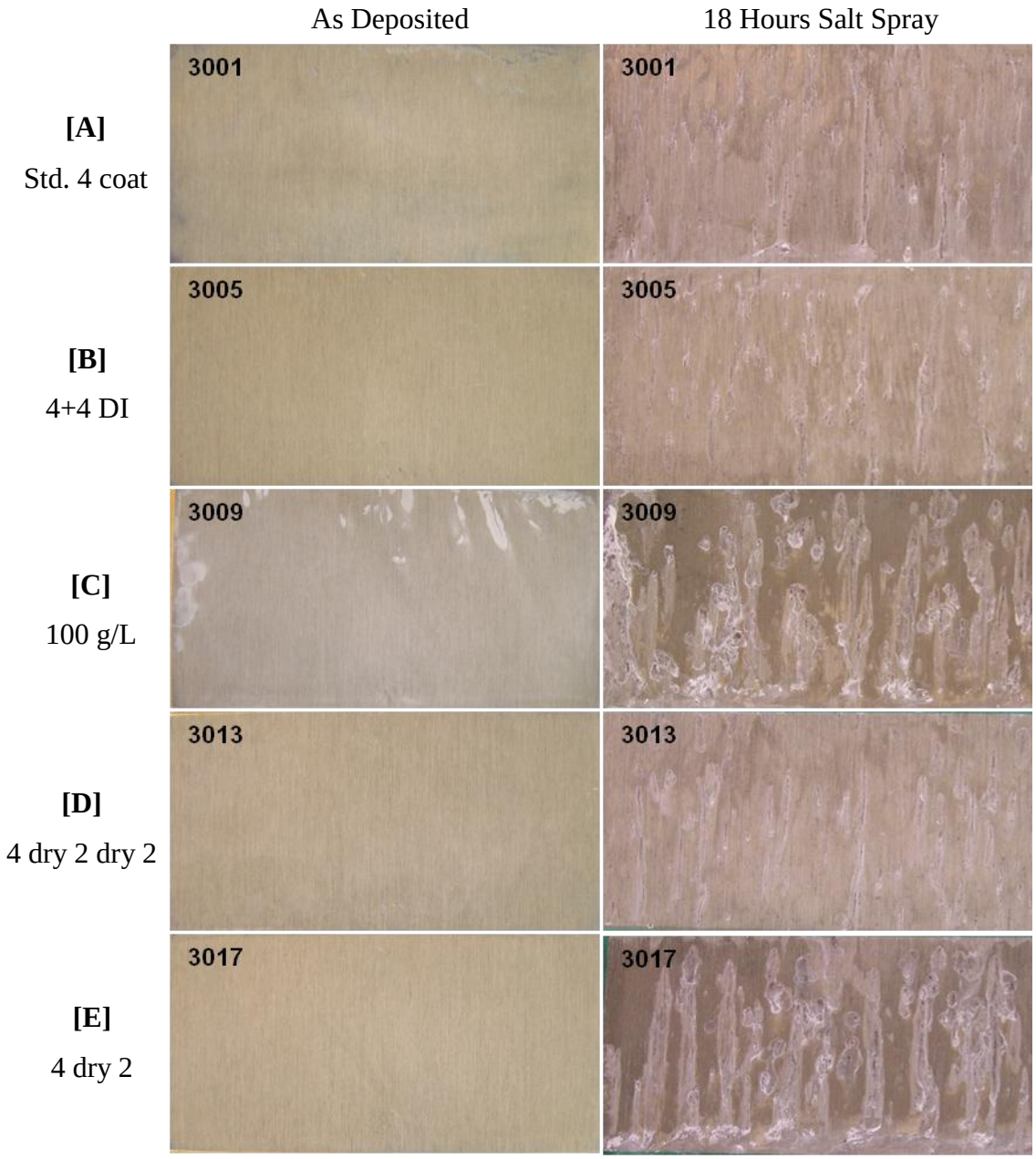

Figure C15. Optical images of direct deposited $CePO_4$ coated substrates, as deposited (left) and after 18 hours of salt spray exposure (right).

Some of the panels did not exhibit good uniformity and several were powdery to the point that the coating could be easily wiped off. The SEM images of each direct deposition condition are similar but exhibit differences in the morphology of the precipitate (Figure C16). Additionally, the as-deposited versus wiped morphologies are consistent for each image set. A precipitate remains loosely bound on the surface of each

of the as-deposited coatings. In each case, the wipe operation was performed by rubbing a gloved finger over the surface of the coating. Upon doing so, a distinct change in the coating's appearance was observed, from a more mottled, darker appearance to a lighter, more uniform appearance. After removing the loose precipitate, the morphology of the coating that remained adhered to the panel could better be characterized. Conditions [A] and [B] exhibit a morphology dominated by nodules or particles, whereas the remaining conditions exhibit a morphology much similar to that observed from a coating prepared using the standard CeCC process, except the cracks are much smaller and more uniform that those present in a sealed CeCC coating.

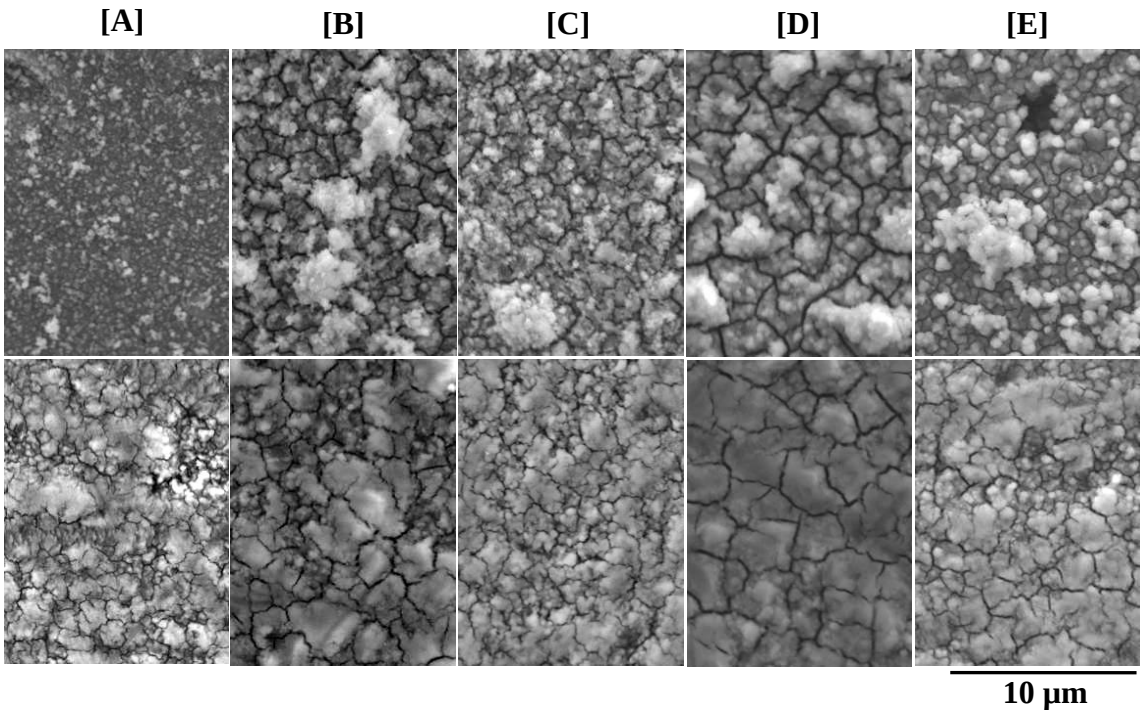

Figure C16. Direct deposited $CePO_4$ coatings, as-deposited surfaces (top), and adhered coatings after removal of loose precipitates (bottom).

Results from pull tab adhesion tests are shown in Figure C17. Conditions [B] and [E] exhibited adhesion strengths similar to the 32 MPa measured for a sealed CeCC, but the other conditions were only 50-75% of that value. Some of the deviation in the data appears to be caused by the non-uniformity of the coating. For a given sample, areas with very little or no coating consistently exhibited better adhesion than areas that were heavily coated.

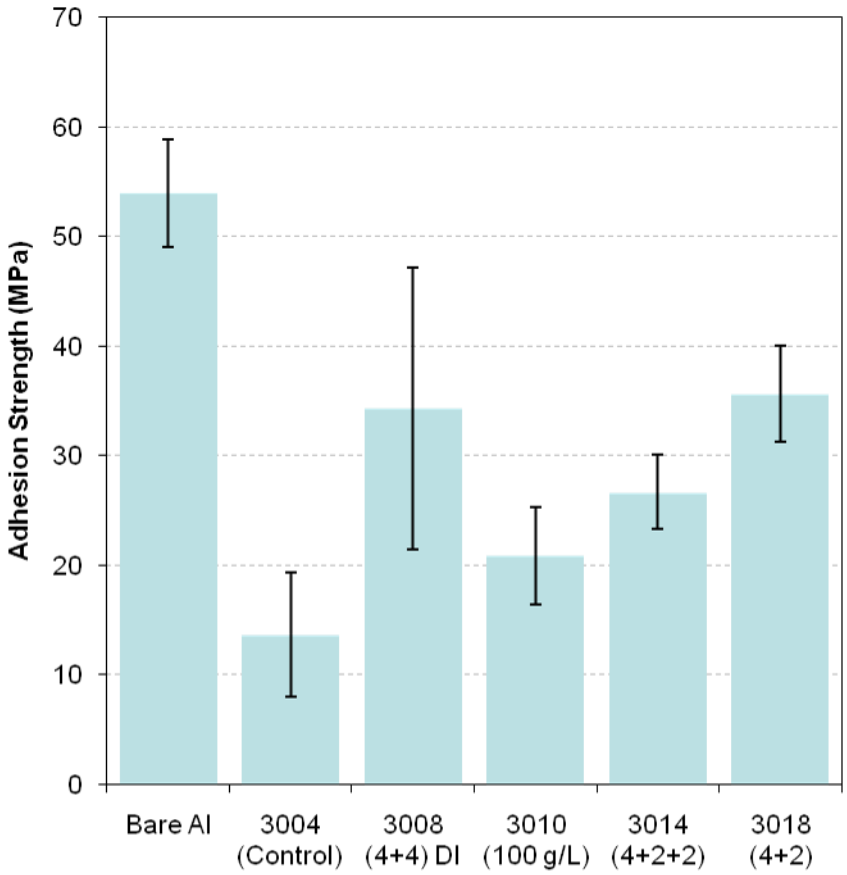

Figure C17. Adhesion tests for coating conditions examined during Round 2. Standard sealed CeCCs have adhesion strength ~32 MPa. Pull tabs loaded at 15lb/s.

Analysis presented in Paper IV established directly deposited $CePO_4$ coatings as a static barrier. This type of coating is unable to prevent corrosion of the substrate that is exposed by defects (i.e., cracks). In an attempt to remove some of the exposed active sites (i.e., intermetallics near the substrate surface, exposed by cracks), two $CePO_4$ coated substrates were immersed for 30 seconds in a 20 % equivalent $NaCl/H_2O_2$ solution of the standard CeCC spray solution and one of the panels was then post-treated in a 2.5 wt% solution of NaH_2PO_4 (5 min, 85 °C). After 18 hours of salt spray exposure the post-treated panel had less corrosion compared to the panel that was not post-treated (Figure C18).

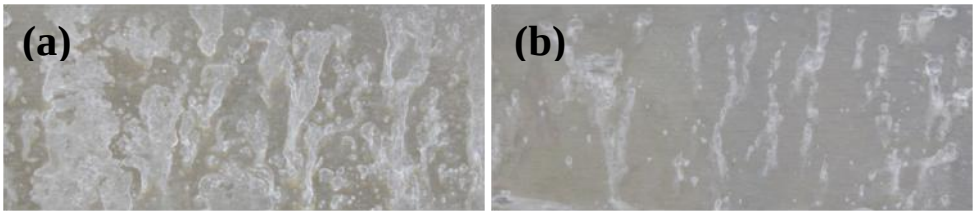

Figure C18. Directly deposited $CePO_4$ coatings after 18 hours of salt spray exposure. Coatings were exposed to 10 % equivalent $NaCl/H_2O_2$ for 30 sec, (a) no post-treatment and (b) with post-treatment.

Powder precipitation

Powders were obtained by adding base (NaOH) to aqueous $CeCl_3$ solutions with compositions based on standard coating solutions. Any precipitate from each condition was then scraped into a post-treatment solution containing 2.5 wt% NaH_2PO_4 at 85 °C and allowed to react for at least 5 min. The resulting powders varied in color, particularly before and after post-treatment. One week after preparation, the precipitate collected from the solutions containing H_2O_2 was a strong orange color compared to a dull grey-brown for the solution that did not contain H_2O_2. The presence of gelatin did not strongly influence the color of the resulting precipitate. When the precipitate from solutions containing H_2O_2 was placed into the sealing solution, the resulting powder showed a strong color change to white (w/ gelatin) and off-white (w/o gelatin). Eight different powders were prepared, each including 10 g of $CeCl_3$ per 250 g of coating solution and varying the presence of gelatin and/or peroxide. The resulting XRD patterns are shown below as Figure C19. Hydrated cerium phosphate was detected in all cases in which the precipitate was post-treated, even in the absence of gelatin. The results indicate a decrease in ceria crystallite size with increased H_2O_2 concentration. This trend does not appear to hold after post-treatment of the precipitate; however, the small amount of powder from the last two conditions shown may contribute to peak broadening.

Solution constituents prior to precipitation by addition of base are listed below. Powders were produced for unsealed and post-treated (85 °C, 5 min) conditions:

- No gelatin, no H_2O_2
- 0.6 g of gelatin per 250 g of coating solution, no H_2O_2
- No gelatin, 20 ml H_2O_2 per 250 g of coating solution
- 0.6 g of gelatin and 20 ml of H_2O_2 per 250 g of coating solution

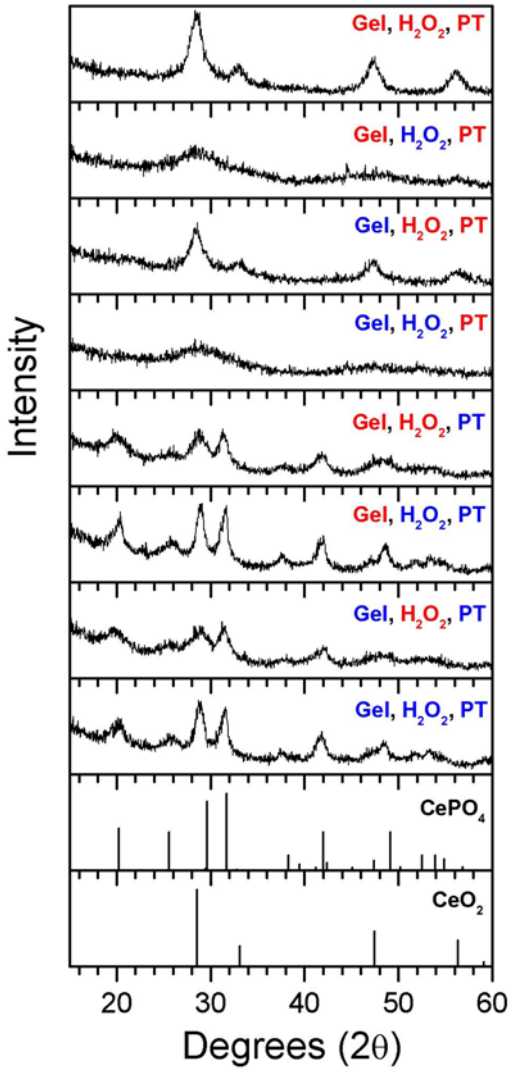

Figure C19. X-ray diffraction patterns obtained from Ce-based powders precipitated under different conditions. Blue indicates the presence of gel, hydrogen peroxide, or post-treatment (PT) and red corresponds to their absence.

After the identification of an interfacial phase (comprised of Ce, Al, and O) that formed at the interface of post-treated CeCCs during salt spray exposure, powders were precipitated from cerium containing solutions in the presence of aluminum chloride. The potential formation of Ce/Al/O compounds during precipitation was characterized using XRD. Initial powders of $Ce(OH)_4$, $CePO_4$, and CeO_2 were placed in two solutions of

$AlCl_3$ (2 g per 150 ml). The pH of the first solution was raised to 12 using NaOH, after which the precipitate was rinsed and filtered. The pH of the second solution was also raised to 12 using NaOH, but was then lowered to a pH of 4 using HCl. Afterwards, the precipitate was rinsed and filtered. The same procedure was used for each of the Ce compounds.

$Ce(OH)_4$ precipitate was produced by preparing a standard coating solution and adding NaOH. A portion of the resulting precipitate was collected and placed into an 85 °C aqueous solution containing 2.5 wt. % NaH_2PO_4, thereby forming $CePO_4 \cdot H_2O$. Commercial CeO_2 powder was used instead of heating the precipitated $Ce(OH)_4$. Analysis of the XRD patterns revealed that aluminum ions did not have a detectable influence on the phase of the precipitated cerium species. Diffraction peaks from the patterns matched with those from patterns collected in the absence of aluminum chloride.

VITA

Daimon K Heller was born in Tulsa, Oklahoma to Lance K and Donna Ruth Heller. Daimon graduated from Broken Arrow High School in May 2002, placing 6th in his graduating class of 1,007 students. He went on to study Ceramic Engineering at the University of Missouri-Rolla (UMR). During his undergraduate tenure, he spent 10 months as a student intern at Sandia National Laboratories in Albuquerque, NM and was honored as the "Outstanding Technical Year-Round Student" in 2005. In December 2006, Daimon received a Bachelor's degree in Ceramic Engineering, magna cum laude, and a minor in Economics from UMR. He then pursued a doctoral degree in Materials Science and Engineering at the Missouri University of Science and Technology (formerly the University of Missouri-Rolla before January 1, 2008), which was awarded in August 2010.